

Development of a Low Inertia Drumless Tether Management System

by

©Haibing Wang

A Thesis submitted to the School of Graduate Studies in partial fulfillment of the requirements for the degree of

Master of Engineering

Faculty of Engineering and Applied Science

Memorial University of Newfoundland

October 2017

St. John's

Newfoundland

Abstract

Oceanography winch system is a very important piece of equipment for ocean research. It is capable of managing cable and towing lines that are connected to the scientific research equipment. Traditional drummed winch systems exhibits issues such as large drum inertia that causes slow response, cable kink and high power consumption. In this thesis, an innovative low inertia drumless winch system that winds cable into a Figure "∞" shape was proposed and prototypes were designed and fabricated to prove the concept.

To estimate the power requirement for the winch system with regard to sensor towing applications, a dynamic mathematical model of the tow cable in two dimensions was developed using lumped parameter modelling. The model was implemented in Matlab, and simulations were done for different towing speeds. Towing forces including analysis of drag on cable, and relative sensor position under varying towing conditions could be estimated from the model.

Two prototypes were designed and built to prove the concept. The first prototype was designed to be a two module system which was planned to achieve reeling, twisting and directing the cable separately by the two modules. Dry running tests of the cable manipulation was performed. Second prototype which consisted of Cable Manipulation Unit and Cable Storage Unit was also designed and built. All three geared DC servo motors are feedback loop controlled using PID controllers, and PID parameters

were manually tuned. Cable winding tests were performed. Prototype one failed at twisting and changing the direction of cable. Prototype two successfully reels in and out the cable and can also change the direction while reeling it, but failed at twisting the cable while it was being reeled. Test results and problems encountered were discussed, possible solutions and future work on how to solve the problems and improve the performance of the system were also discussed.

Acknowledgements

Foremost, I would like to express my sincere gratitude to my advisors Dr. Ralf Bachmayer and Dr. Nick Krouglicof for the continuous support of my Master's thesis project, for their patience, motivation, enthusiasm, and immense knowledge. Their guidance and inspiration have really helped me in all the time of research and writing of this thesis. I would like to particularly thank Dr. Ralf Bachmayer for his very innovative ideas and suggestions on how goals can be achieved differently.

Besides my advisors, I would like to thank the laboratory technologists Tom Pike, Don Taylor, and Greg O'Leary who generously provided many hardware and tools which helped me build my prototypes.

My sincere thanks also goes to my laboratory mates Zhi Li, Mingxi Zhou, Brian Clause and Federico Luchino who have offered generous help, for their encouragement, insightful comments, and hard questions.

Last but not the least, I would like to thank my family: my parents, my wife and two lovely sons, for supporting me spiritually throughout my life.

Table of Contents

Abstract	ii
Acknowledgments	iv
Table of Contents	vii
List of Tables	vii
List of Figures	x
Nomenclature	xi
1 Introduction	1
1.1 Background Information	1
1.2 Literature Review	5
1.2.1 Single Drum Winch System	5
1.2.2 Double Drum Traction Winch System	6
1.2.3 Tether Management System	7
1.3 Motivation and Scope of Work	7
2 Cable Modeling	11
2.1 Overview	11
2.2 Coordinate System and the Method	12

2.3	Rotation Matrix	12
2.4	Kinematics	15
2.5	Internal and External Forces	17
2.6	Mass Matrix and Assembly of Forces	21
2.7	Mathematical Simulation in MATLAB	22
3	Design, Fabrication and Evaluation of Prototype I	27
3.1	Overview	27
3.2	Concept Generation and Analysis	28
3.2.1	Concept One: Rigid Casing with flexible joint	28
3.2.2	Concept Two: Flexible Cable with Active and Passive Profile Rollers Assembly	30
3.3	Prototype I Design	33
3.3.1	Introduction and System Overview	33
3.3.2	Detailed Design	37
4	Design, Fabrication and Evaluation of Prototype II	45
4.1	Mechanical	46
4.2	Electrical/Mechatronics	53
4.3	PID Control of Motors	66
4.3.1	Model of Cable Reeling Mechanism Motor	66
4.3.2	Simulink Model and Simulations for Closed Loop Control of the CRM Motor	71
4.3.3	PID Control Loop Tuning of the CRM Motor in Simulink	73
4.3.4	PID Tuning of the CRM Motor Without Cable	76
4.3.5	Position Synchronization Between CRM and ASM	82
4.4	Test of Full Winch Prototype II and Result	88

5 Conclusion and Future Work	94
Bibliography	98
Appendix	101

List of Tables

2.1 Constants and Parameters for MATLAB Simulation	23
2.2 Forces at Node 0 under Various Towing Speeds	25

List of Figures

1.1 Deep Sea Research Winch	2
1.2 How Slip Ring Works	3
1.3 Seaeye Tiger and a TMS	6
2.1 Coordinate System	13
2.2 Rotation Matrix	14
2.3 Marine Cables	18
2.4 A 2D coordinate system for MATLAB simulation	23
2.5 MATLAB Cable Simulation $V_0 = 1.2\text{ m/s}$	24
2.6 Forces at Node 0 under Various Towing Speeding	25

3.1	Rigid Casing with Flexible Joint Concept	28
3.2	2D representation of Profile rollers assembly driving flexible cable . .	31
3.3	Profile rollers assembly driving flexible cable	31
3.4	Differential Driving Mechanism	32
3.5	Prototype I System Diagram	34
3.6	Prototype I System Setup	35
3.7	Prototype I System Setup	36
3.8	Prototype I Differential Drive Assembly Illustration	38
3.9	Prototype I Twist Assembly Illustration	39
3.10	Rapid Prototyping Microcontroller: MUNder Board	41
3.11	Stepper Motor Driver: Microstepping Driver DCM 8028	42
3.12	L298N Full Bridge Motor Driver on SparkFun Breakout Board	43
4.1	Prototype II Assembly of Cable Manipulation Unit Overview	46
4.2	Cable Reeling Mechanism Illustration	47
4.3	Flexible Coupling and Motor Mount	48
4.4	Cable Reeling Mechanism Top Section View	49
4.5	Front View of Cable Storage Unit Top Section View	51
4.6	Back View of Cable Storage Unit Top Section View	52
4.7	Photo of Controls Electronics	53
4.8	mbd Rapid Prototyping Microcontroller Board	54
4.9	Pololu High Power Brushed DC Motor Driver 36v9	55
4.10	Pittman Brushed Geared DC motor GR 5.9:1	56
4.11	Mechanical Limit Switch	57
4.12	TMS Prototype II Brief System Diagram	58
4.13	Figure "8" Laying Pattern for Cable and Motor Position Relation Cal- culation	59

4.14	Position Relationship Calculation between Sliding Mechanism and Cable Reeling Mechanism	60
4.15	Bar Graphs for CRM Movement: Distance in Inches	64
4.16	Bar Graphs for Motor 2 Movement in Revolutions and Pulses	65
4.17	Typical DC Motor Circuit	67
4.18	DC Motor Transfer Function	68
4.19	Mechanical Assembly Diagram of the CRM	69
4.20	Complete Transfer Function for CRM	71
4.21	Simulink model for DC Servo Motor	71
4.22	Simulink model for CRM Motor Speed Controller	72
4.23	Simulink Motor Model for Controller Design	73
4.24	PID Tuning for CRM Motor, P - gain	74
4.25	PID Tuning for CRM Motor, PD - gain	75
4.26	PID Tuning for CRM Motor, PID - gain	76
4.27	PID Tuning for Motor 1, $K_p = 12$, $K_p/T_i = 0$, $K_p \cdot T_d = 0$	77
4.28	PID Tuning for Motor 1, $K_p = 6$, $K_p/T_i = 0$, $K_p \cdot T_d = 0$	78
4.29	PID Tuning for Motor 1, $K_p = 6$, $K_p/T_i = 0$, $K_p \cdot T_d = 12$	79
4.30	PID Tuning for Motor 1, $K_p = 4$, $K_p/T_i = 0$, $K_p \cdot T_d = 10$	80
4.31	PID Tuning for Motor 1, $K_p = 4$, $K_p/T_i = 0.067$, $K_p \cdot T_d = 10$	81
4.32	Position Synchronization Control Loop for Motor 2	82
4.33	PID Position Control for Motor 2, $K_p = 1$, $K_p/T_i = 0$, $K_p \cdot T_d = 0$	83
4.34	PID Position Control for Motor 2, $K_p = 1$, $K_p/T_i = 0$, $K_p \cdot T_d = 1$	84
4.35	PID Position Control for Motor 2, $K_p = 1$, $K_p/T_i = 0$, $K_p \cdot T_d = 1.5$	85
4.36	PID Position Control for Motor 2, $K_p = 0.5$, $K_p/T_i = 0$, $K_p \cdot T_d = 0.5$	86
4.37	PID Position Control for Motor 2, $K_p = 0.5$, $K_p/T_i = 0.01$, $K_p \cdot T_d = 0.5$	87

4.38	PID Position Control for Motor 2, $K_p = 0.2$, $K_p/T_i = 0.01$, $K_p \cdot T_d =$ 0.2	88
4.39	Illustration of Rubber Roller Twisting Cable	90
4.40	Cable Jammed in Cable Guide Tube	92
5.1	Marine Cable Twist Test Setup	177
5.2	Marine Cable Twist Test Data	178
5.3	Marine Cable Twist Test Chart	179

Nomenclature

P	–	Power needed to control drum
T	–	Torque required for turn winch drum
ω	–	Angular velocity of the drum
J	–	Polar moment of inertia
α	–	Angular acceleration
ϕ	–	Euler angle as X axis fixed
θ	–	Euler angle as Y axis fixed
ψ	–	Euler angle as Z axis fixed
ρ_w	–	Density of sea water
ρ_c	–	Density of cable
ρ_{tf}	–	Density of cable
m_c^i	–	Mass of cable element i
m_{tf}	–	Mass of tow-fish
m_a^i	–	Added mass of cable element i
g	–	Gravitational acceleration
E	–	Young's modulus of cable
A	–	Cross sectional area of cable
A_f	–	Cross sectional area of tow-fish
ε^i	–	Strain of element i

d_c	– Diameter of cable element
d_{pta}	– Pitch Diameter of Timing Pulley A
d_{ptb}	– Pitch Diameter of Timing Pulley B
d_{fr}	– Diameter of Friction Driver Roller
d_{tf}	– Diameter of tow-fish(modeled as a solid sphere with an average density)
V_c	– Volume of one cable element
V_{tf}	– Volume of tow-fish
lu	– Initial length of one cable element
l^i	– Length of cable element i
W_c	– Weight of cable element i
W_{tf}	– Weight of tow-fish
F_c	– Buoyancy force of one cable element
F_{tf}	– Buoyancy force of tow-fish
D_x^i	– Normal drag along x direction in body fixed frame for cable element i
D_y^i	– Normal drag along y direction in body fixed frame for cable element i
D_z^i	– Tangential drag along z direction in body fixed frame for cable element i
f_n	– Normal loading function for determine normal hydrodynamic drag
f_t	– Tangential loading function determine tangential hydrodynamic drag
v_x^i	– x component of velocity of geometric center of element i in the body fixed frame for cable element i
v_y^i	– y component of velocity of geometric center of element i in the body fixed frame for cable element i
v_z^i	– z component of velocity of geometric center of element i in the body fixed frame for cable element i
C_d	– Drag coefficient of the cable
r_{gA}	– Gear Ratio for Motor #1

r_{gB}	–	Gear Ratio for Motor #2
R_A	–	Number of Revolutions for Motor #1
R_B	–	Number of Revolutions for Motor #2
Θ_{twist}	–	Twisted Cable Angle
P_{en}	–	Encoder pulses for cable test
D_{en}	–	Diameter of cable test setup encoder wheel
D_{pu}	–	Diameter of cable test setup pulley wheel
<hr/>		
TMS	–	Tether Management System
FDM	–	Fused Deposition Modeling
RP	–	Rapid Prototyping
ABS	–	Acrylonitrile Butadiene Styrene (a common thermoplastic polymer)
CMU	–	Cable Manipulation Unit
CSU	–	Cable Storage Unit
CRM	–	Cable Reeling Mechanism
ASM	–	Arm Sliding Mechanism
CTM	–	Cable Twisting Mechanism

Chapter 1

Introduction

1.1 Background Information

Oceanographic research winches are vital to oceanographic scientific researches such as sensor towing, ROV operations, and other tethered scientific instruments. For typical underwater sensor towing applications, the motion control of towed equipment is often necessary for obtaining a much more reliable and meaningful set of data. This is due to the fact that the motion of the equipment being towed is affected by unwanted movement of surface vehicle caused by sea waves and wind, and ocean current [1]. The motion of the towed equipment is not usually predictable under any particular sea state. To overcome that unwanted movement of the towed equipment caused by random ocean current and unwanted movement of surface vessel, winch control is required to achieve a precision motion control of the towed equipment. Motion control can be achieved passively by controlling the fin actuators or actively by deploying and retrieving the towing cable. Oceanographic research winches can be categorized into two major types according to the method of driving: Hydraulic and Electric. The discussion will be focused on electric research winches in this thesis if not

indicated otherwise. For the purpose of scientific researches such as data collection of current, temperature, depth and etc., cable being deployed need to have the capability of transmitting power and/or data. A slip ring is integrated into the winch system to achieve this. A typical oceanographic research winch system is composed of the following major components (see figure 1.1):

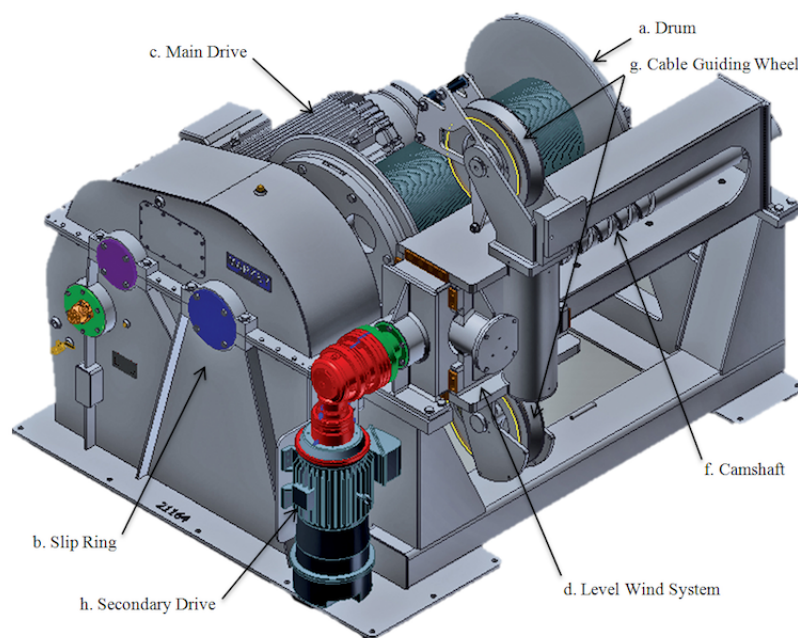


Figure 1.1: Rendering of CAST6-125 Deep Sea Research Winch Designed for AGOR-27 by Mark Jessup (MarEx 2011)

a. Drum

“Drum” is a spool that cable can be wound on and it is driven by a hydraulic or electric motor with reduction gears. The drum stores wound up cable as the data collection is completed.

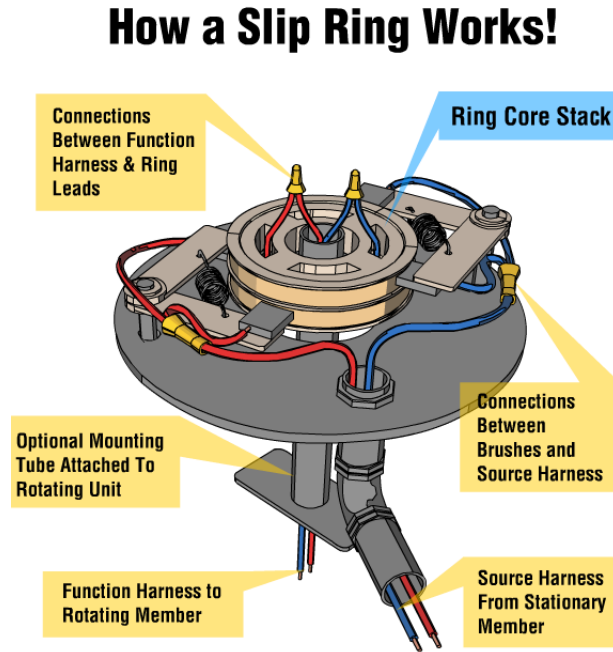


Figure 1.2: This shows how a simple slip ring works (photo courtesy of UEA)

b. Slip ring

A slip ring is an electromechanical device that is able to transmit the power and electrical signals from a stationary to rotating structure [2]. It maintains the power and data transmission between the fixed onboard electronics and the rotating cable that is being wound on drum. A standard slip ring has four basic elements: A ring assembly, brushes, connectors and leads. As shown in figure 1.2, the source harness from stationary member is connected to the electro-conductive brushes which swipe against the copper (silver or gold is used if high quality data transmission is required)

ring in the center as it rotates. The function harness is connected to the rotating member, which is the copper/gold ring that is always in contact with the source harness. No matter what direction or how fast the rotating unit spins, the stationary member can always make contact with the rotating member [3]. There is a variety of design configurations for the slip rings: Concentric ring, back to back, and drum type [4].

c. Main drive

Electric or hydraulic motors are required to drive the drum through reduction gears to control the payout of towing cable. Motors can be AC or DC driven depending on the availability of the electrical services on the surface vessel.

d. Level wind system (Cable guiding mechanism)

Level wind system moves the guiding wheels along the path that is parallel to the axis of the drum, and it synchronizes the position to the movement of the cable so that the cable is wound on the spool in an organized manner layer by layer. The movement and position synchronization is typically done by a cylindrical camshaft (f) whose rotational speed is synchronized to the rotational speed of the drum.

e. Control module

This module contains all electronics that are required to drive the motors and to achieve the speed and/or position control of the motors. While this is not shown in figure 1.1, it can be contained in the enclosure attached to the winch frame or a separated enclosure.

1.2 Literature Review

1.2.1 Single Drum Winch System

The single drum research winch has been the data collection mainstay of oceanographic researches for wire and cable handling and storage [5]. It can be used for a wide variety of applications with cable length capacity range from one hundred meters to 10,000 meters. Smaller and lighter winches are also made available for cost reduction while they are still capable of reaching required depth for most applications. These winches typically provide 5000 - 6000 meters of reach depending on the cable or wire diameter. Portable winch systems are also popular because of their easy manoeuvrability, low cost and light weight, and they typically provide a few hundred meters of reach.

A single drum winch is composed of only one drum, which is driven by a electric or hydraulic motor. Cable deployment or retrieval is directly controlled by the drum rotation, so any cable tension induced by drum action is stored in the wound spool. In many applications where high line pull load exist, the cable bend diameter can reach that of the cable diameter at the cross over points. This combined with high line pull load will result in possible cable damage. Moreover, the cable will penetrate the top layer under extremely high tension. In some cases, the systems are still called single drum winch systems even though multiple drums are used for some particular applications because each drum has its own independent drive and drum rotation is individually controlled.

1.2.2 Double Drum Traction Winch System

A double drum traction winch typically consists of two winding drums or sheaves and a storing drum, and more importantly it provides the capability of traction control for cable or wire rope as they are reeled in or paid out. Typically, the cable or wire rope is wound into the grooves on both torque controlled sheaves to form a single layer, which promotes low line tension on the end where a storage drum can wind the cable in multi-layer format without excessive tension. The idea of traction control has largely extended the life span of cable or wire rope, which saved a lot of time and cost in a long run. For that reason, traction winches have become more and more popular in the oceanographic research industry.

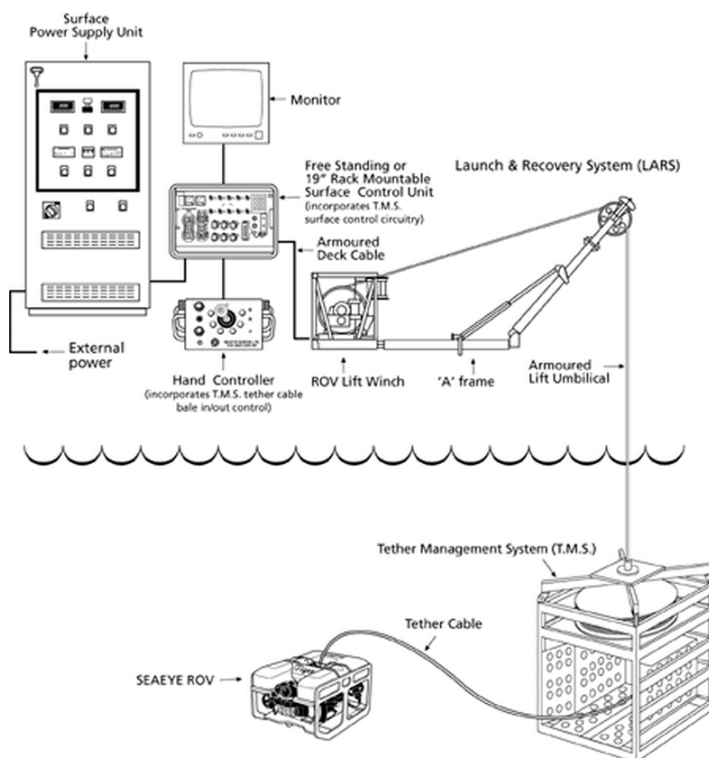


Figure 1.3: A Saab Seaeye Tiger operating from a TMS system

1.2.3 Tether Management System

The tether management system usually refers to a system that stores and deploys tether cable for ROVs (Remotely Operated Underwater Vehicles). A tether management system can decouple a ROV from the motion of the surface vessel so that the vehicle can freely navigate itself within a satisfying operating radius without being affected by any unwanted motion of the tether cable [6]. ROV Tether management systems typically don't involve the control of the winch drum as long as the cable has some slack and the ROV can freely reach its designated spot. The main component of all TMS is an integrated winch system that involves deployment and storage of the tether cable. A popular type of TMS (Tether Management System) is usually submerged in water, so water proof design is the key to the successful operations of these equipment. As shown in figure 1.3, the TMS is lifted by a ROV lift winch on the surface vehicle, and the SEA-EYE ROV is tethered from the TMS which has a winch drum built in for the operations of tether cable. The armoured life umbilical is rated for the weight of TMS and ROV with a reasonable safety factor so that the cable will have a long operating life. The type shown in figure 1.3 is a garage type which has a parking space for the ROV. The ROV can be parked into the TMS before it is lift out of the water. In this system, there are two slip rings since there are two cable drums for the manipulation of tether cables.

1.3 Motivation and Scope of Work

In spite of continuous development and many achievements in Oceanographic research winches, there still exist several serious issues in the area of oceanographic researches especially with the sensor towing applications.

First of all, a slip ring is a part that wears out quickly or breaks down very often, and the repair or replacement cost is very high. If the break down happens while the research is being carried out, not only the cost will arise much more significantly, it will also delay the entire task.

Second of all, the large inertia of the winch drum has made it more difficult to dynamically control the reeling action of the drum. For two main reasons, it is very important for the winch system to be able to dynamically control the tether cable.

Firstly, for small to medium sized ocean research vessels, the ship's motion added to the winch speed can form cable kinks as it is being lowered, and then when the ship motion reverses, the cable can be quickly damaged by the severe snap loads. Secondly, the quality of the data collected will be affected if there is no control of cable reeling action [7].

For power and data cables, the manufacturer specifies a minimum bending radius so that the cable doesn't get damaged and will have a longer life. This factor is always seriously considered when the winch drum is sized, and the drum diameter is sized much more than the minimum because it can promote higher load capacity, increased cable life, less cable layer for more spooling benefit and etc [8]. As a result, the drum becomes a lot larger and heavier. As the cable is wound on the drum, the weight of the wound drum becomes even larger. The heavy drums have large rotational inertia, which is the issue for the dynamic control of reeling action of drums. The power needed for controlling the winch increases significantly as the polar moment of inertia becomes larger.

$$P = T \times \omega \quad (1.1)$$

$$T = J \times \alpha \quad (1.2)$$

Where,

P = power

T = torque

ω = angular velocity

J = polar moment of inertia

α = angular acceleration

As shown in equation 1.1 and 1.2, when J increases with the radius of the drum, the required power increases. The availability of power might not be the most unsolvable issue, but the entire system will cost a lot more because everything has to be sized to the larger power requirement including the motor drive, framing, control module and etc. The large size often will raise another issue of occupying too much deck space.

To solve the existing issues, the design of a new type of winch system with no drum and low inertia was proposed. The elimination of the drum can potentially solve two major issues, which are the difficulty to control the drum and slip ring problem. Several possible conceptual design ideas were considered and a few design iterations were made for the final winch prototype. Subsurface cable modeling was completed using lumped parameter method. One dimensional cable modeling in 3D space was considered sufficient for this application. Each cable element is modelled as a spring

damper system. A tow fish at the cable end was modelled as a point mass with a spherical shape for hydrodynamic drag. Cable towing load was estimated by using the same mathematical model of the cable. The design of the first prototype was carried out and the prototype was made and tested. The first prototype was designed to reel the cable and change the direction of the cable at the same time by driving the cable with two differential friction rollers. It consists of two modules: the first module drives the cable in and out with two differential friction rollers that are controlled by two stepper motors. The second module create a cable twist by moving one roller up and down while keeping the pairing roller in the same height. The created cable twist can assist the cable to be wound into the cable storage unit. It failed to change the cable direction while it tried to reel it at the same time. The investigation was made and then the second method was hatched. The new prototype reels the cable by using a set of friction rollers which are driven by a servo motor, and the arm swing between the left and right position to change the cable direction. This thesis will discuss the concept and the designs with great details to explain how the concept works and why it should solve the existing issues for conventional winch systems.

Chapter 2

Cable Modeling

2.1 Overview

For scientific towing applications, the towing force needs to be estimated for deciding the power requirement when designing such a winch system. Therefore, mathematical modeling and simulation of the underwater towed system needs to be prepared. It is also essential to have a clear understanding of the dynamics of the cable and the towed body.

The dynamics of underwater cable is highly non-linear because of the geometric configuration and the fluid drag force [9] [18], therefore, a numerical approach is taken. In many cases, cable dynamics were studied and analyzed by using lumped mass and spring damper system in a three dimensional space [9] [11] [16] [17] [14] [15]. This chapter will first start the discussion from developing the discretized cable model in a fixed reference frame. The kinematics of the cable elements, internal forces and external forces that act on the cable are all closely looked at. Finally applying Newton's Second Law of Motion to all of the nodes on the cable obtains a set of governing equations of motion. Within the scope of this study, a tow-fish is also

attached to the end of the cable. For simplicity, the tow-fish is modelled as a solid sphere with a certain density.

2.2 Coordinate System and the Method

For the purpose of the cable modeling, we need to define a fixed inertial reference frame along with a sequence of frames that move with the nodes of the cable. The continuous cable is discretized to some number of elements. Each point between any of the two neighboring elements is recognized as a node. See figure 2.1, the inertia reference frame is fixed at sea surface, while the local coordinate system moves with each cable element. A rotation matrix transforms the coordinate system from local to the fixed frame. As shown in the figure, X is positive to the right, Z is positive downward, and Y is positive outward away from the paper. The towed cable can be treated as a series of elastic rods connecting one to another, and each rod element has its spring and damper effect. The uniform mass of each rod element is lumped into the two ends, which are the nodes between the elements.

The figure 2.1 illustrated two example elements (Element i and $i+1$) and 3 nodes ($i-1$, i , $i+1$). The local coordinate or the body fixed frame x - y - z is defined as shown in the figure 2.1 with y and z being normal and x being tangent to the cable element.

2.3 Rotation Matrix

According to Euler's rotation theorem, any rotation may be described using three angles. The rotation matrix R can be expressed as a product of three rotation matrices $R_z(\psi)$, $R_y(\theta)$ and $R_x(\phi)$. ψ , θ and ϕ are the Euler angles, and the rotation directions of the frame are shown in figure 2.2

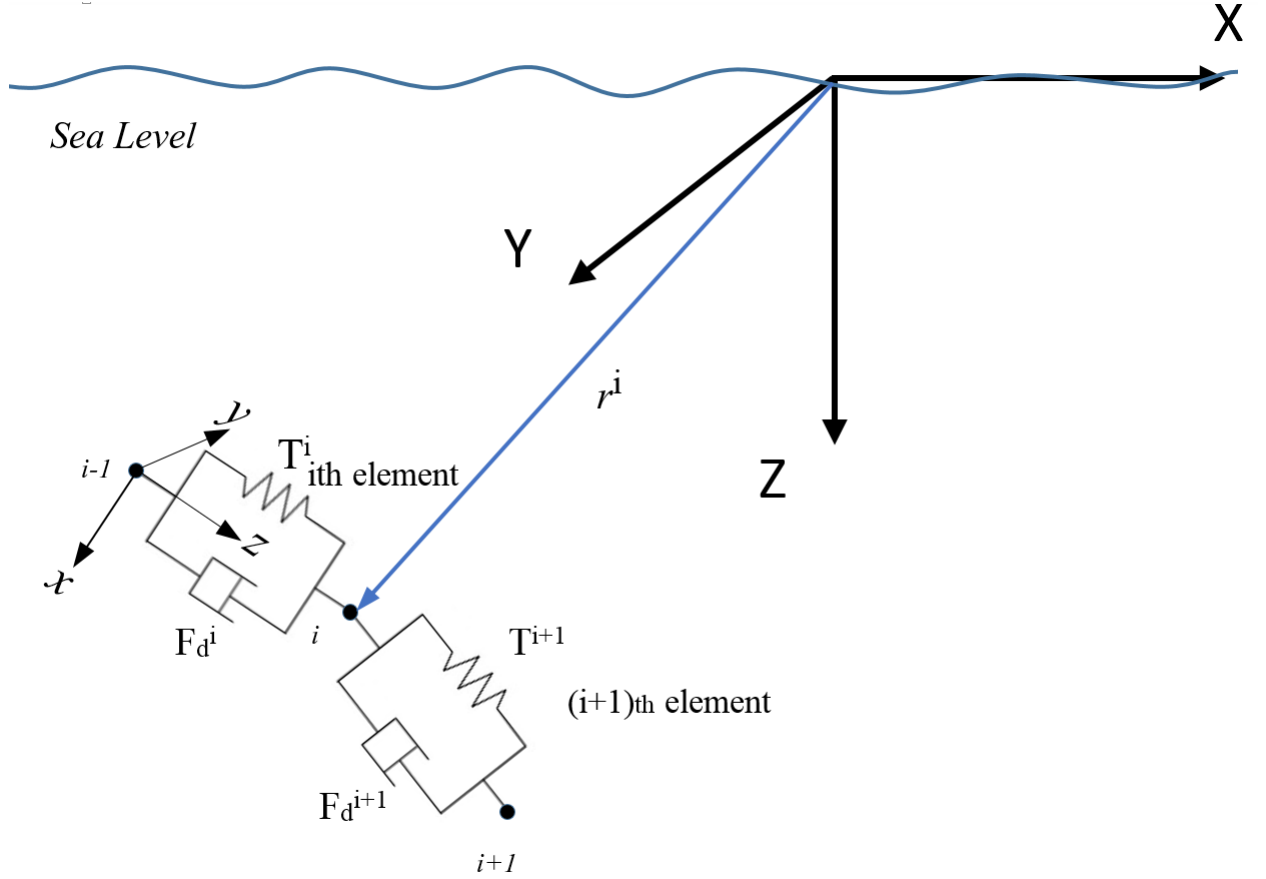


Figure 2.1: The Inertia Reference Frame X-Y-Z and The Local Coordinate System x-y-z on the cable elements

The three rotation matrices $R_z(\psi)$, $R_y(\theta)$ and $R_x(\phi)$ are defined depending on their specific directions of rotations around the axes Z, Y, and X, respectively.

$$R_x(\phi) = \begin{bmatrix} 1 & 0 & 0 \\ 0 & \cos(\phi) & -\sin(\phi) \\ 0 & \sin(\phi) & \cos(\phi) \end{bmatrix}, \quad (2.1)$$

$$R_y(\theta) = \begin{bmatrix} \cos(\theta) & 0 & \sin(\theta) \\ 0 & 1 & 0 \\ -\sin(\theta) & 0 & \cos(\theta) \end{bmatrix}, \quad (2.2)$$

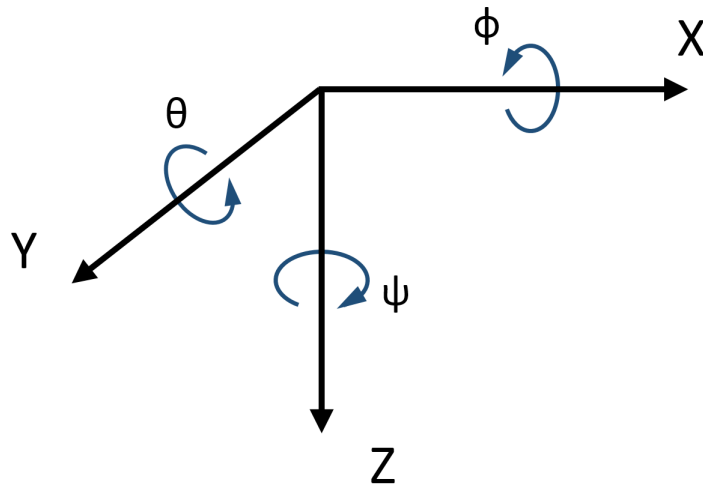


Figure 2.2: The Inertia Reference Frame X-Y-Z and its rotations

and

$$R_z(\psi) = \begin{bmatrix} \cos(\psi) & -\sin(\psi) & 0 \\ \sin(\psi) & \cos(\psi) & 0 \\ 0 & 0 & 1 \end{bmatrix}. \quad (2.3)$$

The Rotation Matrix R is the product of the matrices 2.1, 2.2, & 2.3:

$$\begin{aligned}
R &= Rz(\psi) \times Ry(\theta) \times Rx(\phi) \\
&= \begin{bmatrix} \cos(\psi) & -\sin(\psi) & 0 \\ \sin(\psi) & \cos(\psi) & 0 \\ 0 & 0 & 1 \end{bmatrix} \begin{bmatrix} \cos(\theta) & 0 & \sin(\theta) \\ 0 & 1 & 0 \\ -\sin(\theta) & 0 & \cos(\theta) \end{bmatrix} \begin{bmatrix} 1 & 0 & 0 \\ 0 & \cos(\phi) & -\sin(\phi) \\ 0 & \sin(\phi) & \cos(\phi) \end{bmatrix} \\
&= \begin{bmatrix} \cos(\theta) & 0 & \sin(\theta) \\ 0 & 1 & 0 \\ -\sin(\theta) & 0 & \cos(\theta) \end{bmatrix} \begin{bmatrix} 1 & 0 & 0 \\ 0 & \cos(\phi) & -\sin(\phi) \\ 0 & \sin(\phi) & \cos(\phi) \end{bmatrix} \\
&= \begin{bmatrix} \cos(\theta) & \sin(\theta)\sin(\phi) & \sin(\theta)\cos(\phi) \\ 0 & \cos(\phi) & -\sin(\phi) \\ -\sin(\theta) & \cos(\theta)\sin(\phi) & \cos(\theta)\cos(\phi) \end{bmatrix}
\end{aligned} \tag{2.4}$$

Since within the scope of this study, torsional motion and force are not considered, therefore, ψ is set to zero eg. $\psi = 0$. The two of the three Euler angles are sufficient to describe the orientation of the cable elements [11] [16]. In Equation 2.3, $R(\psi)$ becomes an identity matrix, thus we can obtain a slightly simplified orthogonal rotation matrix R as seen in equation 2.4.

2.4 Kinematics

In this section, a sample element and its neighboring element and nodes are denoted as element i , element $i+1$, node $i-1$, node i , and node $i+1$ (as shown in figure 2.1). The orthogonal rotation matrix for the i^{th} element becomes the following:

$$R^i = \begin{bmatrix} \cos(\theta^i) & \sin(\theta^i) \sin(\phi^i) & \sin(\theta^i) \cos(\phi^i) \\ 0 & \cos(\phi^i) & -\sin(\phi^i) \\ -\sin(\theta^i) & \cos(\theta^i) \sin(\phi^i) & \cos(\theta^i) \cos(\phi^i) \end{bmatrix} \quad (2.5)$$

At any instant, the Euler angles θ and ϕ can be calculated if the end points of the cable elements are known [11]. In the finite element method, every element is of equal size and the initial positions of the each cable element are known in both frames [19]. For the end point i , x and y coordinates are equal to zero in the local body fixed frame since the cable element is in line with z axis. If the length of the element i at any instant is l^i , then

$$R^i \begin{bmatrix} 0 \\ 0 \\ l^i \end{bmatrix} = \begin{bmatrix} r_X^i - r_X^{i-1} \\ r_Y^i - r_Y^{i-1} \\ r_Z^i - r_Z^{i-1} \end{bmatrix} \quad (2.6)$$

Thus,

$$\begin{bmatrix} \cos(\theta^i) & \sin(\theta^i) \sin(\phi^i) & \sin(\theta^i) \cos(\phi^i) \\ 0 & \cos(\phi^i) & -\sin(\phi^i) \\ -\sin(\theta^i) & \cos(\theta^i) \sin(\phi^i) & \cos(\theta^i) \cos(\phi^i) \end{bmatrix} \begin{bmatrix} 0 \\ 0 \\ l^i \end{bmatrix} = \begin{bmatrix} r_X^i - r_X^{i-1} \\ r_Y^i - r_Y^{i-1} \\ r_Z^i - r_Z^{i-1} \end{bmatrix} \quad (2.7)$$

Since the length of the element i can be calculated as follows,

$$l^i = \sqrt{(r_X^i - r_X^{i-1})^2 + (r_Y^i - r_Y^{i-1})^2 + (r_Z^i - r_Z^{i-1})^2} \quad (2.8)$$

and \mathbf{r}^i , and \mathbf{r}^{i-1} are the position vectors with the vector components being r_X^i, r_Y^i, r_Z^i and $r_X^{i-1}, r_Y^{i-1}, r_Z^{i-1}$, the following set of non-linear equations can be obtained combining

the above ones from 2.5 through 2.8:

$$l^i \sin(\theta^i) \cos(\phi^i) = r_X^i - r_X^{i-1} \quad (2.9)$$

$$-l^i \sin(\phi^i) = r_Y^i - r_Y^{i-1} \quad (2.10)$$

$$l^i \cos(\theta^i) \cos(\phi^i) = r_Z^i - r_Z^{i-1} \quad (2.11)$$

Take equation 2.9 and divide it by 2.11 we can get

$$\tan(\theta^i) = \frac{r_X^i - r_X^{i-1}}{r_Z^i - r_Z^{i-1}} \quad (2.12)$$

Then we can get,

$$\theta^i = \text{atan2}(r_X^i - r_X^{i-1}, r_Z^i - r_Z^{i-1}) \quad (2.13)$$

Once θ^i is calculated, Euler angle ϕ^i can then be obtained by equation 2.10 and 2.9 or 2.11. For best numerical stability, we choose to use one of the equations 2.9 or 2.11 based on the value of $\cos(\theta^i)$ and $\sin(\theta^i)$. The mass matrix can then be obtained provided that the rotation matrix R^i is known now. The dynamics of the cable element is discussed in the next subsection where the internal and external forces involved will be studied.

2.5 Internal and External Forces

The method for calculating the internal forces within cable elements has been discussed well in Huang's paper [9]. Essentially these forces exist because of the elastic behavior of the towing cable. These include tension force, and damping force. The bending and torsional moment are not considered because the tow cable is modelled as a series of discrete elastic rods chained together one after another, and the joints

between the elements i.e. the nodes are frictionless.

For any element, we have

$$\sigma = \frac{T}{A} = E\varepsilon \quad (2.14)$$

where σ is the stress when the element is subject to a load, E is the Young's Modulus of the cable, and ε is strain under the tension force. If the unstretched length of element i is l_u^i , the current length of the element is l^i , then $\varepsilon^i = \frac{l^i - l_u^i}{l_u^i}$. T represents the tension force and A is the cross sectional area of the towing cable. Thus the tension force within element i can be calculated by the following:

$$T^i = EA\varepsilon^i \quad (2.15)$$



Figure 2.3: Sectional View of Typical Marine Cables: Xtreme Cat Underwater Network Data/Power Cable

As shown in figure 2.3, typical marine towing cable is composed of layers that are made from different materials. The outer protective layer can be various types of materials such as Polyethylene, Polyurethane and etc. depending on the specific applications. In between the jacket and conductors there is a reinforcement layer, which can be fiber or steel. As the cable is being stretched under tension and then

restored to its original position, a damping effect is created by the friction between the layers of different materials. The damping force is proportional to the rate of change of its tangential strain ε . For Element i , the damping force can be calculated as follows,

$$F_d^i = C_v(v_z^i - v_z^{i-1}) \quad (2.16)$$

Where C_v is the viscous damping coefficient that can be obtained through the experimental method, and v_z^i is the tangential component of the velocity of node i in the local coordinate frame.

To obtain a simulation model as close as possible to real towing, all of the external forces should be added. As we are only studying the dynamic behaviour of the submerged portion, the cable is subjected to gravitational and buoyancy forces. Since the cable is towed through water, the hydrodynamic drag is also significant and should be considered.

The weight of one element can be calculated based on its volume and density. The density of the cable along the longitudinal direction is considered uniform. The buoyancy force of each element is also easily calculated as shown in equation 2.18

$$W_c = m_c g = \rho_c V_c g \quad (2.17)$$

$$F_c = \rho_w V_c = \rho_w \frac{\pi d_c^2}{4} l_u \quad (2.18)$$

The tow-fish is also subject to weight and buoyancy force:

$$W_{tf} = m_{tf}g = \rho_{tf}V_{tf}g \quad (2.19)$$

$$F_{tf} = \rho_w V_{tf} = \rho_w \frac{\pi d_{tf}^3}{6} \quad (2.20)$$

For the hydrodynamic forces that are acting on the cable and the tow-fish, we are going to adopt the approach that has been done in papers [17] [11] [18] [20] [21]. The drag forces in x, y and z direction of the body fixed frame is generated as follows:

$$D_x^i = -\frac{1}{2}\rho_w C_d d_c l_u^i f_n |\mathbf{v}^i|^2 \frac{v_x^i}{\sqrt{(v_x^i)^2 + (v_y^i)^2}} \quad (2.21)$$

$$D_y^i = -\frac{1}{2}\rho_w C_d d_c l_u^i f_n |\mathbf{v}^i|^2 \frac{v_y^i}{\sqrt{(v_x^i)^2 + (v_y^i)^2}} \quad (2.22)$$

$$D_z^i = -sgn(v_z^i) \frac{1}{2}\rho_w C_d d_c l_u^i f_t |\mathbf{v}^i|^2 \quad (2.23)$$

In equation 2.21, 2.22 and 2.23, there are loading functions f_n and f_t in the normal and tangential direction, respectively. The loading functions distribute the drag into the normal and tangential component nonlinearly. As discussed in Driscoll and Nahon's paper [17], the loading functions are expressed as follows,

$$f_n = 0.5 - 0.1 \cos \gamma + 0.1 \sin \gamma - 0.4 \cos 2\gamma - 0.011 \sin 2\gamma \quad (2.24)$$

$$f_t = 0.01(2.008 - 0.3858\gamma + 1.9159\gamma^2 - 4.16147\gamma^3 + 3.5064\gamma^4 - 1.187299\gamma^5) \quad (2.25)$$

$$0 < \gamma < \frac{\pi}{2} \quad (2.26)$$

where γ is the relative angle between cable element and the fluid flow. Assume there is no current existed while cable is being towed. γ is then the relative angle between cable element and the opposite of the towing direction. Once the drags are calculated for the element i and $i + 1$ (see figure 2.1), half of each drag is applied to node i . Weight and buoyancy force on the node are calculated using the same method.

2.6 Mass Matrix and Assembly of Forces

As added mass should be accounted for motion of underwater bodies, the cylindrical cable element i has an added mass of

$$m_a^i = \rho_w V_c^i \quad (2.27)$$

for the normal direction, but no added mass is considered in the tangential direction because the effect will be relatively small compared to the normal directions. The mass matrix of element i in the body fixed frame then becomes,

$$M_B^i = \begin{bmatrix} m_c^i + m_a^i & 0 & 0 \\ 0 & m_c^i + m_a^i & 0 \\ 0 & 0 & m_c^i \end{bmatrix} \quad (2.28)$$

For the element $i + 1$, we have

$$M_B^{i+1} = \begin{bmatrix} m_c^{i+1} + m_a^{i+1} & 0 & 0 \\ 0 & m_c^{i+1} + m_a^{i+1} & 0 \\ 0 & 0 & m_c^{i+1} \end{bmatrix} \quad (2.29)$$

, and so on.

As we need to lump the mass of element i and $i + 1$ to the node i under this lumped mass spring damper system method, we then obtain the mass representation for node i in the inertia reference frame X-Y-Z:

$$\mathbf{M}^i = \frac{1}{2}\mathbf{R}^i\mathbf{M}^i(\mathbf{R}^i)^T + \frac{1}{2}\mathbf{R}^{i+1}\mathbf{M}^{i+1}(\mathbf{R}^{i+1})^T \quad (2.30)$$

To obtain the final equation of motion, apply Newton's Second Law to each node,

$$\mathbf{M}^i\ddot{\mathbf{r}} = -(\mathbf{T}^i + \mathbf{F}_d^i) + (\mathbf{T}^{i+1} + \mathbf{F}_d^{i+1}) + \frac{1}{2}(\mathbf{D}^i + \mathbf{D}^{i+1}) + \mathbf{W}_c - \mathbf{F}_b \quad (2.31)$$

where $1 < i < n - 1$, if there are a total of n nodes with the last node being the tow-fish. In equation 2.30 and 2.31, bold letters represent mass matrix or the vector form of the forces which includes the x, y and z component. Since the weight and buoyancy force of each element are the same, lumped weight and buoyancy force are equal to that of a single element's. In equation 2.31, it is only valid to the second last node before the point of attachment of the tow-fish, which is modeled as solid sphere for simplification. Care should be taken when the model is implemented in MATLAB, and the first and last node are the special conditions. See the next section for details for MATLAB implementation of the dynamic cable towing model.

2.7 Mathematical Simulation in MATLAB

The main purpose of the towing simulation is to understand the dynamic behavior of the towed system, which includes finding the towing force at node 0. This is required for the power estimation of the reeling motor during the preliminary design of tether management system. Within the scope of this study, the main work is focused on the design, fabrication and testing of the TMS prototype. Further more, the main

Table 2.1: Constants and Parameters for MATLAB Simulation

$Cd = 1.2$	– Drag coefficient
$Cv = 0.1$	– Damping coefficient
$lu = 0.5\text{ m}$	– Unit length of unstretched cable element
$E = 2 \times 10^9$	– Young's Modulus of cable
$d_c = 0.011\text{ m}$	– Diameter of cable
$g = 9.81\text{ m/s}^2$	– Gravitational acceleration
$\rho_w = 1100\text{ kg/m}^3$	– Density of seawater
$\rho_{tf} = 3000\text{ kg/m}^3$	– Density of tow-fish
$d_{tf} = 15\text{ cm}$	– Diameter of tow-fish

purpose is to figure out the towing dynamics as the towing vessel is traveling straight without turns. Thus, only a two dimensional model is implemented in MATLAB to obtain an estimate of the dynamic behavior. For simulation, a set of constants and parameters are assumed to be as shown in table 2.1. The two dimensional frame used in the MATLAB simulation is shown in figure 2.4

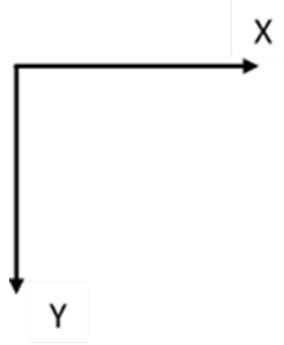


Figure 2.4: 2D coordinate system used in MATLAB simulation

In the simulation, initial state is that the cable is vertically hanging under the seawater, then an initial speed is given to node zero at the surface. The number of elements is 20, and each element is 0.5m long. Therefore the total length of simulated cable is 10 meters. Figure 2.5 shows the cable position for every 0.2 second. The stars represent the nodes. The MATLAB code also calculates the forces at Node 0.

$$F_{tx} = -137.1498N \quad (2.32)$$

$$F_{ty} = 173.128N \quad (2.33)$$

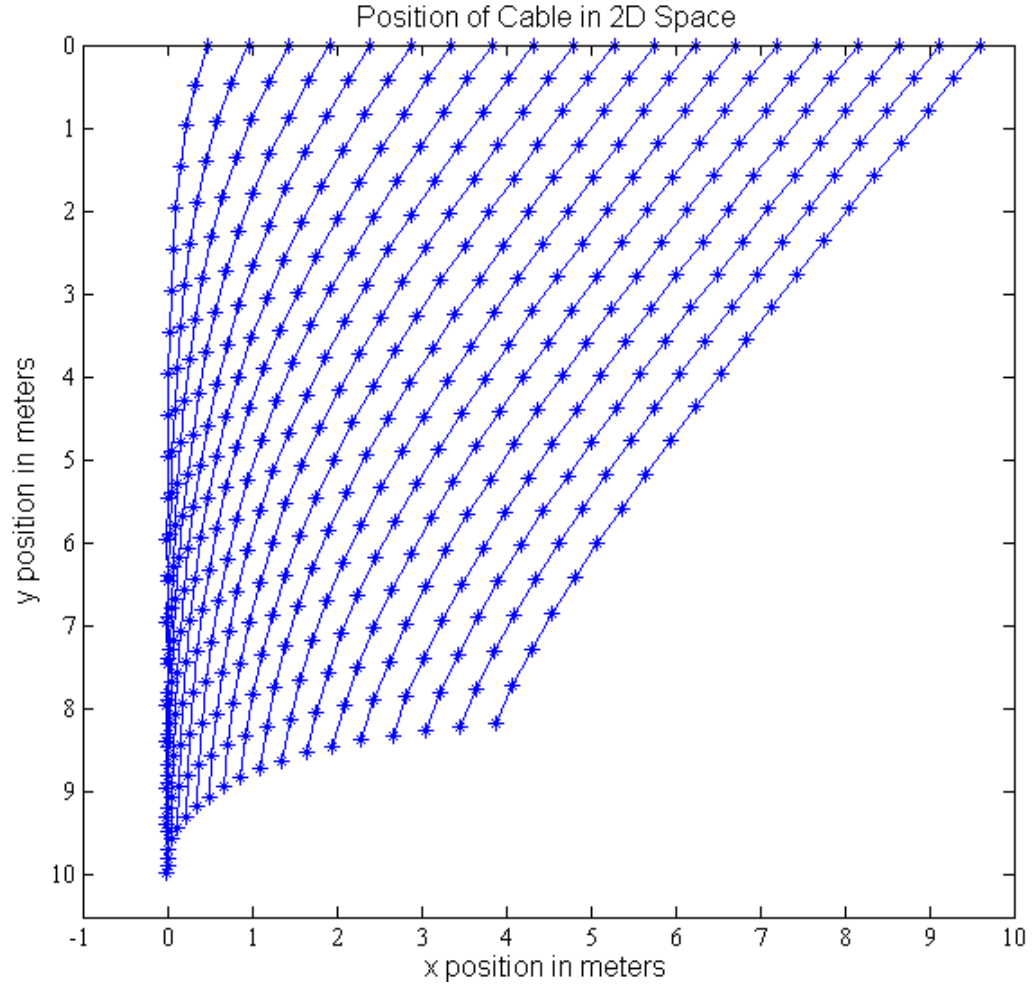


Figure 2.5: MATLAB Cable Simulation: $V_0 = 1.2 \text{ m/s}$

Table 2.2: Forces at Node 0 under Various Towing Speeds

Speed(m/s)	F_{tx}	F_{ty}	F
0.2	-5.9756	66.2440	62.53
0.4	-19.4182	68.8865	71.57
0.6	-38.0506	77.4051	86.25
0.8	-62.8189	95.6557	114.44
1.0	-95.9843	127.8405	159.86
1.2	-137.1498	173.128	220.87
1.4	-181.6247	224.7379	288.95
1.6	-227.568	279.5172	360.44

Equation 2.32 and 2.33 are the forces exerted on Node 0 by the moving cable. The total force acting on the node is then calculated to be 220.87 N. The various towing speeds are also simulated in MATLAB and the corresponding tow forces are tabulated in table 2.2.

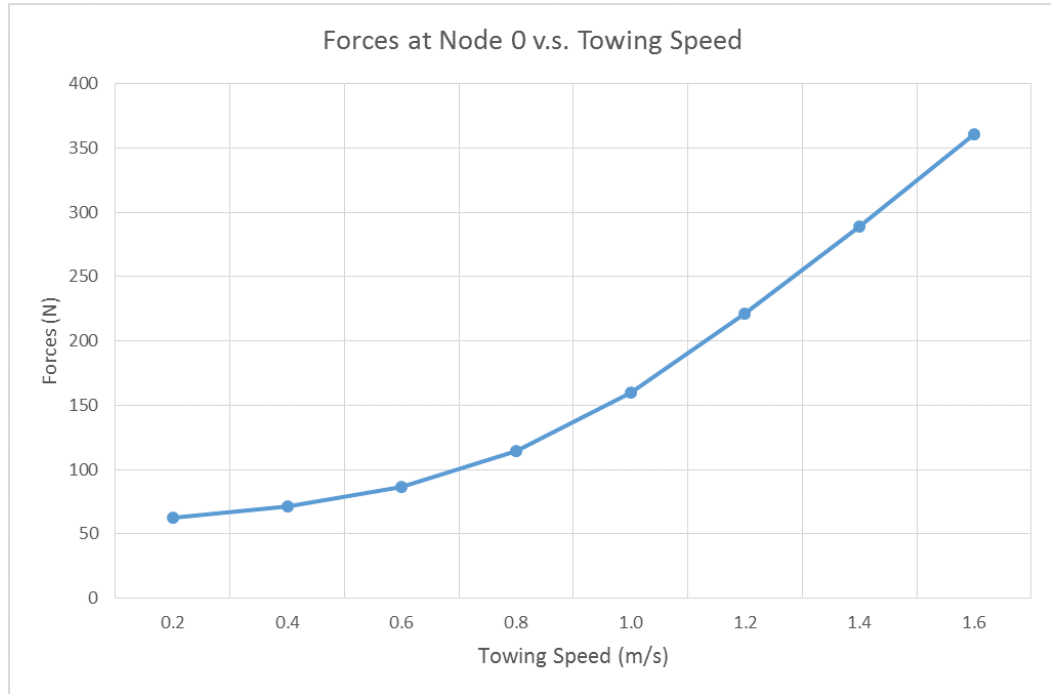


Figure 2.6: Forces at Node 0 under Various Towing Speed

In Figure 2.6, the resultant force acting on Node 0 increases with the increasing

towing speed. While the MATLAB simulation model can effectively estimate the towing force, it provides critical information for the design of the prototype. In the next chapter, the complete development process of the tether management system will be discussed, which includes conceptual designs, concept models and testing, improved design, and design of required electronics.

Chapter 3

Design, Fabrication and Evaluation of Prototype I

3.1 Overview

In this chapter, a few conceptual designs are discussed and each concept is analyzed for its viability and feasibility, and then a final design is proposed. During the concept generation process, some rapid mock ups and simple models were made to help with the design. Reasons are explained why they were not adopted and how the improved design was proposed. The integrated electronics which includes the rapid prototype microcontroller board, stepper and DC servo motors are also discussed in details.

3.2 Concept Generation and Analysis

3.2.1 Concept One: Rigid Casing with flexible joint

This is the very first concept generated during the first team meeting. The idea is to achieve fast deployment and retrieve of the cable without having to use a slip ring mechanism by combining the rigid sections and the flexible joint. The far end of the tether storage unit has a fixed cable connection so that when the cable is reeled out or in, it would not be necessary to involve a slip ring for data and power transfer. This is also one of the main objectives of this research project. To assist the concept generation process and better understand the mechanism, a quick mock up of the model was fabricated(see figure 3.1) using bamboo skewers and springs.

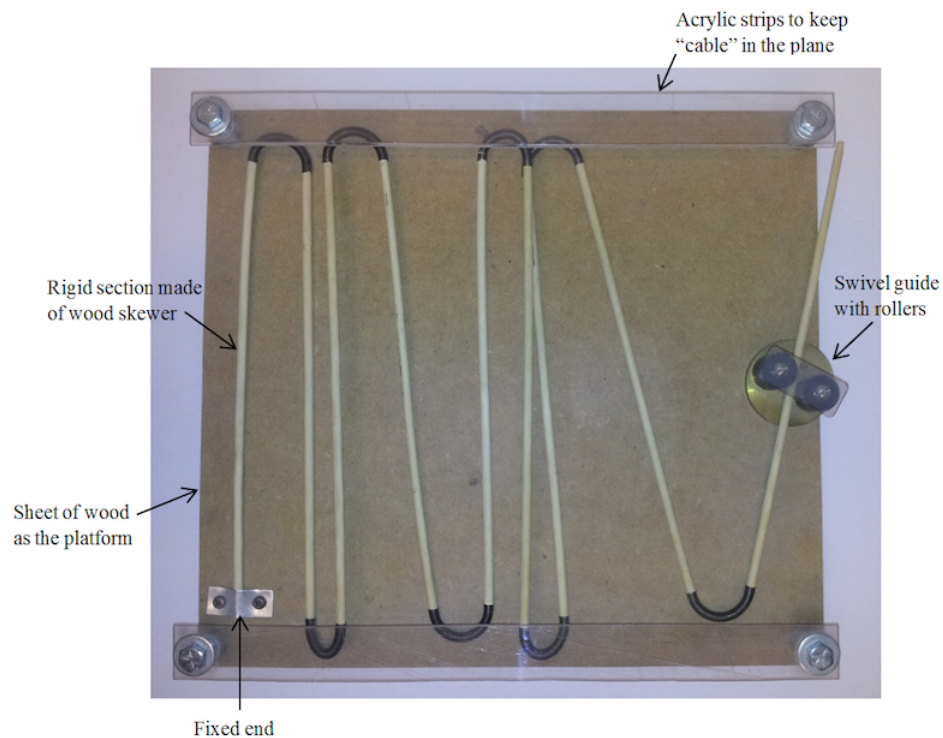


Figure 3.1: Rigid casing with flexible joint concept mock up

The connected "cable segments" are fixed onto a wood platform at one end by a metal

bracket. The other end can move freely to simulate the retracting and deploying action of the "cable". Two pieces of acrylic strips are tied down to the wood platform leaving a gap for the flexible part of the "cable" as well as keeping it from moving upward. This is to reduce the degrees of freedom of the "cable" so it only moves within the plane that is parallel to the wood platform. The swivel guide is composed of a brass wheel which has a shaft on the other end that turns inside the hole in the wood platform and two guiding rollers that are made of Delrin plastic. This mock up helped with the further design idea generation and feasibility study.

This concept did not work out very well because of several reasons, one being that the swivel cable guide requires a certain distance between itself and the retrieved portion of the cable. This is due to the fact that all rigid casing sections have to pass the cable guide in the middle and the rigid casing needs some space as it is being drawn into the unit. This greatly reduces the cable packing capability of the TMS. The bent section also requires that a minimum bending radius should be used. This also increase the volume of the storage unit since the bending radius is generally at least ten times the cable diameter. The cable packing capability refers to the ability that the system has to store cable. Packing density is usually used to measure how dense a tether management or winch system is able to store the cable. It can be calculated as follows:

$$\rho_{pack} = \frac{L_{cable}}{V_{unit}} \quad (3.1)$$

In equation 3.1, ρ_{pack} is the packing density of the unit, L_{cable} is the total length of cable, and V_{unit} refers to the total volume of the storage unit. Based on this concept, a rough estimation of the packing density can be calculated. Another important reason is that the rigid casing adds some unwanted swing motion to the towed object as it's being retrieved or paid out. The rigid section tends to swing from the left to the

right back and forth when it is guided through the cable swivel guide. Being able to manage the cable inside the storage unit is also a big challenge in this case. For the above reasons, it was chosen to abandon this concept. Although this idea did not work out, it is quite innovative and encouraging.

3.2.2 Concept Two: Flexible Cable with Active and Passive Profile Rollers Assembly

While the rigid cable casing idea was not adopted, ordinary flexible towing cable idea was brought back to the discussions. The main idea of this concept is to drive the cable in and out by a set of friction rollers with one being active and the other passive, and store it in a cable storage unit with a figure "8" shape. This concept was inspired by the fact that winding or unwinding cable in a figure "8" shape cancels out the cable twist. This is a great advantage because cable twist creates a huge issue during cable deployment and retrieval. The cable twist is one of the most common causes of cable damages. As seen in figure 3.3 of the idea demonstration, the two rollers are concave shaped all around. In this demo, both rollers can rotate freely about their own axis, and the left roller can also move up and down as it is rolling while the right roller stays in the middle. The advantage of this setup is that cable twist can be created if the left roller is set up to move up and down. Figure 3.2 is a 2D representation drawing of the setup seen below in Figure 3.3. The left roller is rotating clockwise and the right one is rotating counterclockwise, and the cable is being driven out toward the reader. The direction of the created cable twist depends on the moving direction of the active roller. The idea of the concaved profile is to have a high probability of keeping the cable at the lowest potential as the cable is being twisted while there is chance of slippage, which will drive the cable outside of the rolling surface and lose control of the cable manipulation. In the first fabricated

prototype, this profile was not implemented because of the cost of custom making is quite high. To show the proof of concept, it is not an absolutely necessary item on the list.

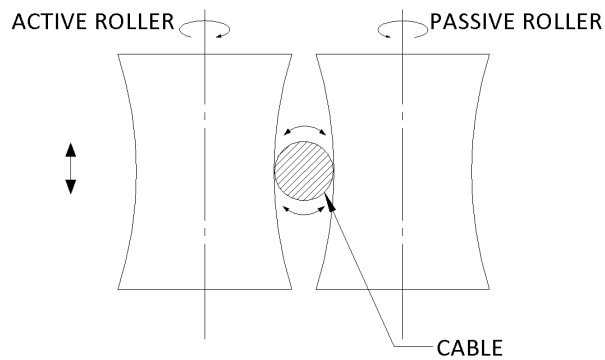


Figure 3.2: 2D representation of profile rollers assembly driving flexible cable

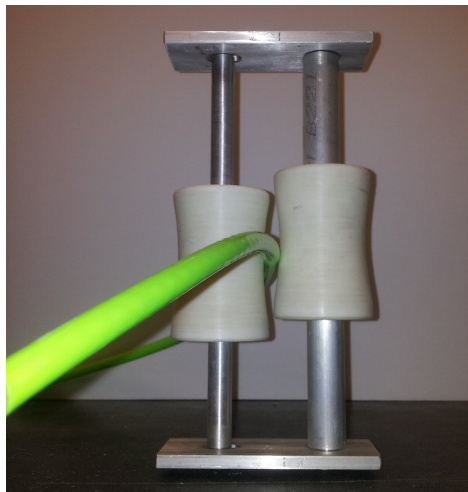


Figure 3.3: Profile rollers assembly driving flexible cable

Additional feature of this setup is the differential drive mechanism. The differential drive mechanism can be used to change the direction of the cable payout which is essential as the cable is driven into the storage unit. The cable needs to change its

moving direction from left to right or vice versa to finish the figure "∞" shape. The idea is to drive one roller faster than the other to create a difference in the driving friction force. This will be discussed in the next section as it uses two active drives instead of one active drive and one passive drive.

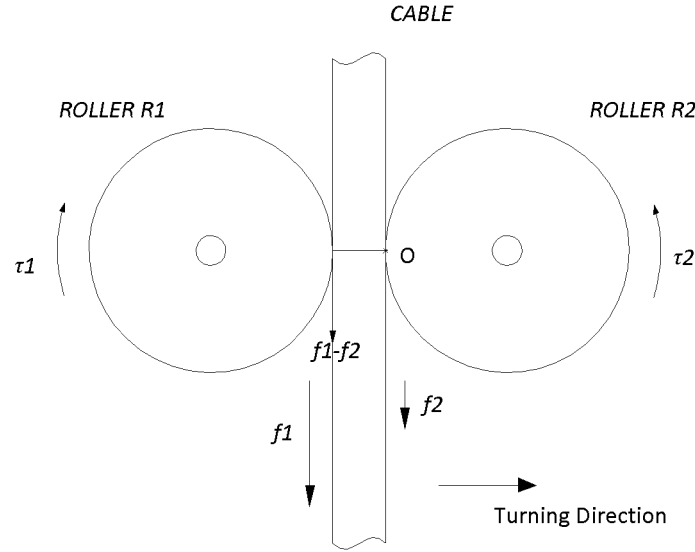


Figure 3.4: Differential Driving Mechanism Idea Demonstration

As shown in Figure 3.4, Roller R1 and Roller R2 are being driven at two different speeds, and $\tau_1 > \tau_2$, then, the friction forces produced at the cable and roller interface f_1 and f_2 are also different. Under the assumed conditions shown in the figure, driving friction force f_1 will be greater than f_2 . The differential force $f = (f_1 - f_2)$ will produce a torque on the cable around point O, thus turning the cable to the right as shown in Figure 3.4. As this idea was finalized, the first prototype was designed and built based on it. The details on the design and fabrication of the initial prototype will be discussed in the next section.

3.3 Prototype I Design

3.3.1 Introduction and System Overview

As discussed in the previous section, the differential drive mechanism is able to perform a few satisfying tasks such as rolling, twisting, and bending of the underwater towing cable, which are the demanding features for manipulating the cable into the storage unit. The reason being is that as the cable is laid into the figure "∞" shape, it is bent and twisted. Although the mechanism seems to be very compact, it is not viable because the complexity of it. First of all, integrating all the actuators and mechanical parts into one set of rollers will require many components to be custom made and compact sized actuators to be purchased, which in the end will lead to a very high cost prototype. Second of all, it will consume too much time to have the system designed, built and tested since more complex system tends to exhibit more problems and it will be more difficult to troubleshoot.

To solve this issue, a twin module cable driving mechanism design is considered and at this stage, the storage unit was not designed and built. The focus is to investigate if the concept works for cable manipulations. This arrangement separates the fully integrated set of rollers into two modules. One does the twisting motion of the cable by shifting one of rollers in the vertical direction while keeping the other at certain height. The shifting roller is driven by a NEMA 17 lead screw stepper linear actuator. The other module manages to roll the cable in or out in the horizontal direction, and each of the two friction rollers has its own independent drive, an NEMA 17 bipolar stepper motor. All the motors are controlled by the "MUNder Board", which is readily available through the mechanical engineering mechatronics laboratory. The MUNder board is powered by a PIC microcontroller chip 18F4550. Two of the

NEMA 17 bipolar stepper motors are driven by two L298 Dual Full Bridge Drivers. The lead screw stepper motor is driven by the Haydon DCM8055 microstepping driver. All boards and drivers are powered by the BK Precision 1672 power supply and it is an open loop system. The system diagram is shown in Figure 3.5.

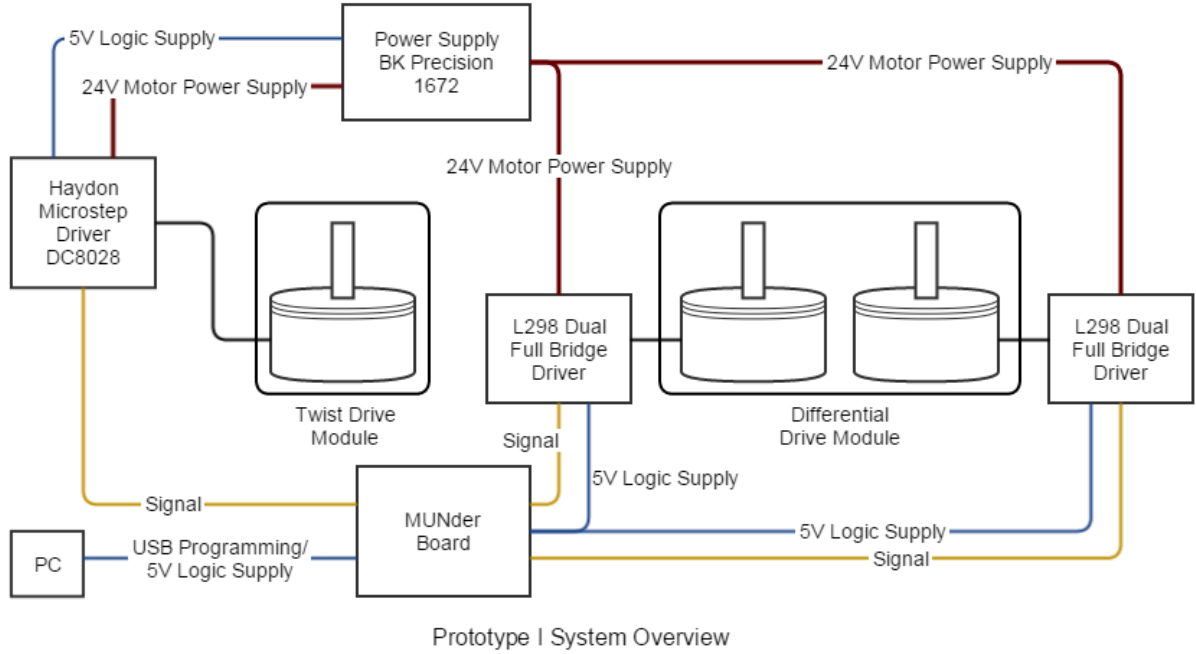


Figure 3.5: Prototype I System Diagram

Figure 3.6 shows the system setup with the FALMAT XtremeCat underwater network data/power cable in the modules. Figure 3.7 a,b,c,d shows the setup in different angles and closeups. As shown in Figure 3.7, the cable is reeled out by two friction drive rollers.

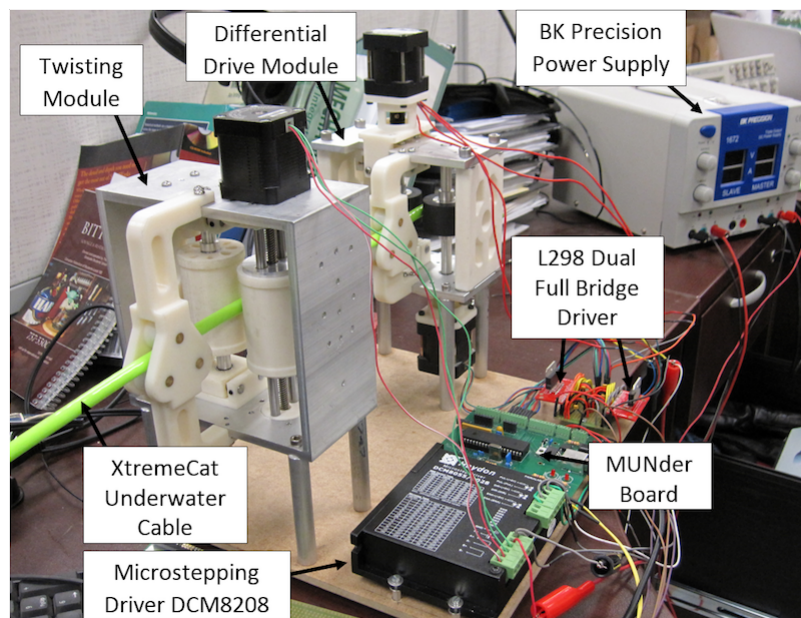
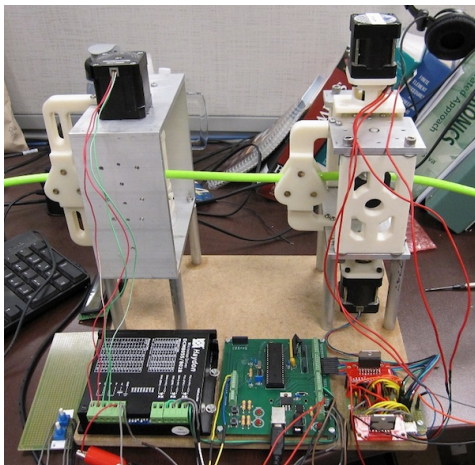
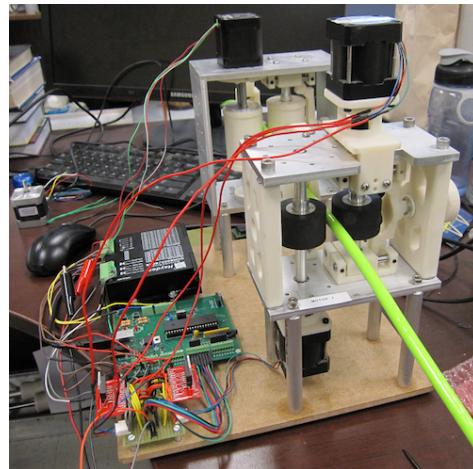


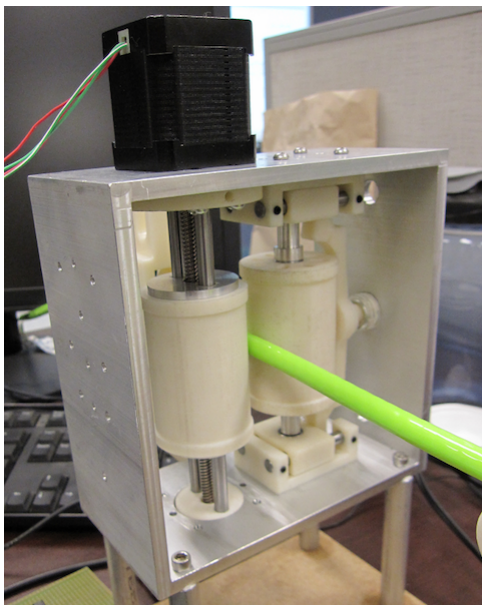
Figure 3.6: Prototype I System Setup



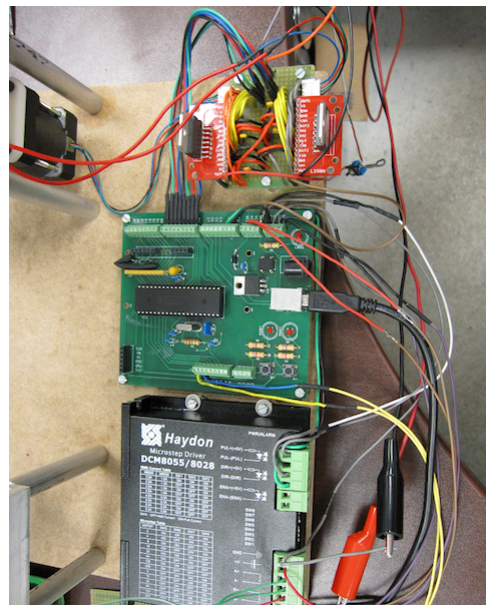
a



b



c



d

Figure 3.7: Prototype I System Setup

3.3.2 Detailed Design

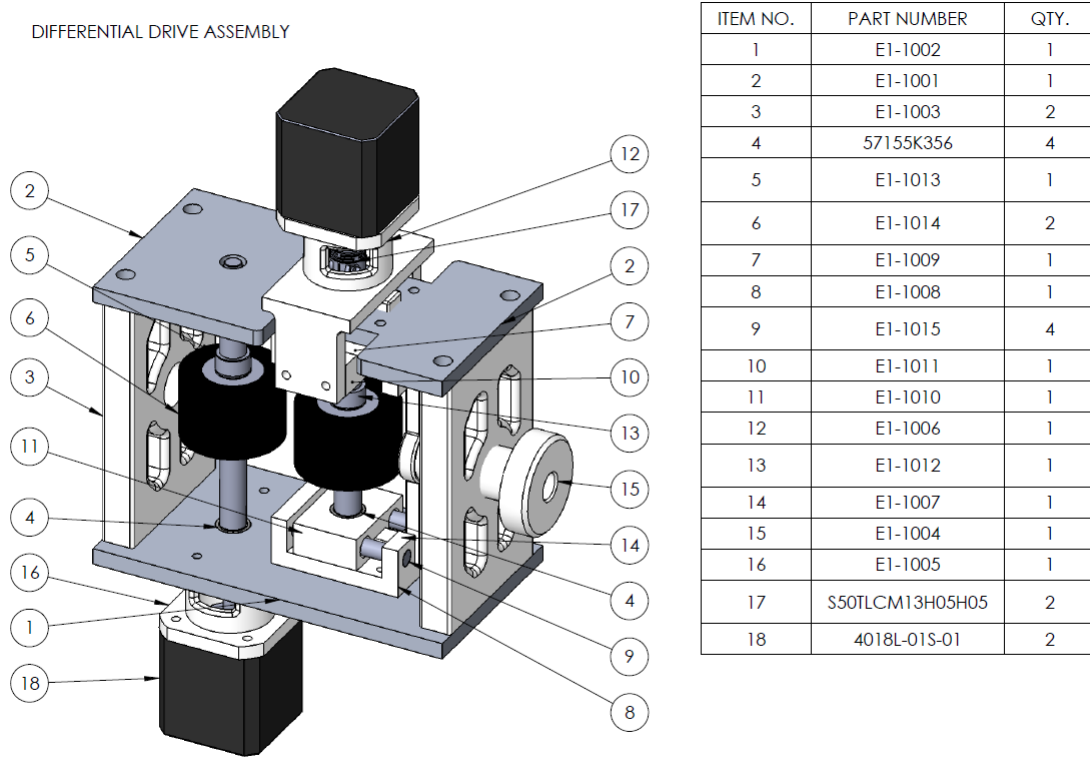
In this section, both mechanical and electronics design are illustrated in more details. Mechanical design includes motor power and torque calculations, Solidworks 3D modelling. In the electronics design, the setup and implementation of microcontroller and motor drivers are discussed.

Mechanical Design:

Design of the Differential Drive Assembly E1, Twist Assembly E2

As mentioned in the introduction, Prototype I is composed of two main mechanical module assemblies, the Differential Drive Assembly E1 and the Twist Assembly E2. Figure 3.8 is the roller module assembly, which reels the cable in and out by driving the two friction rollers (Item #6, Part No: E1-1014). The intention was also to change to direction of the cable while it is being rolled by differentiating the speed of the two rollers, thus, two stepper motors are used for this purpose. The friction rollers have aluminum core sleeves that can be press fit onto a shaft, which is suitable for transmitting power in low-speed and low torque applications. The roller has a bore diameter of 1/2", an OD of 1", and a width of 1". Roller surface is soft neoprene that has a durometer of 55A, which creates a good grip between the roller and the underwater towing cable, whose surface is relatively smooth compared to other data cables. One of the roller shafts (Item #5, Part No: E1-1013) is installed in between the top and bottom plate (Item #2, Part No: E1-1001 and Item #1, Part No: E1-1002) with two miniature steel ball bearings (Item #4, Part No: 57155K356). The other assembled shaft is installed in between two sliding blocks (Item #11, Part No: E1-1010) so that the distance between the two rollers can be adjusted by a spring loaded fork (Item #14, Part No: E1-1007), which is controlled by twisting the adjusting knob (Item #15, Part No: E1-1004) The sliding blocks slide on two parallel steel

shafts (Item #9, Part No: E1-1015) that seat in the shaft blocks (Item #8, Part No: E1-1008).



FOR FIGURE IN THESIS

Figure 3.8: Prototype I Differential Drive Assembly E1 Illustration

Two stepper motors are mounted onto the motor mounting brackets (Item # 16 and 7, Part No: E1-1005 and E1-1009, respectively) and connected to the roller shafts through flexible coupling (Item #17, Part No: S50TLCM13H05H05)

As shown in Figure 3.9, the Twist Assembly E2 uses one stepper motor with a lead screw shaft and nut so as the motor turns, the lead screw nut moves along up and down along the shaft when a part is fixed to it, the roller core (Item #8, Part No: E2-1010) in this case. There is also a roller shell (Item #10, Part No: E2-1008), which rotates around on the outside of the roller core that allows the motion of the cable in the reeling direction. The roller on the other side is seated in between two

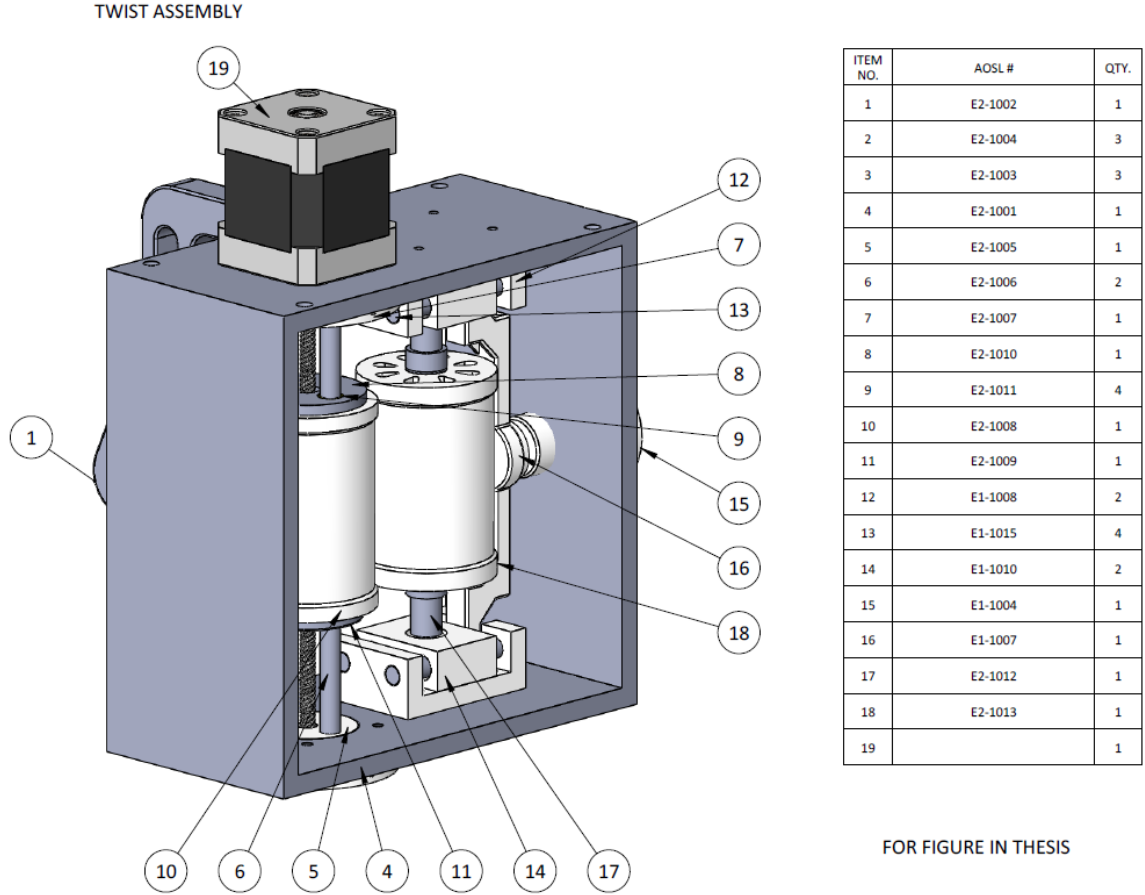


Figure 3.9: Prototype I Twist Assembly E2 Illustration

slider blocks (Item #14, Part No: E1-1010) so that the distance between the two rollers can be adjusted, and is similar to the arrangement in the Differential Drive Assembly E1. The compression force on the fork (Item #16, Part No: E1-1007) can be adjusted by twisting the knob (Item #15, Part No: E1-1004).

Fabrication of Differential Drive Assembly E1, Twist Assembly E2

To reduce the cost of prototyping and time of fabrication, many of the parts are produced by the method of FDM (Fused Deposition Modelling). FDM is one of the RP (Rapid Prototyping) processes in which a part is produced using layer-by-layer deposition of thermal plastic materials [22]. Such process is almost fully

automated by single board computers. Although the technology evolves quickly in today's demanding market, and more and more materials are made available to the users, ABS is probably still the most popular material used for its good mechanical properties good economical values. The parts made by the RP method are Item #3, 7, 8, 10, 11, 12, 14, 15, and 16 (As shown in Figure 3.8). Making rapid prototyped parts are quick and easy, however, it does have some disadvantages. The stepper motor mount(E-1005, E-1006), slider blocks(E-1010, E-1011) and shaft blocks (E-1008, E-1009) showed cracks after several experiments were run on the assembly. One of the reasons is that most of these parts require relatively high strength and the aluminum alloy was selected for the material originally. The other important reason is that threads are directly tapped into the ABS materials where inserts should have been used. It is realized that the suitability of the material has to be closely checked and design modifications might be necessary if such fabrication method is to be adopted. The roller shafts are machined on the lathe in the student machine shop, tolerances are carefully controlled so that bearings and the press fit rollers are installed properly. The top and bottom plates are milled on the milling machine in the same shop, aluminum 6061 is used for these parts.

Electronics Design:

To control the Differential Drive Assembly E1 and the Twist Assembly E2, the MUNder board is used. The MUNder board is microcontroller rapid prototype board designed by the Faculty of Engineering and Applied Science at Memorial University. It is primarily used for the Engineering One course ENGI 1040.

As shown in Figure 3.10, the MUNder Board has made 27 digital I/O pins, 8 analog I/O pins available. It also allows users to add serial communication module to the board through a 6 pin female connector for convenience. The board has a USB

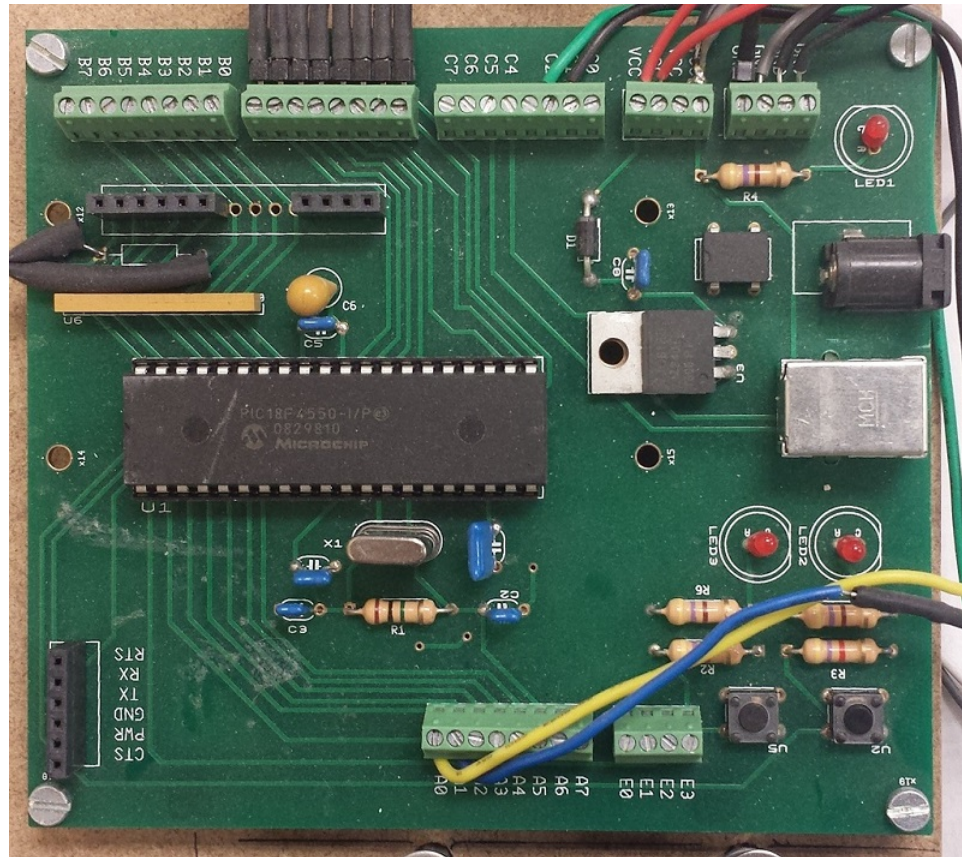


Figure 3.10: Rapid Prototyping Microcontroller: MUNder Board

connector for programming the PIC microcontroller and logic power, and it also has a 5V barrel power jack for external power input. The MUNder board is chosen because it is very easy to set up and use, and it is readily available. MPLAB was used for developing applications for the MUNder board and is a free software downloaded from Microchip website, and the C18 compiler is also free to use. The two stepper motors in differential drive assembly E1 were controlled through digital output pins D0-D7, 4 pins for each. The motor signal was then sent to L298 driver. The third motor for the twist assembly E2 was controlled by a pulse signal and a direction signal which is either high or low. It is made much simpler because of the powerful microstepping driver module DCM8208.

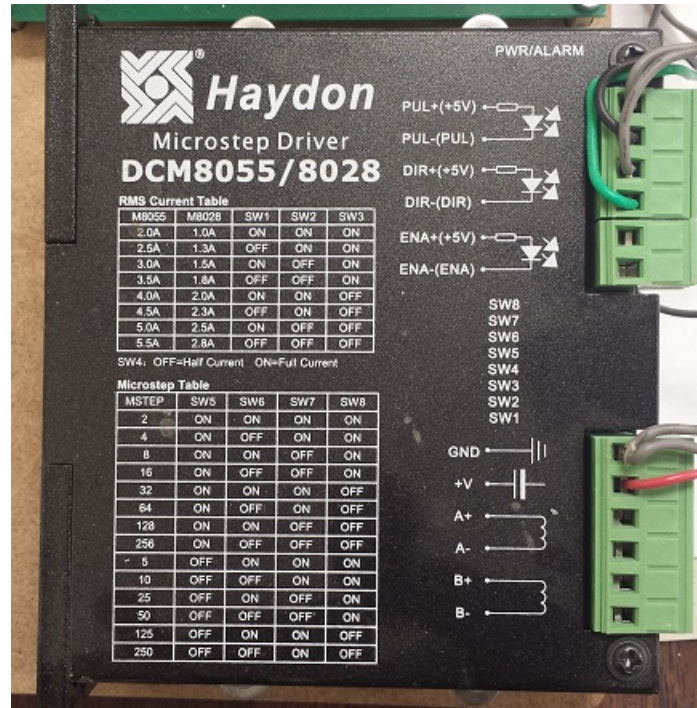


Figure 3.11: Stepper Motor Driver: Microstepping Driver DCM 8028

As shown in Figure 3.11, the two phases of a stepper motor can be connected to A+, A-, B+, B-. The driver then only takes a pulse and a direction signal to gain the full control of the motor. Microstepping is easily set by different combinations of the four DIP switches shown in the table, SW5-SW8. The driver also has a current setting that is configured in a similar way by choosing the "ON" or "OFF" state combinations of the three DIP switches SW1 - SW3. The immediate advantage of pulse signal control method is that it uses less I/O pins and is reduces the complexity of the code. The other two stepper motors have to be controlled through interrupt service routines to avoid skipping steps or malfunctioning of the motors, which in turn reduces torque and speed.

The other two stepper motors in the differential drive assembly E1 are driven by the full bridge motor driver L298N. This is a high voltage, high current dual full

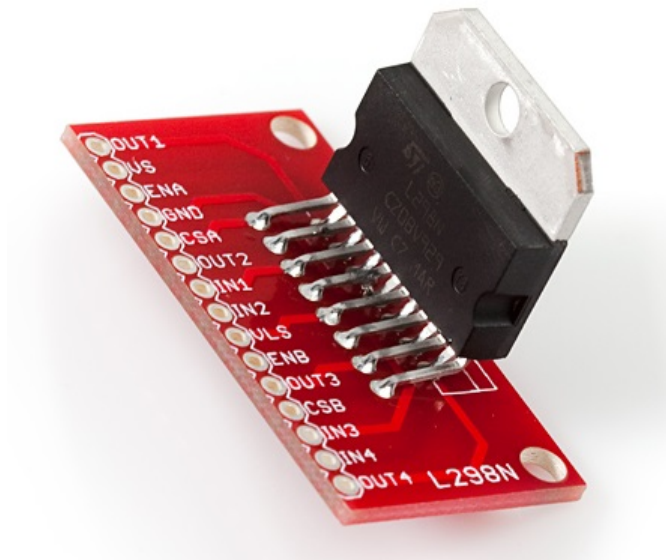


Figure 3.12: L298N Full Bridge Motor Driver on SparkFun Breakout Board

bridge motor driver to accept standard TTL logic levels and drive inductive load such as DC and stepping motors. As shown in Figure 3.12, it is a Multiwatt15 package with 15 stagger leads. For more details and specifications of the chip please refer to the product data sheet [23]. For easy connections, a SparkFun breakout board is used, which avoids the messy and unreliable connections for the rapid prototype purpose. This full bridge allows the stepper motor to run at maximum continuous current of up to 2A, and the maximum voltage supply can be up to 50V. The enable Pin allows the easy and independent control of the motor despite the coil signals. This is also a motor driver chip that is very popular and easily accessible at the Engineering Faculty at MUN.

The two stepper motors that are used in the differential drive assembly E1 are size NEMA 17 with model number 4018L-01S-01 from LIN ENGINEERING. This model has a full step angel of 1.8° and a rated current of 0.56 A per phase. The nominal holding torque reaches 41.86 oz·in (i.e. 29.6 N·cm) according the data sheet

from the manufacturer. These are also chosen because they are readily available. The real biggest advantage is that the entire system was put together very quickly and evaluated.

As seen in the Prototype I System Diagram/System Overview in Figure 3.5, all stepper motors are supplied with 24V DC voltage through the motor drivers, which is also supplied with a logic 5V either by a power supply or the MUNder Board. The MUNder Board is powered through 5V USB connection from a PC for easy modifications and program debugging.

Chapter 4

Design, Fabrication and Evaluation of Prototype II

In this chapter, the complete development of Prototype II which includes design, fabrication and evaluation will be discussed.

Since the Prototype I failed to perform changing directions of cable, the main purpose of designing and building the second prototype is to address this issue. For the Prototype II, the directional change of the cable manipulation is accomplished through directly swinging an arm that reels in and out the cable using friction rollers. The twist of the cable is done by turning the friction roller module around the longitudinal axis of the cable with a belt driven mechanism. On the opposing side along the same level, there is a cable receiving and storage unit that has a unique figure "∞" shaped cavity where the cable is wound and stored passively. In other words, the total assembly of prototype II includes two main units: A. Cable Manipulation Unit and Cable Storage Unit. The details on how it works will be discussed in the following paragraphs and illustrated with pictures and drawings of 3D models completed in Solidworks.

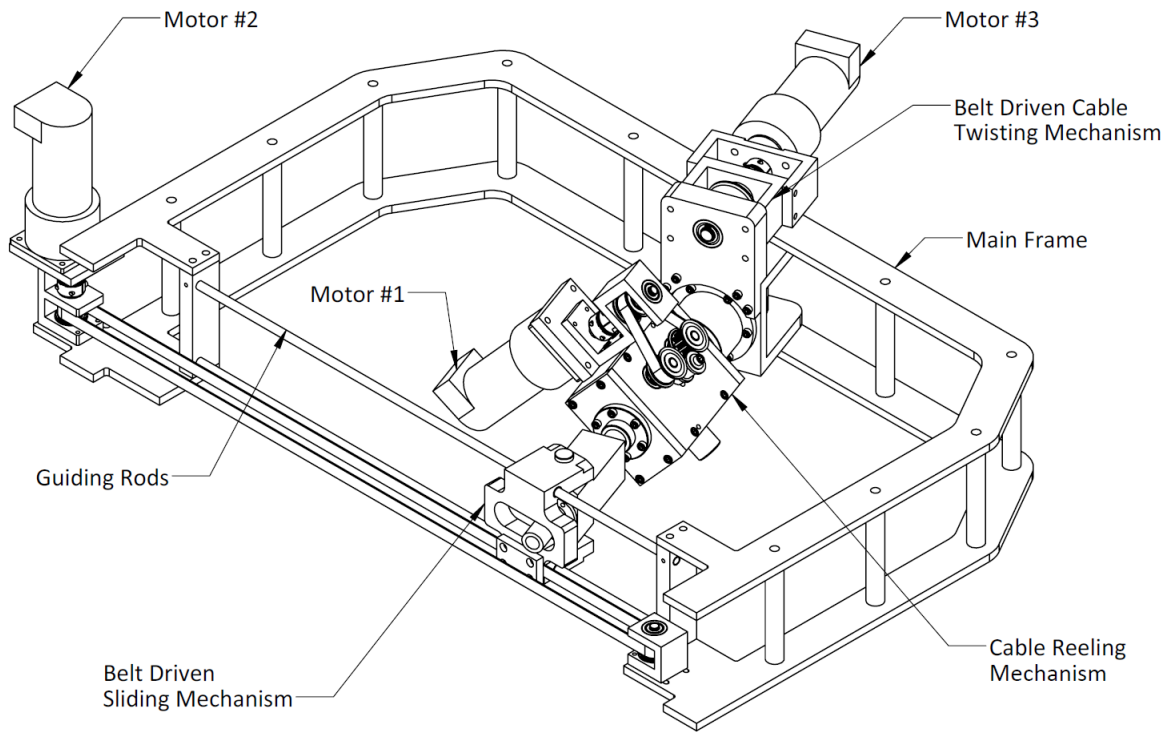


Figure 4.1: Prototype II Assembly of Cable Manipulation Unit Overview

4.1 Mechanical

The Cable Manipulation Unit Assembly is composed of three active driving mechanisms:

1. Cable Reeling Mechanism (*Motor #1*)
2. Arm Sliding Mechanism (*Motor #2*)
3. Cable Twist Mechanism (*Motor #3*)

All motors are Pittman geared servo motors equipped with optical encoders that has a resolution of 512 pulse/s. Further details on the motors will be explained in

the following section "Electrical/Mechatronics". All belts are fiberglass reinforced neoprene timing belt.

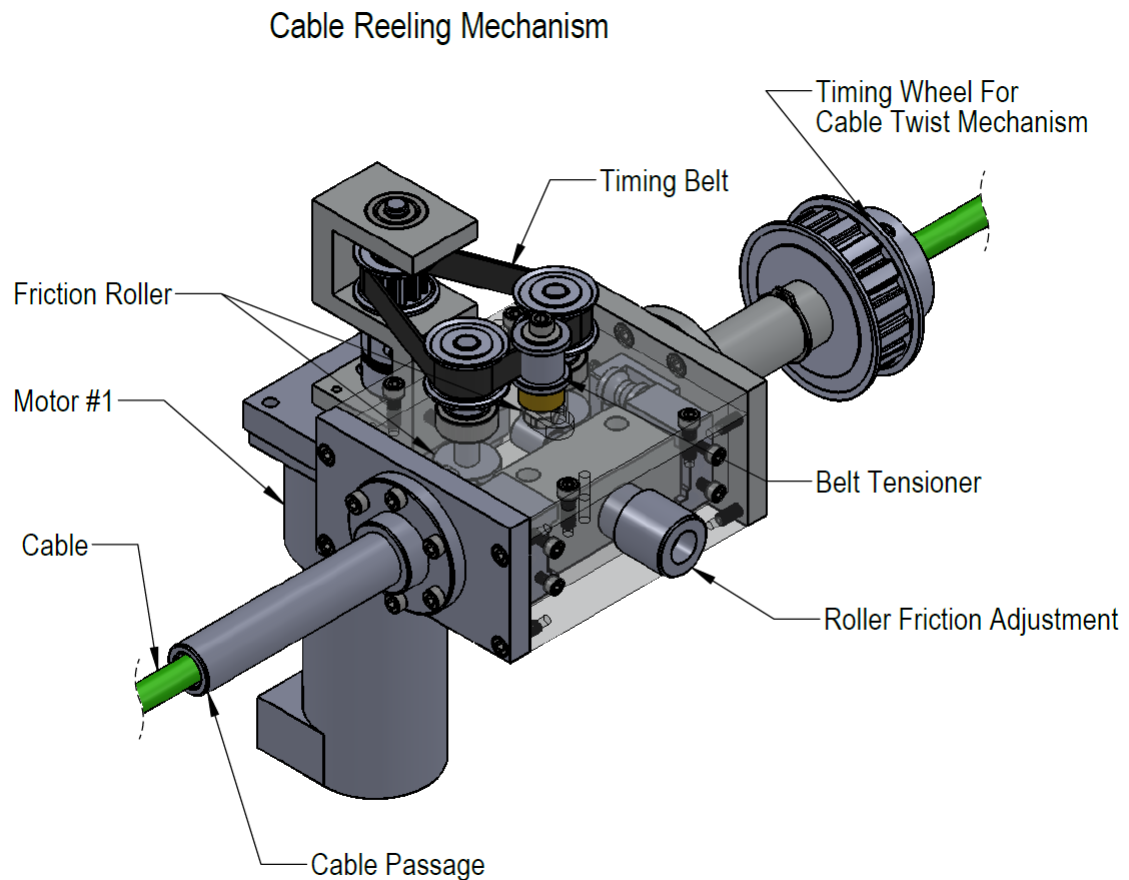


Figure 4.2: Cable Reeling Mechanism Illustration

As shown in Figure 4.2, the cable reeling mechanism is driven by servo motor #1 through timing belt on the top. The two friction rollers seated on two parallel shafts rotate and roll the cable with the other two idler friction rollers pressed against the cable thus forming the frictional rolling force. Both of the two friction rollers connected to the timing pulleys are actively controlled at the same speed by the same motor, this is to gain more traction on rolling the cable. The more the contact surface area between the rollers and the cable, the more friction force it has on the

cable. The friction force can be adjusted by changing the pressure that is applied onto the passive rollers through the Roller Friction Adjustment Knob as seen in the figure. The speed and the position of the friction rollers can be closed-loop controlled through the motor's encoder. The timing belt is tensioned through an adjustable Delrin idler roller. At the entrance and exit of the rollers enclosure, there is a set of plastic profiled rollers to keep the cable in the correct position at all times. The guiding rollers are mounted to the enclosure using shoulder screws and "L" Shaped mounting bracket. In other words, the cable is kept within the width of rollers. As shown in the top section view in Figure 4.4, the cable will not slip off from the rollers. On the left, the inner tube of a telescopic mechanism is mounted to the exit end of the roller enclosure. The inner tube is seated inside the outer tube to form a telescopic assembly where the cable travels through. This mechanism is required because as the Cable Reeling Mechanism swings from the side to side, the distance from the Cable Reeling Mechanism to the sliding rod of the Belt Driven Sliding Mechanism varies as seen in Figure 4.1. Motor #1 is mounted to the enclosure through a "S" shaped mounting bracket which contains both the timing pulley and the flexible shaft coupler.

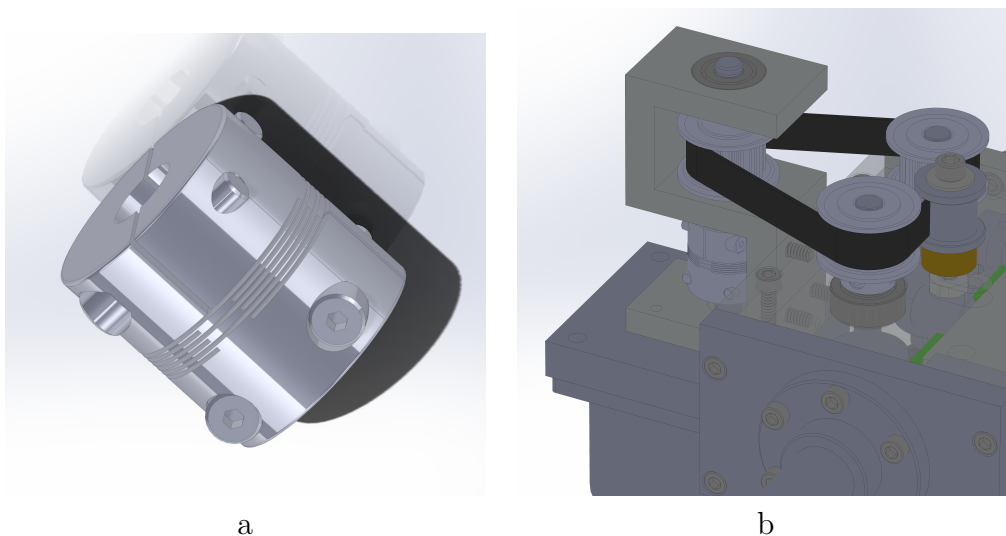


Figure 4.3: Flexible Coupling and Motor Mount

Figure 4.3a is a picture of the flexible shaft coupler which has a bore diameter of 1/4" on both ends with the split hub option. The split hub tightening feature does not damage the shafts like set screws and can transmit a great amount of torque by tightening the screws properly. Figure 4.3b shows how the "S" shaped motor mounting bracket is mounted to the enclosure and the motor. This configuration simplifies the design by only machining one single piece mounting bracket which connects the roller enclosure and the motor. The flexible motor shaft coupling greatly reduces the side loading on the motor shaft and allows a certain amount of misalignment between two shafts. All the timing pulleys are mounted onto the shafts by using set screws and shaft flats are machined in order for the set screws to transmit the required torque.

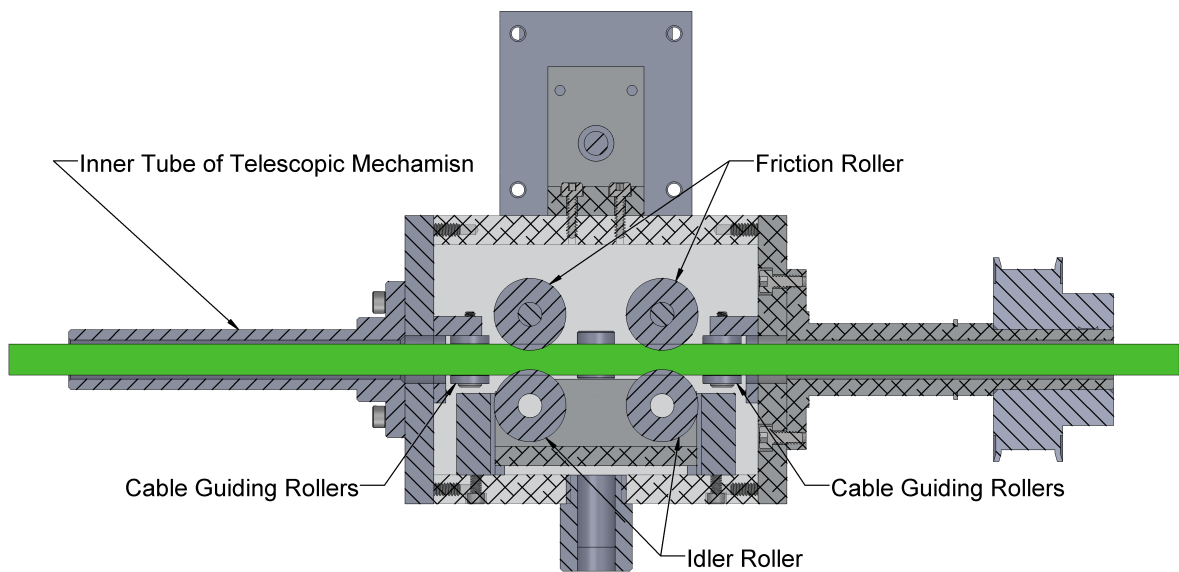


Figure 4.4: Cable Reeling Mechanism Top Section View

The friction drive rollers have an outer diameter of 3/4" and 55A durometer of neoprene rubber which is bonded to the aluminum hub. Since softer rubber deforms more, thus creates more surface contact area with cable, it has a higher friction force than hard rubber material under the same applied pressure, however, the softer rubber

is less durable and become worn much faster than the harder ones. On the opposite side of the friction rollers across the cable, there mounted two idler wheels with the same type of rubber sleeves to couple with the friction rollers. In Figure 4.4, a timing belt pulley is mounted on the tube to the right side of the roller enclosure. Motor #3 drives this pulley to create twist motion of the entire Cable Reeling Mechanism assembly, which satisfy the need for shaping the cable into a figure "∞" pattern. The Cable Reeling Mechanism is driven by Motor #1 through the timing belt as shown in Figure 4.1. The rotational speed and position can also be close loop controlled under the assistant of the motor encoder.

The housing of Cable Reeling Mechanism, all mounting brackets, and main frame of assembly are constructed using Aluminum 6061, which is a common type of structural materials that has high strength to weight ratio, economical and easy for fabrication. Guiding rods are made of shaft grade hardened steel which has higher rigidity for better sliding action of the sliding mechanism. The main frame plates are water-jet cut and bolted together on the aluminum rods to give a rigid support for all the mechanisms mounted to it.

On the other side, it is the Cable Receiving/Storage Unit, as shown in Figure 4.5 and 4.6. The entire prototype CSU housing is made of ABS by 3D rapid prototype machine. Since the unit is relatively large, it was designed and printed in small pieces with sparse construction print mode and then assembled together. The back pieces as seen in Figure 4.6, are bolted to a piece of acrylic sheet with bolt pattern cut by laserjet for precise fit. The CSU is setup so that the center of the CSU is aligned with the center point of the CMU as shown in Figure 4.1. The figure "∞" groove is wider at the entrance and becomes narrower as the cable goes in deeper. The wider entrance makes it easier for the cable to be wound and has less chance to get tangled at the top. Once the cable is settled in the CSU, the narrow channel keeps the cable

layer in right order so one layer of cable does not cross over to the next layer.

Besides the 3D rapid prototyped CSU and two limit switch mounts, the rest of the parts are designed and modelled in Solidworks and fabricated using lathe, milling machine and other common machine shop tools. Most of metal parts are made using economical structural aluminum grade 6061 T6 for maximum strength and minimal fabrication effort.

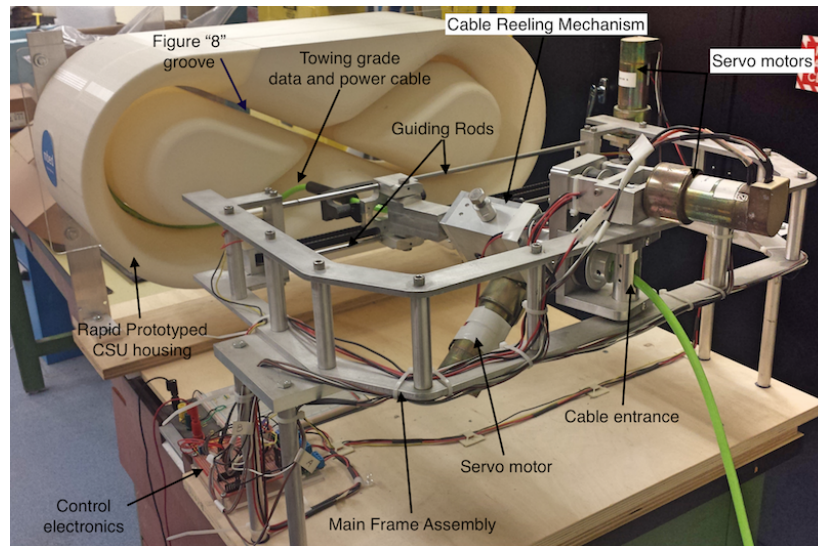


Figure 4.5: Front View of Cable Storage Unit

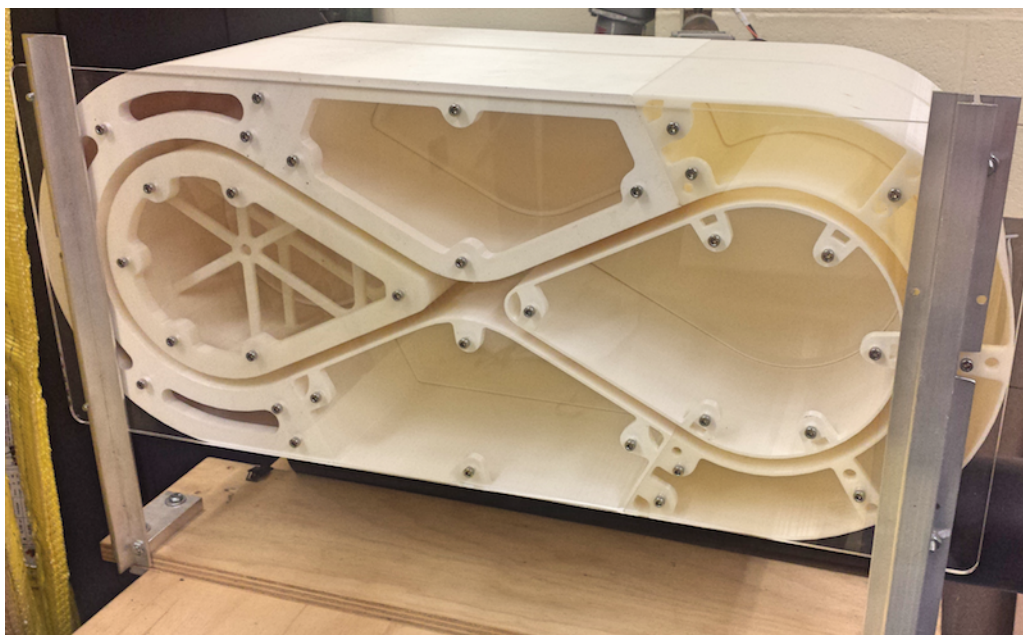


Figure 4.6: Back View of Cable Storage Unit

4.2 Electrical/Mechatronics

As shown in Figure 4.5, all the control electronics are installed right below the left side of the CMU. The active Cable Manipulation Unit is driven by three Pittman Geared Servo Motors, and the Pololu High-Power DC Motor Drivers are used to drive the motors. A mbed LPC 1768 rapid prototype microcontroller was used as the controller to execute the tasks.

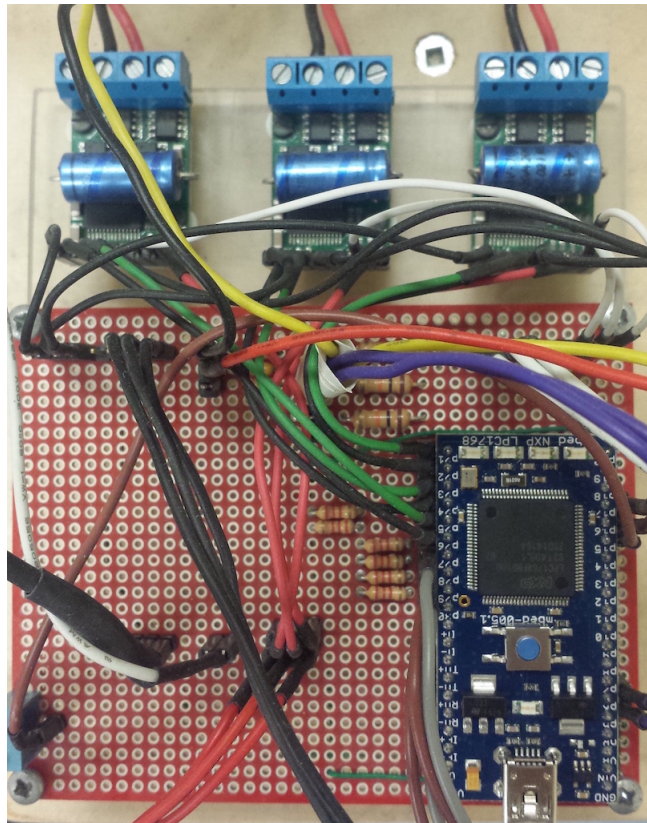


Figure 4.7: Photo of Controls Electronics

1. Mbed MicroController Board

Mbed LPC1768 is a 32-BIT ARM CORTEX-M3 based rapid prototype microcontroller, which runs at 96 MHz and has 512KB flash, 32 KB RAM and a variety of interfaces including built in Ethernet, USB host and device, CAN,

SPI, I2C ADC, DAC, PWM and other I/O interfaces [24]. Mbed uses a web-page online compiler that is compatible to many operating systems. Programs can be compiled and saved to an online compiler account and downloaded to mbed. There is also a generous number of libraries available in the compiler that can be used without spending a lot of time developing your own libraries, which makes it a lot easier for rapid prototyping.

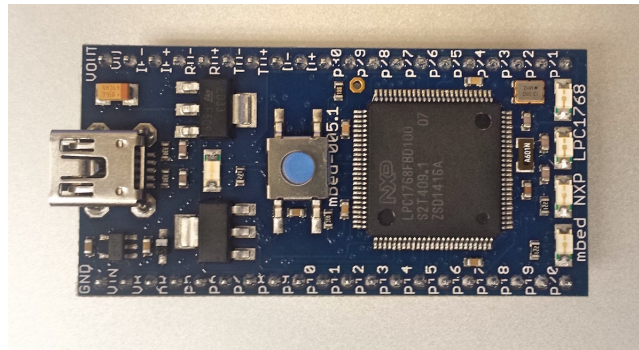


Figure 4.8: mbed Rapid Prototyping Microcontroller Board

2. Pololu High-Power DC Motor Drive 36v9

The Pololu High-Power Motor Driver is a discrete MOSFET H-Bridge designed to drive large DC brushed motors [25], which has a nominal voltage of 36 volts and can be driven at 9A of continuous current. This driver controls a motor by outputting a PWM signal which corresponds to a input PWM signal from the microcontroller. A direction pin controls the direction of the motor. Other features includes reset and fault flag pins that will help with the proper function of the motor. Figure 4.9 is a photo is the driver, and it has screw type terminal block for easy connection of the supply power and motor power output. Logic circuit can also easily be connected with a single row male header pins.

3. Pittman Geared Servo Motors

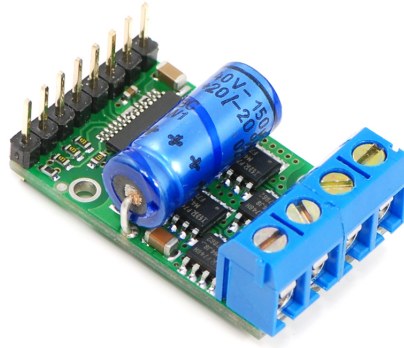


Figure 4.9: Pololu High Power Brushed DC Motor Driver 36v9

The two Pittman Geared Brushed DC Motors with encoders are model #: GM9236C534-R2 and model #: GM9414J561, and the gear ratios are 5.9:1, 19.7:1, respectively. Both motors have a rated voltage of 30.3V. The encoder that is integrated into the motor is a two channel quadrature 512 CPR(counts per revolution)optical encoder with index output, the model # is HEDS-9100 from Avago Technologies.

Motor Specifications (AOSL Lab Tested @ 30.3 volt DC):

Armature Resistance: 5.6 Ω

Inductance: 3.27 mH

DC current: 84 mA

No load speed: 849.3 RPM

Length: 5"

Shaft: 0.25" dia X0.75" L

Weight: 1.5 lbs

NOTE: The power requirement estimation for the motor should have been based on the towing capacity and control capability of the towed device, and system efficiency(including factors like friction, acceleration of cable) and etc. It is not estimated within the scope of the study. Only bench dry test was conducted

at low speeds toward the end of the project. To save cost, the motors were acquired from another completed project within the lab.



Figure 4.10: Pittman Brushed Geared DC motor GR 5.9:1

4. Mechanical Limit Switches

To easily reverse the direction of the swing of the Cable Reeling Mechanism, two mechanical roller switches are mounted to both ends of the guiding rods as shown in Figure 4.5, and it simply generates a ON/OFF digital signal to the mbed while it is triggered at mechanical contact. As shown in Figure 4.11, when the roller is mechanically contacted, the switch close the loop of the digital-in circuit and generates a "1" signal thus telling mbed to reverse the swing direction of the Cable Reeling Mechanism.

As shown in Figure 4.12, a brief system diagram illustrates the basic electrical connections of the main components for the prototype. The mbed microcontroller outputs 3 PWM control signals and 3 digital direction signals to control the direction and speed of the motors. The Pololu motor drivers are supplied with 24 volts DC current since it is tested to be sufficient to drive the mechanism while the motor's rated voltage is 30.3 volts. The motor driver outputs "+V" and "-V" through two



Figure 4.11: Mechanical Limit Switch

wires that are varied by the direction and PWM input pins. the Pololu motor driver is also supplied with a logical 5 volts to power the controlling electronics on board.

The motor's encoder has a 4 wire lead which includes 2 channel output A and B, 5 volts logic power supply and GND. The two channel quadrature encoder detects speed, direction and position of a shaft that is mounted to the decoder wheel. The two channel of signals are 90° out of phase and provides direction of spin by checking whether the leading channel is A or B. One can extract the speed and position information by counting and timing the pulses.

With the position feedback information from these encoders, the motors can be close-loop controlled and position synchronized, which is required by this particular application. All the three actions includes cable reeling, arm sliding, and cable twist-

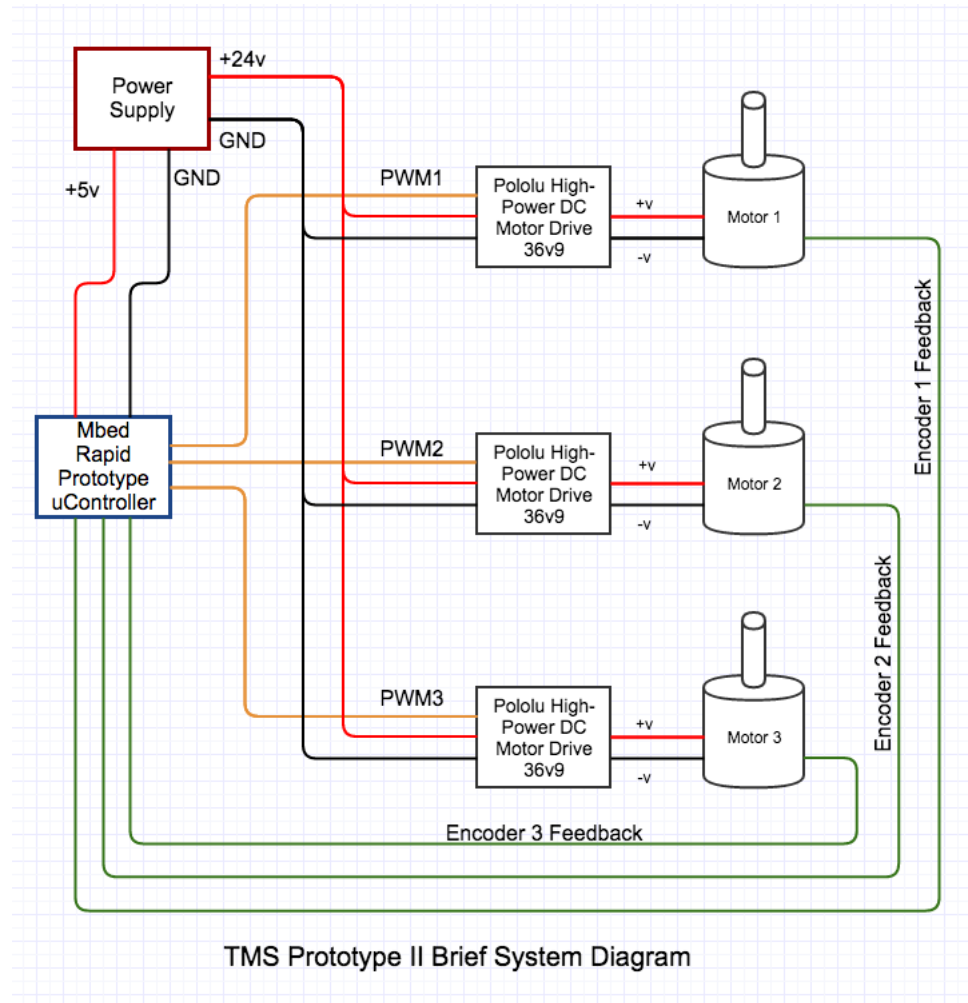


Figure 4.12: TMS Prototype II Brief System Diagram

ing actions have to be position synchronized to properly manage to wind the tow cable into the CSU.

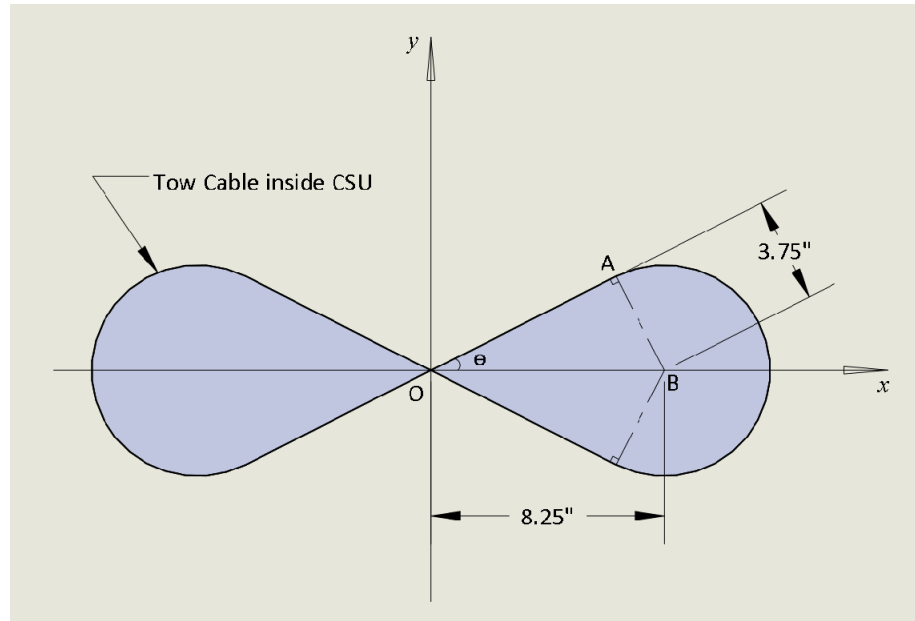


Figure 4.13: Figure "8" Laying Pattern for Cable and Motor Position Relation Calculation

A figure "8" laying pattern for the cable is designed for this prototype before the CSU was designed and built, as shown in Figure 4.13. The radius of the circular portion is 3.75 inches, which is 0.75 inches larger than the minimum bend radius for this particular cable according to the manufacturer supplied data (Falmat Custom Cable Technologies). This results in a safety factor of 1.25. This is to satisfy the requirement for compact design as the system occupies less space. The selected cable has a diameter of 0.34 inches and minimum bending radius of 3.0 inches. The cable has a towing capability of 1200 lbs or less. For power and communications, it has 12 24-AWG conductors and is capable of CAT-5e. There is no power conductors in this cable but the available conductors can be used as power line as long as the current is within the safe limit.

To calculate the torque required for twisting the cable, a cable twist test setup was designed and fabricated. The cable twist test was carried out, so readers can refer

to the Appendix A.4 for more details.

The width of the CSU and CMU is arbitrarily chosen and can be varied within a small range based on the minimum requirements, and it is not the main focus of the research in this project. The distance OB from the center of the CSU unit O and the center of the circular portion of figure "8" B is 8.25 inches. Based on this configuration, the formula for calculating the position relationship between both cable reeling (calculation of length of the cable laying path: combination of straight lines and arc as shown in Figure 4.13) and arm swinging can be developed as follows:

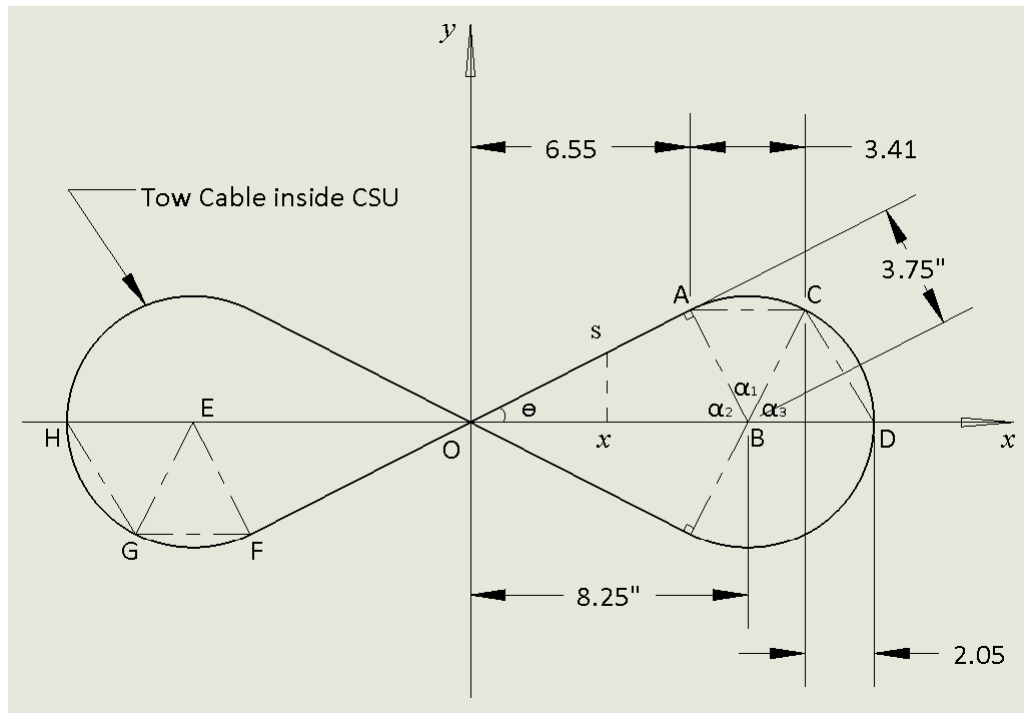


Figure 4.14: Position Relationship Calculation between Sliding Mechanism and Cable Reeling Mechanism

As shown in Figure 4.14, the x position of the cable exit on the sliding mechanism has a relationship with the actual length that is reeled out/in. As the cable exit moves from point H to point D, the amount of cable that is reeled in/out has to match the track length of the groove, which is composed of sections of straight lines and arcs

shown in Figure 4.14, Arc HG, GF, straight line FA, Arc AC, DC. Since the figure "∞" shape is symmetric, one can focus on the first quadrant.

$$\frac{s}{x} = \frac{OB}{OA} = \frac{8.25}{7.35} = 1.12 \quad (4.1)$$

for $-6.55 < x < 6.55$

From the above equation, one can get

$$s = \frac{OB}{OA} \cdot x = 1.12x \quad (4.2)$$

x - variable for cable exit position of sliding mechanism

s - corresponding cable length at the same x position on figure "∞" track

For calculating the ratio of cable length and movement of sliding mechanism in segment AC and CD, one needs to calculate angle $\angle\alpha_1$ and $\angle\alpha_3$.

Since $\angle\alpha_2 = \angle\alpha_3$,

$$\angle\alpha_1 = 180 - 2 \cdot \angle\alpha_2 \quad (4.3)$$

$$\angle\alpha_2 = \angle\alpha_3 = \arccos \frac{AB}{OB} = 62.96^\circ \quad (4.4)$$

Substitue 4.4 into 4.3, one can get $\angle\alpha_1 = 54.07^\circ$

To calculate the arc length of AC and CD

$$\widehat{AC} = \frac{\angle\alpha_1}{360^\circ} \cdot \pi \cdot d = 3.54 \text{ Rad} \quad (4.5)$$

$$\widehat{CD} = \frac{\angle\alpha_3}{360^\circ} \cdot \pi \cdot d = 4.12 \text{ Rad} \quad (4.6)$$

Length of straight line AC and CD can be obtained based on the geometric relation of the Figure "8" track:

$$AC = 3.41, CD = 3.92$$

From the above calculations, one can develop a formula for the ratio between the amount of cable and horizontal movement of the sliding mechanism:

$$s = \begin{cases} 1.12x & -6.55 \leq x \leq 6.55 \\ 1.04x & -9.96 \leq x < -6.55 \text{ or } 6.55 < x \leq 9.96 \\ 2.01x & -11.97 \leq x < -9.96 \text{ or } 9.96 < x \leq 11.97 \end{cases} \quad (4.7)$$

This equation is used to program the position synchronization for position feedback control between Motor #1 and Motor #2, eg. cable reeling mechanism and sliding mechanism motor, respectively. Point H and D are approximately where the limit switches are, any slight difference between cable exit and limit switch is compensated when programming motor position relations. This allows the cable exit of the sliding mechanism to move accordingly along the track while the cable is being laid into the CSU, without other sensors measuring the cable reeling, the cable should be laid inside the CSU relatively accurately assuming the speed of the entire operation is low enough so that any cable slippage does not happen. The distance between Point H and D as shown in Figure 4.14, is 24 inches while the maximum span (horizontal movement) of the cable exit of the sliding mechanism is only 15.5 inches, therefore, the swing movement of the sliding mechanism needs to be scaled down to accommodate this difference. If the actual movement of the cable exit end can be represented by variable x' , then

$$x = \frac{24}{13.98} \cdot x' \quad (4.8)$$

then one can get the update ratio equation combining Eq. 4.7 and 4.8

$$s = \begin{cases} 1.92x' & -3.81 \leq x' \leq 3.81 \\ 1.79x' & -5.80 \leq x' < -3.81 \text{ or } 3.81 < x' \leq 5.80 \\ 3.45x' & -6.99 \leq x' < -5.80 \text{ or } 5.80 < x' \leq 6.99 \end{cases} \quad (4.9)$$

Eq. 4.9 provides the position synchronization ratio for Motor #1 and Motor #2, When converted to motor rotational position ratios (ratio of number of motor rotations), the gear ratio, the radius of the timing pulley wheel and friction rollers are taken into account. The rotational ratio for the motors is then converted into ratio of encoder count pulses, which is the same as rotational ratio since the two encoders have the same resolution.

Calculation for the number of revolutions for both motor #1 and motor #2 under a linear movement of l :

$$R_A = \frac{l}{\pi \cdot d_{fr}} \cdot r_{gA} \quad (4.10)$$

$$R_B = \frac{l}{\pi \cdot d_{ptb}} \cdot r_{gB} \quad (4.11)$$

From Eq. 4.10,

$$l = \frac{R_A \cdot \pi \cdot d_{fr}}{r_{gA}} \quad (4.12)$$

And from Eq. 4.11,

$$l = \frac{R_B \cdot \pi \cdot d_{ptb}}{r_{gB}} \quad (4.13)$$

Based on the derived equations above, the rotational relationship between Motor #1 and #2 is as follows:

$$\frac{R_B}{R_A} = \begin{cases} \frac{d_{fr}}{1.92d_{ptb}} & -11.23 \leq R_B \leq 11.23 \\ \frac{d_{fr}}{1.79d_{ptb}} & -17.10 \leq R_B < -11.23 \text{ or } 11.23 < R_B \leq 17.10 \\ \frac{d_{fr}}{3.45d_{ptb}} & -20.61 \leq R_B < -17.10 \text{ or } 17.10 < R_B \leq 20.61 \end{cases} \quad (4.14)$$

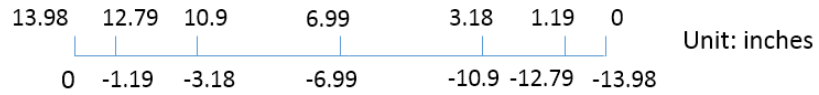
Since $d_{fr} = 0.75$, $d_{ptb} = 0.637$,

$$\frac{R_B}{R_A} = \begin{cases} 0.613 & -11.23 \leq R_B \leq 11.23 \\ 0.66 & -17.10 \leq R_B < -11.23 \text{ or } 11.23 < R_B \leq 17.10 \\ 0.34 & -20.61 \leq R_B < -17.10 \text{ or } 17.10 < R_B \leq 20.61 \end{cases} \quad (4.15)$$

NOTE: In the above equations , R_A and R_B are in revolutions.



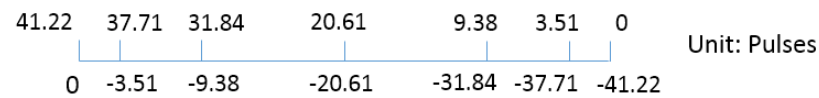
Available Travel Distance for Cable Exit End Bar - A



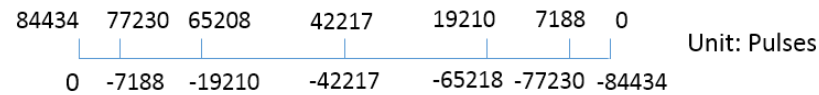
Available Travel Distance for Cable Exit End Bar - B

Figure 4.15: Bar Graphs for CRM Movement: Distance in Inches

To better illustrate how it works, some bar graphs were created. In Figure 4.15, the bar graphs show the lateral travel distance that is available to the Cable Reeling Mechanism (CRM) Arm on the cable exit end. The first bar in the Figure indicates that the cable exit end of the CRM ARM can travel 6.99 inches in both directions from the center point (the origin of travel). However, in a practical mechatronics sense, the origins are better recognized at both ends of the sliding bar (shown in the second bar graph in Figure 4.15).



Available Travel Distance for Motor 2 in # of Revolutions: R_B



Available Travel Distance for Motor 2 in # of Pulses

Figure 4.16: Bar Graphs for Motor 2 Movement in Revolutions and Pulses

In Figure 4.16, the movement was converted to number of revolutions and pulses for Motor #2, which was required for mechatronics implementation. The encoder provides the motor 2 position by sending number of pulses accumulated to the mbed microcontroller. The limit switches at both ends trig an interrupt and reset to the Motor #2 encoder to zero whenever the switch is pushed. As seen in Figure 4.16, the total number of revolutions by Motor #2 is 41.22, which was converted from the

number of pulses sensed by the encoder. The actual travel distance was also verified by measuring it in both the Solidworks model and the prototype. To obtain the number of pulses of Motor #2, a test was carried out. The CRM Arm was programmed to run back and forth between the two limit switches, and the pulses that it generated were recorded and averaged to be 84433.71, which was rounded to a whole number of 84434. This provides necessary position information while implementing the motor position synchronization. The positional ratio of Motor #1 and Motor #2 varies at different regions as shown in the bar graphs, which corresponds to the ratios developed in the Figure "∞" calculation shown in Figure 4.14.

4.3 PID Control of Motors

4.3.1 Model of Cable Reeling Mechanism Motor

It would be beneficial to understand the dynamic behaviour of the cable reeling mechanism since that is the essential part of the cable manipulation system. Therefore a dynamic mechatronics model was developed to assist with better understanding of the system and closed loop control of the mechanism.

The Cable Reeling Mechanism consists of a few simple elements, the DC servo motor, 5.9:1 ratio gear box, 1:1 pulley assembly, and friction rollers.

The CRM model can be developed as a Brushed DC motor with attached gearbox and timing pulley assembly.

Electrically, the motor itself can be modelled based on a simple circuit that is composed of the following elements: Motor Supply Voltage V_m , Armature Resistance R_A , Winding Inductance L_A , and Voltage that represent back EMF V_B , as shown in Figure 4.17:

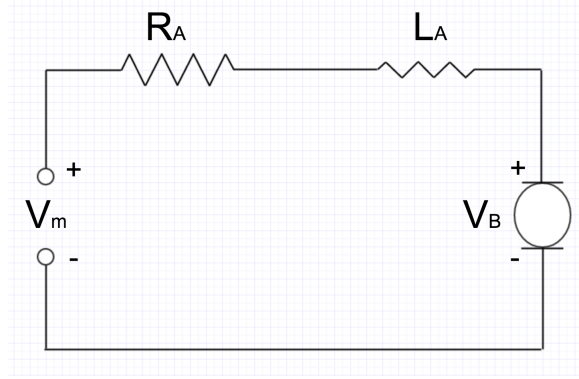


Figure 4.17: Typical DC Motor Circuit

The torque produced by DC motor is proportional to the armature current, then one can get:

$$T_m = I_A \cdot K_T \quad (4.16)$$

And the back EMF voltage V_B , also has a linear relationship with the motor shaft speed ω_m , then:

$$V_B = K_E \cdot \omega_m \quad (4.17)$$

Where K_E is the back EMF constant, which normally has the same numerical value as the torque constant, K_T , given the condition that SI unit is used for both equations, eg. $K_E = K_T$.

By applying Kirchhoff's law to the armature circuit shown in Figure 4.17, one can get:

$$\Sigma V = 0 = -V_m + R_A I_A + L_A \frac{dI_A}{dt} + V_B \quad (4.18)$$

Substitute Equation 4.17 into 4.18,

$$V_m - K_E \omega_m = R_A I_A + L_A \frac{dI_A}{dt} \quad (4.19)$$

Given that I_A is zero, the Equation 4.19 can be written in the Laplace domain as follows:

$$V_m - K_E \omega_m = R_A I_A + L_A s I_A \quad (4.20)$$

then,

$$I_A = \frac{V_m - K_E \omega_m}{R_A + L_A s} \quad (4.21)$$

Now that we have current expressed in the Laplace domain, we can substitute 4.21 into Eq. 4.16 to get:

$$T_m = K_t \cdot I_A = K_t \cdot \frac{V_m - K_E \omega_m}{R_A + L_A s} \quad (4.22)$$

Based on the above equations and findings, the transfer function of the DC motor itself can be expressed as shown in Figure 4.18,

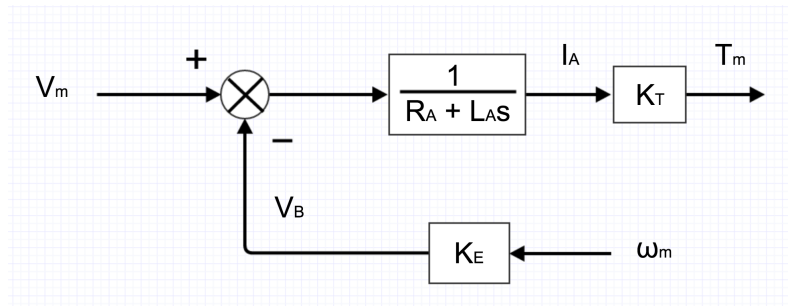


Figure 4.18: DC Motor Transfer Function

To complete the transfer function, a mechanical model of the motor and its attached elements also needs to be developed. As we can see in the above derivation, a torque

T_m was produced by the motor at the given armature current I_A , and this torque drives the motor shaft, gearbox, shaft coupler, timing pulley assembly and finally the friction rollers and the load.

By applying Newton's second law of motion to the rotating mechanism, the following can be obtained:

$$\Sigma T = J_T \cdot \alpha_m \quad (4.23)$$

Where ΣT is summation of torques generated within the system, J_T is the total mass moment of inertia, and α_m is the angular acceleration of the motor. The mechanical assembly diagram for CRM is shown in Figure 4.19,

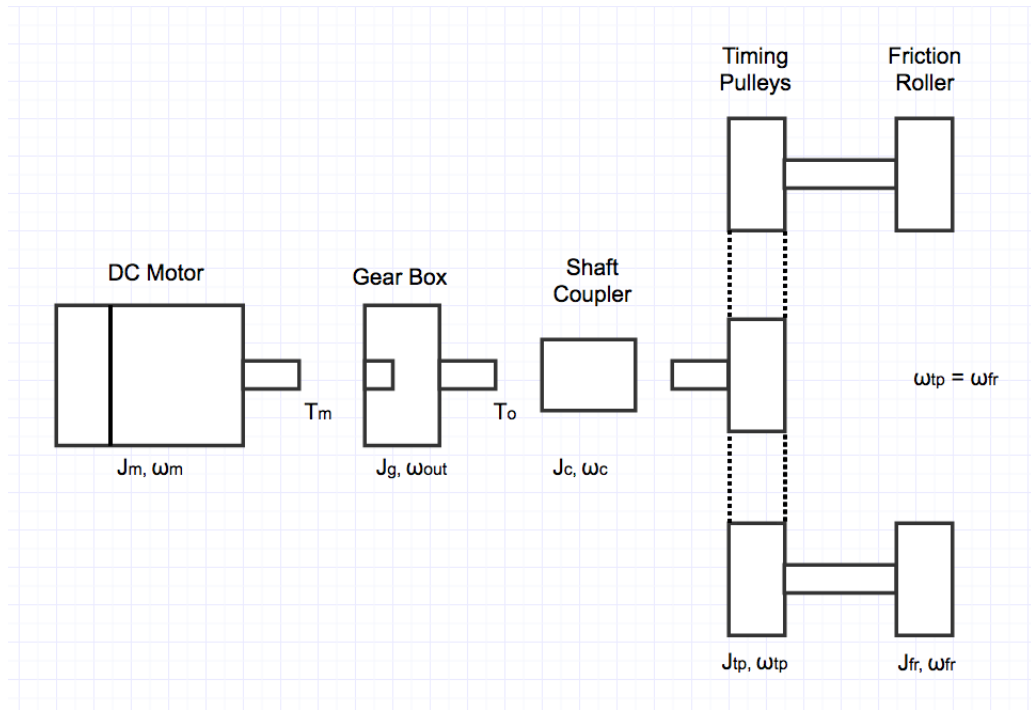


Figure 4.19: Mechanical Assembly Diagram of the CRM

Since a gearbox exists in this assembly, the torque and speed at the output shaft of the gearbox as well as the friction rollers has a ratio of the gearbox, which in this case

is 5.9:1. Assuming N is the gearbox ratio for the motor, one can obtain the following:

$$\omega_{out} = \omega_c = \omega_{tp} = \omega_{fr} = \omega_m/N \quad (4.24)$$

$$T_L = T_m \cdot N \quad (4.25)$$

According to Eq. 4.23, one can get:

$$T_m - (f_m\omega_m + f_L\omega_{fr}) = (J_m + J_L/N^2) \cdot \frac{d\omega_m}{dt} \quad (4.26)$$

and in the above equation, the term $f_m\omega_m$ is viscous friction torque inside the DC motor, $f_L\omega_{fr}$ is a lumped viscous friction torque caused by the gearbox, timing pulley systems and bearings. J_L/N^2 is the equivalent mass moment of inertia caused by the combined effect of gearbox, shaft coupler, timing pulleys, friction rollers.

Substitute Eq. 4.24 into 4.26, one can get,

$$T_m - (f_m\omega_m + f_L\omega_m/N) = (J_m + J_L/N^2) \cdot \frac{d\omega_m}{dt} \quad (4.27)$$

By assuming zero initial conditions, Eq. 4.27 can be rewritten to:

$$T_m - (f_m\omega_m + f_L\omega_m/N) = (J_m + J_L/N^2) \cdot s \cdot \omega_m \quad (4.28)$$

Rearrange to get,

$$\frac{\omega_m}{T_m} = \frac{1}{(J_m + J_L/N^2) \cdot s + (f_m + f_L/N)} \quad (4.29)$$

The transfer function can then be completed as follows,

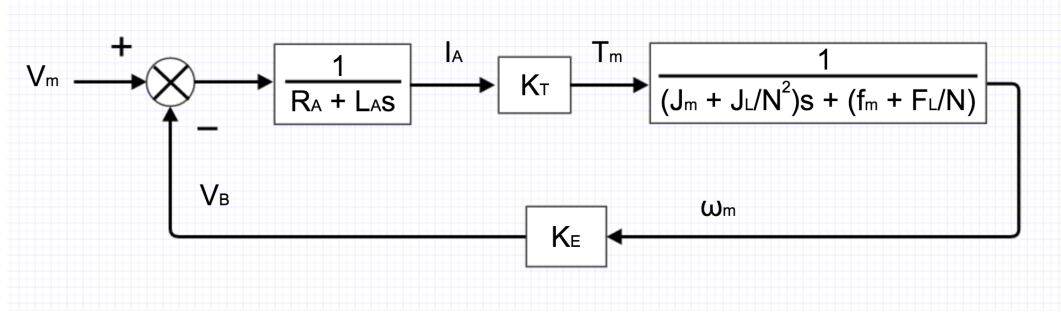


Figure 4.20: Complete Transfer Function for CRM

4.3.2 Simulink Model and Simulations for Closed Loop Control of the CRM Motor

Based on the developed model, a Matlab Simulink model was also obtained as follows,

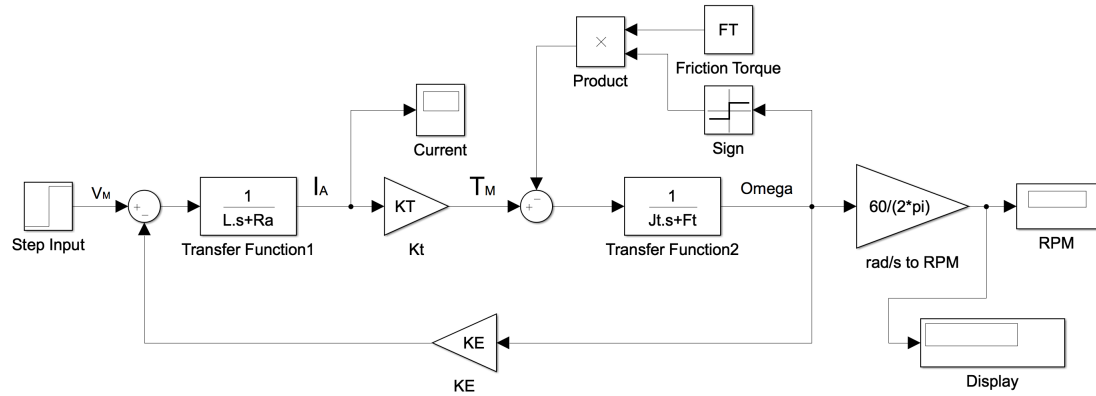


Figure 4.21: Simulink model for DC Servo Motor

In Figure 4.21, J_t represents the total inertia and F_t represents the lumped friction coefficient of viscous damping. They are equivalent to the ones in the Eq. 4.29. FT is a constant friction torque within the system and is not dependent on rotational speed of the elements, which is different than the viscous damping of the motor and gearbox. The step input voltage is 24 volts, which is the chosen voltage for the system for it is sufficient to drive the mechanisms for testing purposes. K_E represents the

back EMF constant. The conversion equation at the end converts the angular velocity from rad/s to RPM, which is often most desired in many cases.

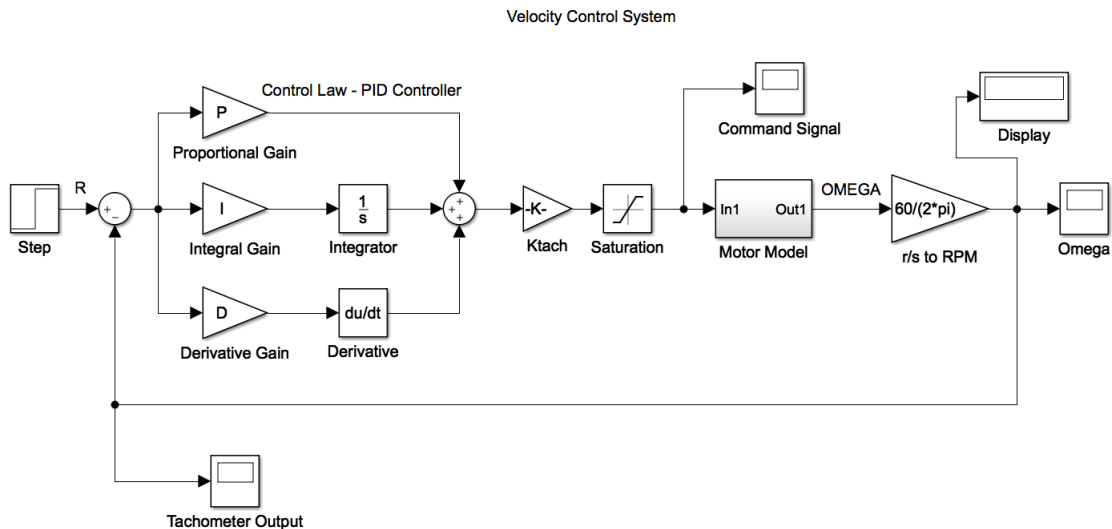


Figure 4.22: Simulink model for CRM Motor Speed Controller

In Figure 4.22, it shows the PID speed controller of the CRM motor and as shown in the figure, the motor model in the controller was developed as seen in Figure 4.23, which was replaced by a blackbox block with one input port and one output port. Right before the motor model, there are the PID gains followed by the saturation block, which is simply limiting output voltage. On the right hand side of the motor model, the output port produces the rotation speed, which is again converted to RPM. To run the simulation, a parameter .m file is run to generate all necessary numbers such as friction coefficient, motor resistance, torque constant. However, some parameters could not be obtained through the available datasheets or tested with the available lab equipment, such as the mass moment of inertia of gears, timing pulleys and friction rollers. Assumptions were made for these parameters to carry on the simulations. The assumed values are shown in Appendix A2.

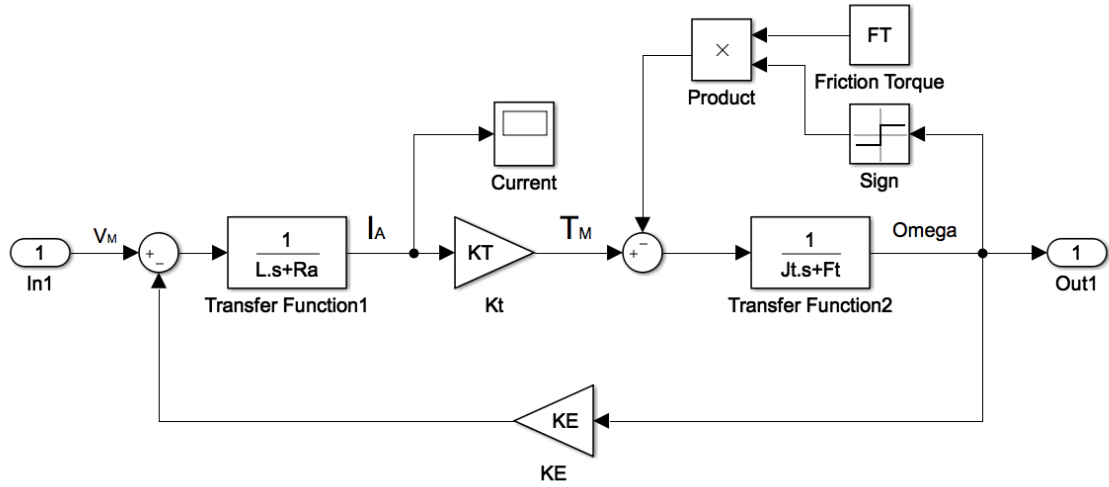


Figure 4.23: Simulink Motor Model for Controller Design

4.3.3 PID Control Loop Tuning of the CRM Motor in Simulink

PID tuning in Matlab Simulink can help understand the real system response. At the first step, only the proportional gain was introduced. Since the CRM mechanism is a relatively slow response system of running at low speed, that is, below 100 RPM of friction rollers, a conservative P-gain was chosen. A relatively low P-gain would be less aggressive and could extend the useful life of the actuator. In this simulation, a step input of 600 RPM was used. This is the speed of the motor itself and does not include the gear box. As seen in the Figure 4.24, the P-gain was set to 12, and the settling time of around 0.012 is still very satisfying to the system. The system overshoots three times for the entire oscillation, which is normally a reasonable number. The rotational speed then settled at 584, which is 16 RPM less than the input speed.

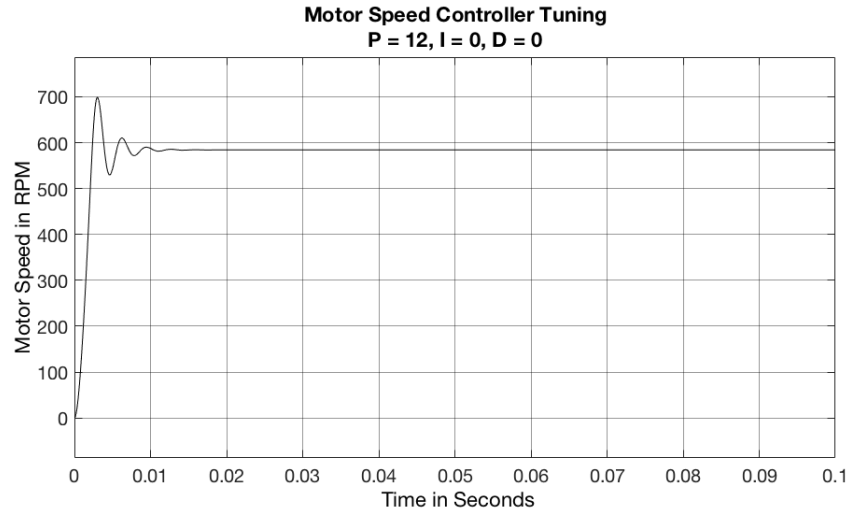


Figure 4.24: PID Tuning for CRM Motor, P - gain

At second step, a derivative gain of 0.1 was introduced to remove the oscillations and overshoots, this is desirable because it can make the system responses less violently and more stable, it often reduces the settling time. In this case, it did not reduce the settling time because a relatively high gain was chosen. The settling time of less than 0.05 seconds is acceptable. The offset to the setpoint speed remains unchanged at this point. If a fast response is a requirement for the system, then a low D - gain can be chosen in order to reduce the settling time.

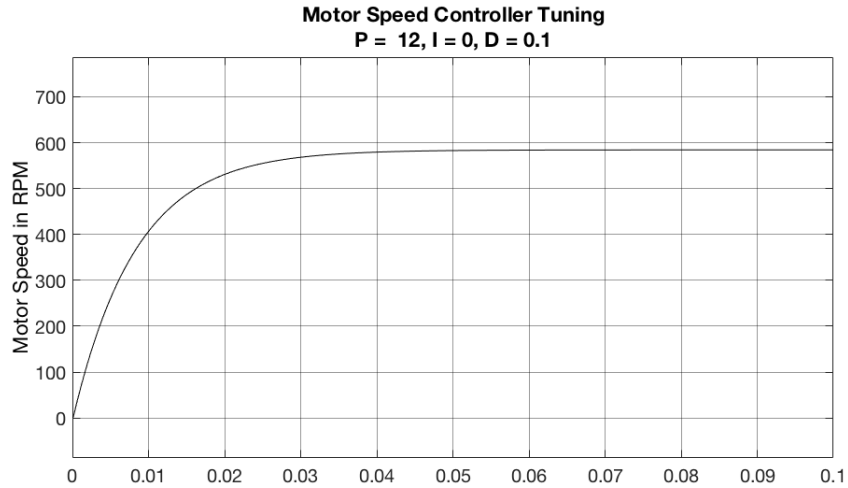


Figure 4.25: PID Tuning for CRM Motor, PD - gain

At last step, the integral gain was set to 35 to bring the final motor speed as close as possible to the setpoint speed of 600 RPM. There could be many more multiple combinations of PID gain values, most importantly, it should fit what is required by the system or design requirement. In this project, PI Controller or PD Controller could also be implemented to satisfy the needs of the project.

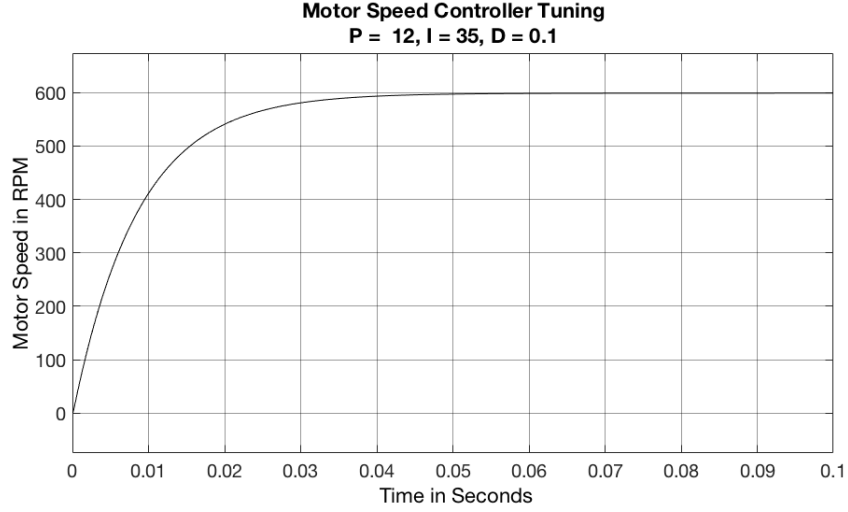


Figure 4.26: PID Tuning for CRM Motor, PID - gain

4.3.4 PID Tuning of the CRM Motor Without Cable

In this section, PID controller tuning of Motor #1 will be discussed. The motor was set to a setpoint speed of 600 RPM and all PID gain parameters were tuned. The approach was to combine the Simulink result, Ziegler–Nichols method, and manual tuning to reduce the time and steps of obtaining the final satisfying gain parameters. A standard form of the PID controller was used in this test, as seen in Eq. 4.30 [26] [27], which is the most common form used in the industry,

$$MV(t) = K_p(e(t) + \frac{1}{T_i} \int_0^t e(\tau)d(\tau) + T_d \frac{d}{dt}e(t)) \quad (4.30)$$

Where,

MV is manipulated variable

T_i is the integral time

T_d is the derivative time

The approach was used is to manually set the proportional gain to aim a reasonable

amount of overshoot first, which is somewhere between 25% to 50%. From the Matlab Simulink model and simulation results, K_p is set to 12, so setting $K_p = 12$ was first tried and it resulted both excessive overshoot and high amplitude oscillations, as shown in Figure 4.27. This indicated that the chosen proportional gain was too high and it needs to be reduced.

The rotational speed of the motor is calculated in the mbed source code by converting counts/ms to Rev/min(RPM) based on the read values of the motor #1 encoder position in pulses at two consecutive PID loops. The PID loop was executed every millisecond by running an Interrupt Service Routine (ISR) called 'ticker' in mbed.

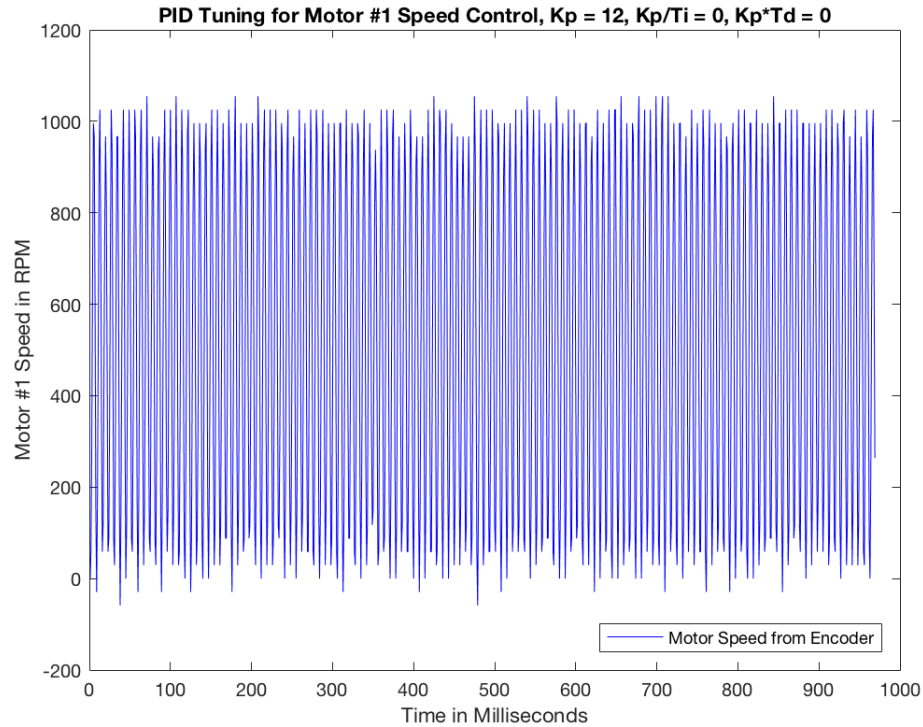


Figure 4.27: PID Tuning for Motor 1, $K_p = 12$, $K_p/T_i = 0$, $K_p \cdot T_d = 0$

At second try of the proportional gain, $K_p = 6$ was used and it resulted an acceptable amount of overshoot and oscillation was removed, as shown in Figure 4.28. The

proportional gain still seemed a bit high by looking at the overshoot, but it was kept at this step. The settled speed of the motor was mostly bouncing between 470 and 500. This was not due to the unstable oscillations of the motor itself but rather the resolution of the encoder. At a motor speed of 600 RPM, number of encoder counts should be equal to 20.48/ms, but the pulses taken by mbed only allows integers. As the little variation in motor speed causes the number of counts per millisecond to change ± 1 counts, the RPM of the motor will vary ± 29.3 , which is a conversion factor from counts/ms to RPM.

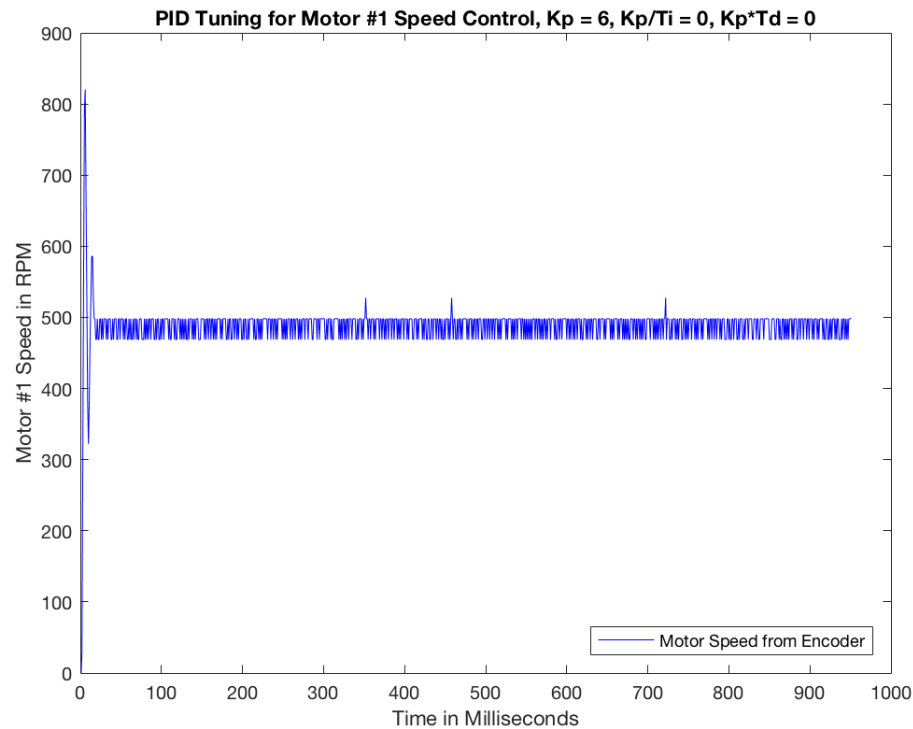


Figure 4.28: PID Tuning for Motor 1, $K_p = 6$, $K_p/T_i = 0$, $K_p \cdot T_d = 0$

A derivative gain was applied to the controller to reduce the amount of overshoot, the result is as shown in Figure 4.29, the overshoot was significantly reduced, but not removed completely, so further tweaking is needed.

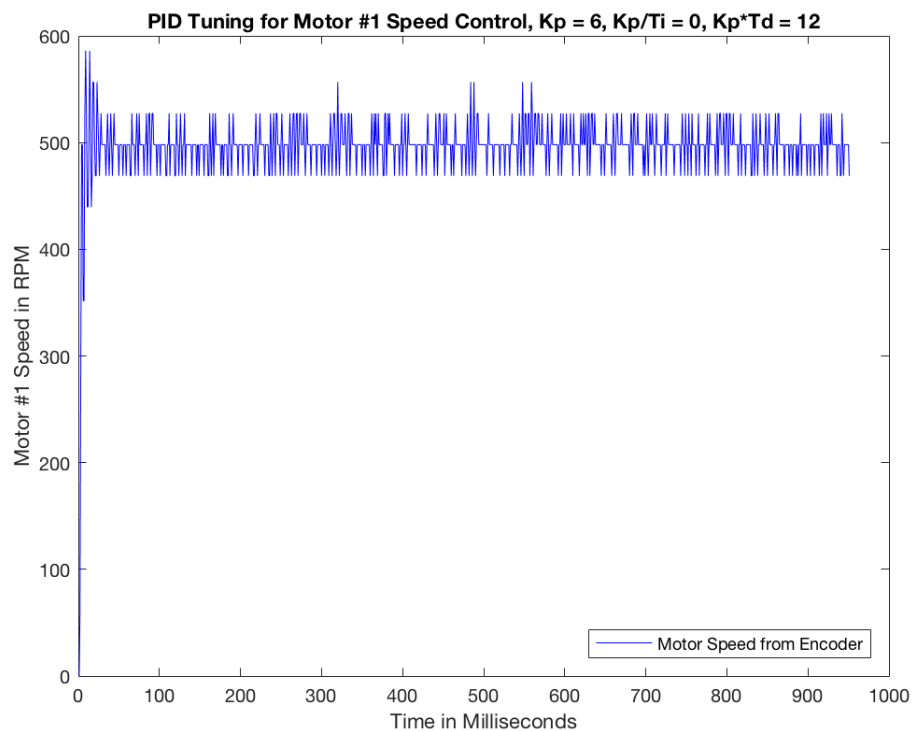


Figure 4.29: PID Tuning for Motor 1, $K_p = 6$, $K_p/T_i = 0$, $K_p \cdot T_d = 12$

Since the proportional gain was still considered relatively high (high amplitude of overshoot), it was further reduced to $K_p = 4$, and as a result the derivative gain was also reduced even though T_d was increased to 2.5. The result shows that overshoot has been removed as seen in Figure 4.30,

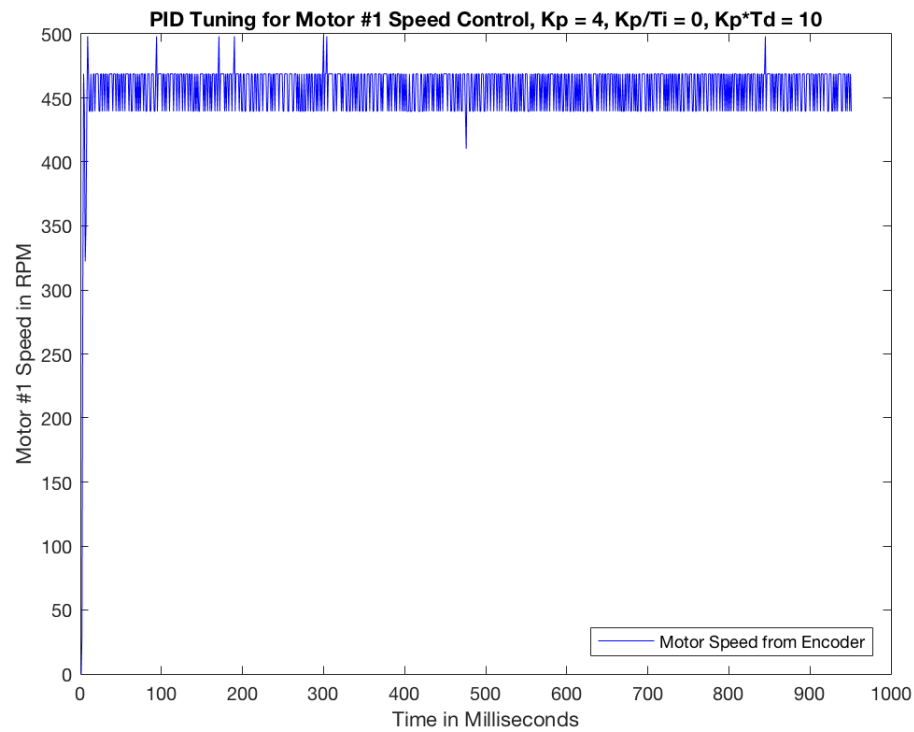


Figure 4.30: PID Tuning for Motor 1, $K_p = 4$, $K_p/T_i = 0$, $K_p \cdot T_d = 10$

As noticed in Figure 4.30, the settled motor speed is just a little over 450 rev/min. Therefore, the last step is to add an integral gain to the controller to bring the motor speed as close as possible to the setpoint, which is 600 RPM.

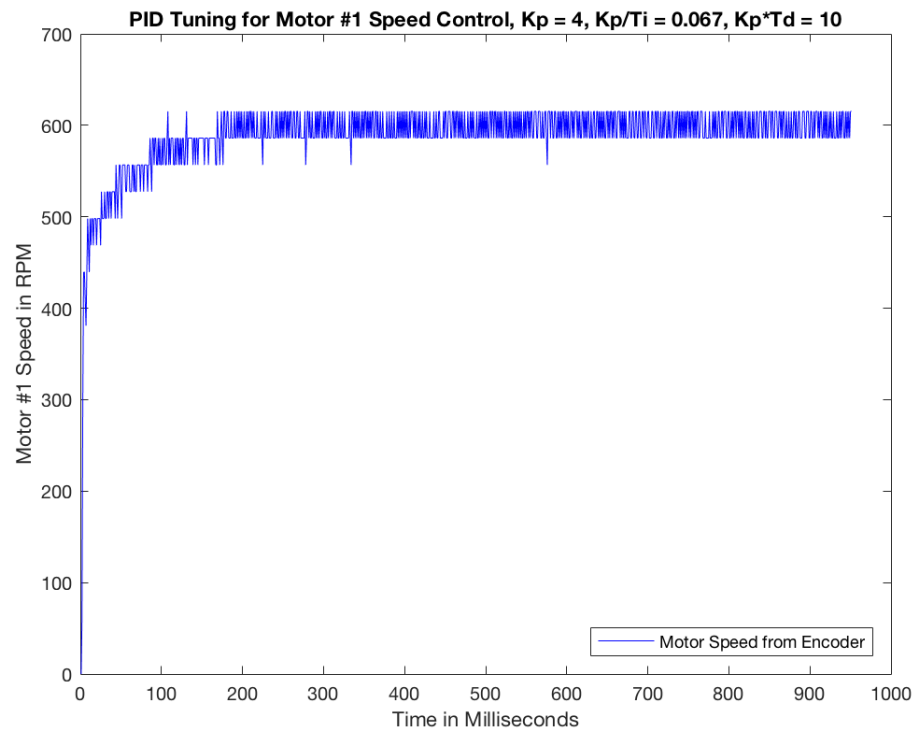


Figure 4.31: PID Tuning for Motor 1, $K_p = 4$, $K_p/T_i = 0.067$, $K_p \cdot T_d = 10$

To add an integral gain, start with a large number of T_i so that the gain is small, then slowly increase the value of K_p/T_i . After a few trials, T_i was set to 60 and $K_p/T_i = 0.067$. The motor speed was settled at 600 rev/min and the settling time is observed to be 0.2 second, which is acceptable in this application.

4.3.5 Position Synchronization Between CRM and ASM

The Motor #2 for the Arm Sliding Mechanism (ARM) has to be position synchronized with the Motor #1 of the Cable Reeling Mechanism (CRM) because there is a fixed position relationship between the amount of cable reeled and laying of the cable inside the Cable Storage Unit (CSU).

The way Motor #2 is controlled is to assign the position value of Motor #1, the angle information in this case, to the setpoint of Motor #2 control loop, with a scaling factor. The scaling factor in this case is the position relationship between Motor #1 and Motor #2, which was developed in Equation 4.15 in this Chapter. The update frequency of this setpoint assignment is 1 KHz. This method of position synchronization worked out effectively since its a relative slow system but the position following has a sufficient update rate.

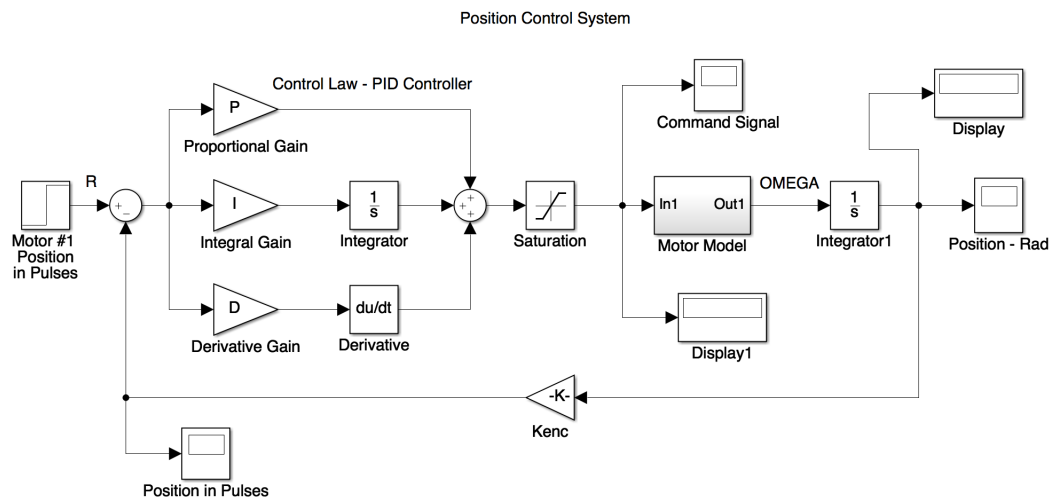


Figure 4.32: Position Synchronization Control Loop for Motor 2

As shown in Figure 4.32, the reference input is the position information in pulses from the Motor #1 encoder, and Motor #2 encoder returns a pulse value as well to

compare with the reference position and gives an error. In the mbed microcontroller, this digital signal from the encoder was converted to a percentage which has a value between -1.0 to +1.0, it is then tuned by PID parameters to output a PWM motor control signal, this signal is checked for saturation before it is sent to the motor. The motor model outputs a rotational speed OMEGA, which was integrated once more to get the angle position value in rad/s. Kenc is the encoder gain that converts the shaft position from rad/s to pulses. In this case, the motor shaft position is represented in pulses, and each full rotation of the shaft is 512 pulses (However, mbed microcontroller is capable of X4 encoding for the quadrature encoding which in this case, is 2048 counts/rev).

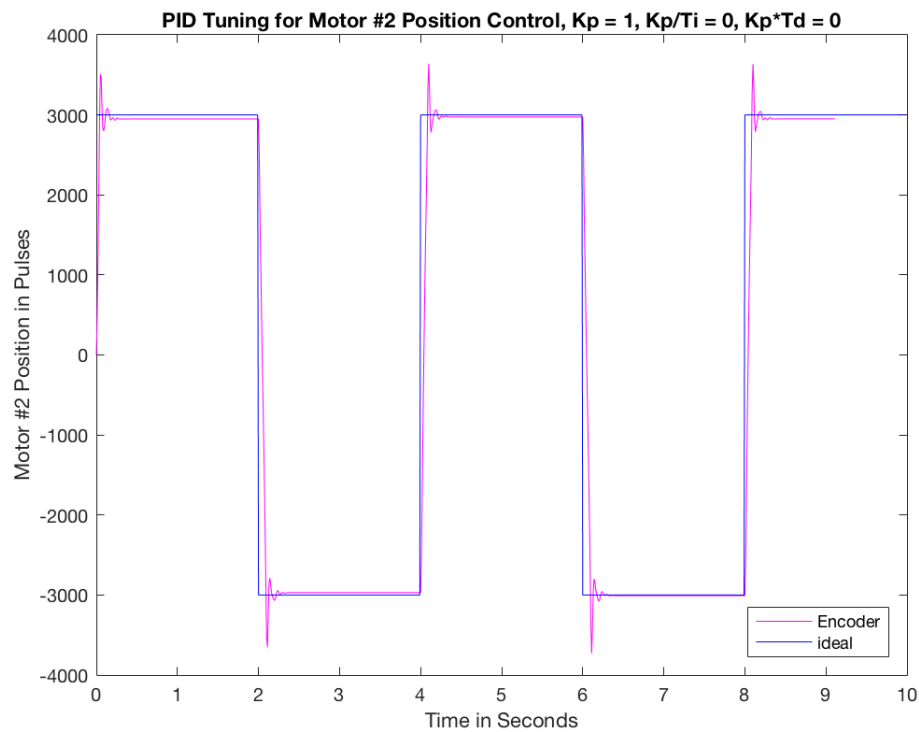


Figure 4.33: PID Position Control for Motor 2, $K_p = 1$, $K_p/T_i = 0$, $K_p \cdot T_d = 0$

The second motor was position closed loop controlled. For the tuning purpose, the

setpoint position was set to ± 3000 pulses, which converted to be $3000/2048/5.9 \cdot \pi \cdot P.D.\text{timing pulley} = 0.5\text{ inch}$. As shown in Figure 4.33, the blue plot is the setpoint target, which switches between ± 3000 pulses, and the magenta plot shows the step response. In this plot, one can notice the overshoot but the position was quiet close to the set point. To remove the overshoot, a derivative gain was added and the result was plotted in Figure 4.34 and 4.35

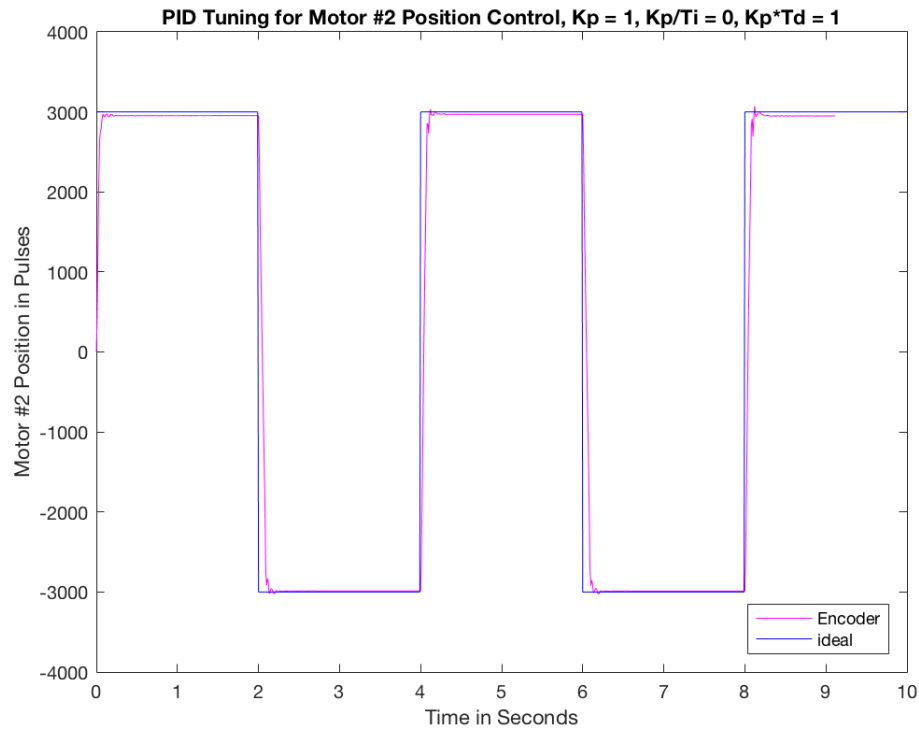


Figure 4.34: PID Position Control for Motor 2, $K_p = 1$, $K_p/T_i = 0$, $K_p \cdot T_d = 1$

As the derivative gain of 1 was added to the controller, the overshoot was drastically reduce to almost zero, however the response still contained small magnitude of oscillations, so the derivative gain was further increased. As shown in Figure 4.35, the oscillation became a little more violent. From this point on, the derivative gain did not work, so the proportional gain was reduced to remove the overshoot.

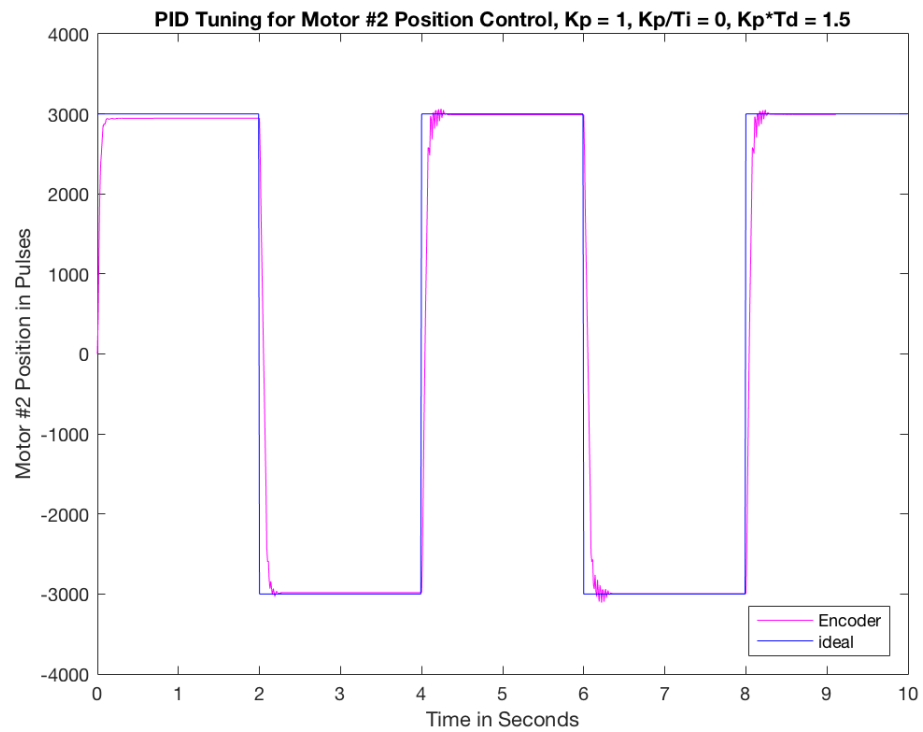


Figure 4.35: PID Position Control for Motor 2, $K_p = 1$, $K_p/T_i = 0$, $K_p \cdot T_d = 1.5$

The proportional gain was then set to 0.5, and derivative gain was set back to 1 again. The step response seen in Figure 4.36 showed a much promising result.

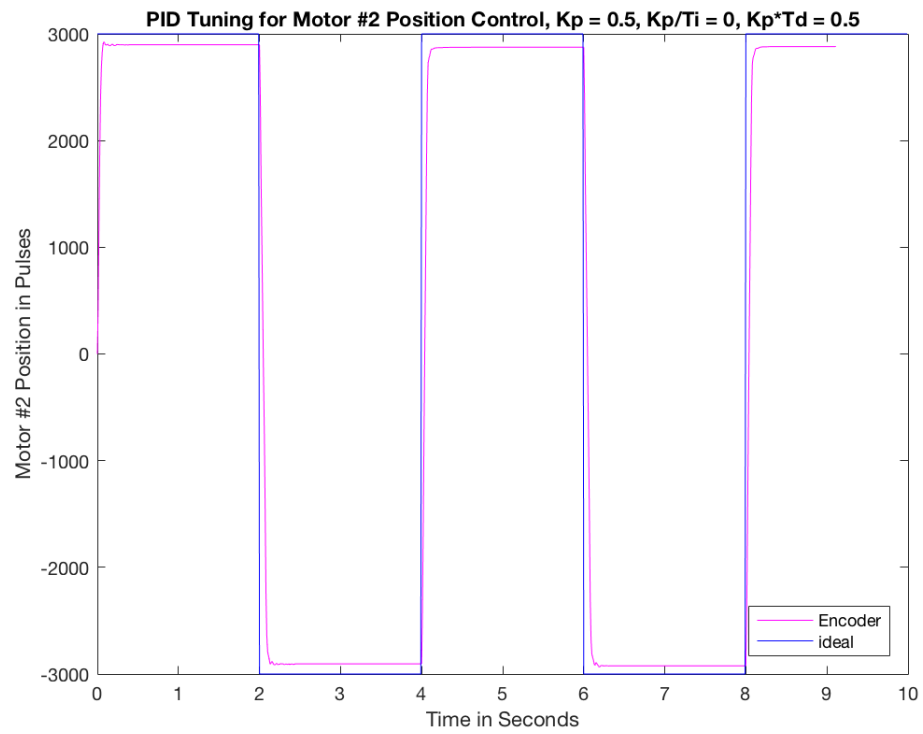


Figure 4.36: PID Position Control for Motor 2, $K_p = 0.5$, $K_p/T_i = 0$, $K_p \cdot T_d = 0.5$

However, the position offset from the setpoint had been increased as a result of that adjustment, therefore, an integral gain was required to properly bring the position back to the setpoint target of 3000 pulses.

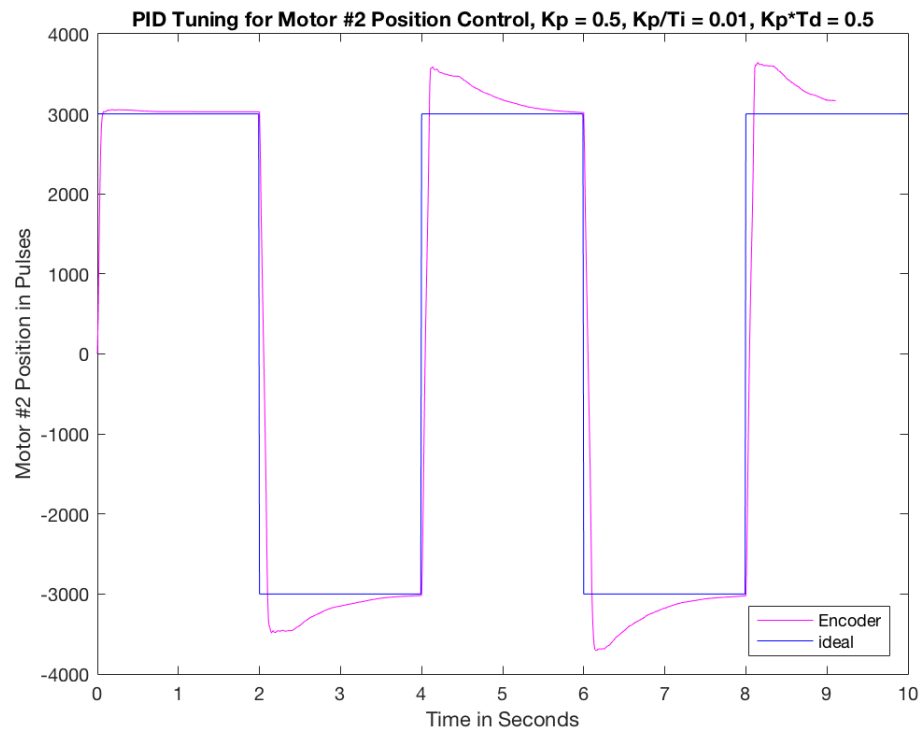


Figure 4.37: PID Position Control for Motor 2, $K_p = 0.5$, $K_p/T_i = 0.01$, $K_p \cdot T_d = 0.5$

From Figure 4.37, the overshoot had occurred again because the added integral gain. Further reducing the proportional gain was necessary. After a few tries, the proportional gain was set to 0.2, integral gain was set to 0.01, and derivative gain was set to 0.5. The step response then became the following, as shown in Figure 4.38.

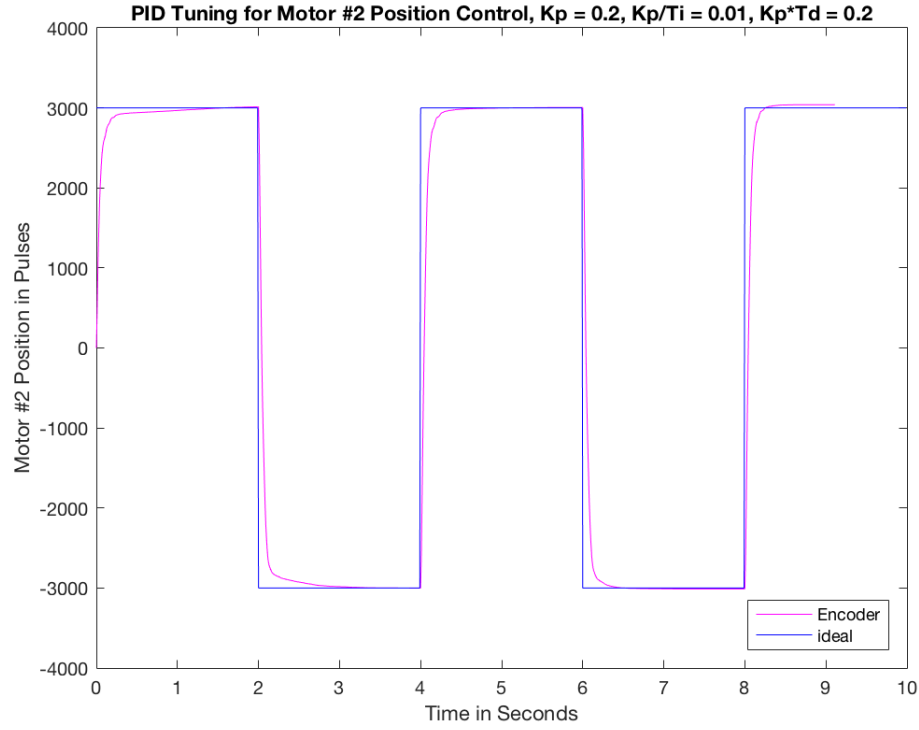


Figure 4.38: PID Position Control for Motor 2, $K_p = 0.2$, $K_p/T_i = 0.01$, $K_p \cdot T_d = 0.2$

4.4 Test of Full Winch Prototype II and Result

After the entire system was setup and all motors controllers were tuned, it was tested for winding cable into the Cable Storage Unit (CSU) in Figure "∞" pattern. To prove the concept and feasibility, the system was only tested at a relatively low speed, so the performance with regard to speed and accuracy of the operations was not a focus at this stage of the project. The varying parameters include the distance between CSU and CMU d_u , Motor #1 speed, compression load by spring loaded adjustment screw F_c , and positional relationship between Motor #1 and Motor #2 R_m .

TEST 1 All three motors are tested without manipulations of the cable and the use of Cable Storage Unit. Motor #1 was velocity controlled using PID control algorithm and Motor #2 was run by following Motor #1 using PID position control loop, and Motor #3 was also run by applying position synchronization control loop following Motor #1. All components including motors, encoders, timing pulley systems, friction rollers functioned properly and showed no sign issues. Firstly, Motor #1 was tested at three different speed: 200, 600, and 2000 RPM for 10 minutes. The Cable Reeling Mechanism arm worked properly and had no known issues by visual observing. Secondly, Motor #2 were tested while running Motor #1 at same three different speeds for 10 minutes. Lastly, all three motors were tested at the same time for three different speed of Motor #1 for 10 minutes. No issues were found by visually checking the Cable Manipulation Unit.

TEST 2 After the system was tested without any load, cable reeling test was carried out. The cable was reeled forward and backward by just running Motor #1, the other two motor were turned off. Three speeds of 200, 600 and 2000 RPM were tested, observation found no issues. Only the Cable Manipulation Unit was tested, cable was not being wound into the Cable Storage Unit. Then Motor #2 was also switched on following the position of Motor #1. Cable were reeled forward and backward for three different speeds of 200, 600, and 2000 RPM. No noticeable operation issues were discovered by visual inspection during the test. However, some black powder like substance with small grain sized particles were found in the area of cable inlet and outlet. The visual inspection of components after disassembling the Cable Reeling Mechanism suggested that this was due to the wear of the rubber friction rollers. The wear had not compromised the friction drive capability of the rollers. The rest of the test was carried out. Motor #3 was turned on while running the other two motors to

twist the cable for 234° at near each end of the Cable Manipulation Unit. The cable twist angle is directly related to the angle of the circular segment of the Figure " ∞ ", whose angle is calculated to be 234° based on the geometry. No operational issues were found but the third motor had little effect on twisting the cable. Taking a closer look at the cause of the result, it was suggested that the rubber rollers lose deformation when they try to twist the cable while reeling it at the same time.

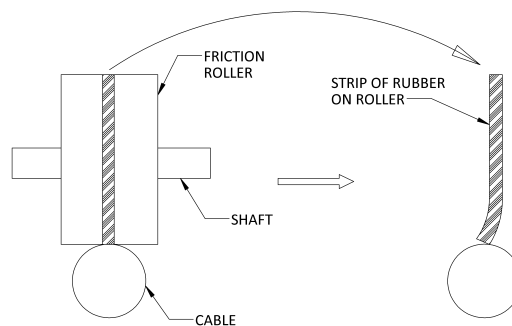


Figure 4.39: Illustration of Rubber Roller Twisting Cable

As shown in Figure 4.39, the portion of the roller that is in contact with the cable will deform as it rotates around the cable twisting it. The deformation creates a force to cause the cable to turn. However, if the roller also tries to rotate around its own shaft, the undeformed portion that will be in contact with the cable at the next moment does not create enough deformation as it walks around the cable at the direction of twist. The following tests were carried out without running Motor #3 due to this result.

TEST 3 Test 3 involved running the entire system with cable, that is to wind cable into the Cable Storage Unit in a Figure " ∞ " shape. Motor #1 speed was set to 200 RPM, so the friction rollers speed was $200/5.9 = 33.9$ RPM. The speed of cable payout

was then calculated to be $33.9 \cdot \pi \cdot 0.75 = 79.9 \text{ in/min}$. The test speed was considered to be slow given the capability of the motor and the system. The goal of the test was to test the functionality of the system, that was, the cable figure " ∞ " winding and storing capability.

The initial distance between the Cable Manipulation System and the Cable Storage Unit was set to 7.5 inches. Before the cable test was carried out, the synchronization ratio between Motor #1 and Motor #2 were set according to the ones that were developed in Eq. 4.15. The result showed that the system performed relatively well in the center region but poorly when the CRM ARM was close the the ends. The cable seemed to have enough stiffness to be pushed into the slot but it was easily jammed as the cable guide moved away from the ends. This was due to two main reasons: The first reason was that when the cable guide assembly moved close to the ends, the extension tube tilted toward the ends at a relatively large angle that would cause it to jam the cable as the cable was being fed through it laid into the slot of the storage unit. As the tilt angle got large enough, the cable was bent at a much smaller radius that would cause too much friction at the entrance of the extension tube. It also made the extension tube difficult to slide freely inside slot of the cable guide bracket. The second main reason was that the cable was not deflected or guided properly while it was being wound at both ends. The test showed that a better cable deflector needed to be designed to better guide the cable into the slot of the storage unit.

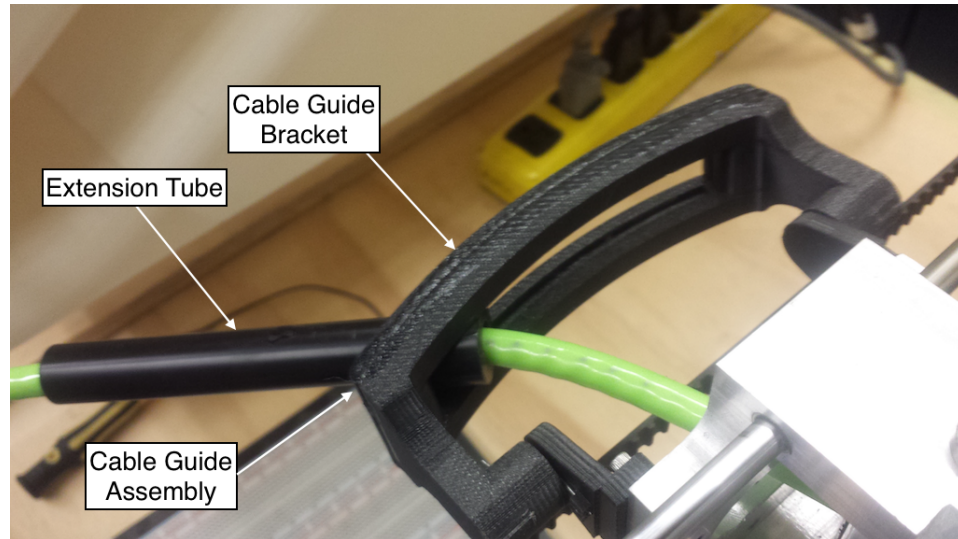


Figure 4.40: Cable Jammed in Cable Guide Tube

As the cable was jammed, the CRM Arm kept moving, the winding process had to be completely disengaged since the cable feeding and CRM Arm movement would immediately break out of synchronization. Slippage between cable and friction rollers would occur whenever the Cable Reeling Mechanism encountered large resistance along the cable. To keep two actions in synchronization, cable slippage detection should be implemented.

To reduce the risk of cable jam, the distance between the CMU and CSU was adjusted to 8.5 inches which in turn reduced the tilt angle of the cable guide extension tube. This resulted in a better result which had a better success rate at the two ends of the unit. To carry on the test with less interruptions due to cable jams, helping deflecting the cable with fingers made a positive impact especially at the two ends where the change of deflect angle at the inlet of the CSU was needed.

Second major issue found in the experiment was that sometimes the cable would get jammed between the walls of the slot. Closer observations suggested that the possible cause was the surface roughness of the rapid prototyped unit was a bit too

high, which caused large unwanted friction. This also happened more often as the cable started to make turns toward the ends.

Lastly, the depth changing cable laying method could cause potential problems too. The depth changing cable laying means that when cable is continuously laid into the slot of the CSU, the depth of the slot is reduced by one thickness of the cable after each loop. Since the linear cable stiffness is generally consistent throughout the length of the entire cable, the laying force generated would change as the distance changes. This could cause the system to not have enough stiffness to properly push the cable into the designated space, and it also could cause the cable to have too much stiffness so that the top layer would compress the layers below.

Chapter 5

Conclusion and Future Work

In this thesis project, a low inertia drumless winch system was proposed. Issues often encountered when operating traditional winches were discussed. Active motion control of towed sensor equipment requires agile response of the winch system. This is difficult to achieve by winches that have large drum and cable inertia. Some novel and innovative concepts were generated and discussed. Finally, designing a mechanism that was able to wind cable into a Figure "∞" shape was chosen since it had many advantages over other concepts including elimination of drum and cancellation of cable twist. In addition, no slip ring was required for power and data transmission. This could increase system reliability and reduce maintenance cost.

A dynamic mathematical cable model was developed and implemented in Matlab using lumped parameter modelling. Simulations were carried out under different speed from 0.2 m/s to 1.6 m/s. The corresponding forces at node zero, which was the anchor point for towing, were calculated and projected in Table 2.2. The required force varies from 62.53 N to 360.44 N based on the towing speed. The position of the sensor (tow fish) was also estimated and demonstrated in Figure 2.5. The tow fish was modelled as a spherical body that has a diameter of 15 centimetres. The density of tow fish was

set so that it was neutrally buoyant. The cable length was assumed to be 10 meters long, each element was 0.5 meters long. The resolution was set low to reduce the time cost of simulation yet still provide a reasonable result.

The first prototype with the two modules was designed and built. The first module was consisted of two friction rollers that were driven separately by two step motors. This module was not only to reel the cable but also changing the feeding direction of the cable. The test result showed that reeling mechanism worked well. However, changing the feeding direction required a substantial amount of motor torque which the step motors were not able to provide. As the speed of the motors were set slightly different, they started to skip steps. There was no effect of direction changing for feeding the cable. The second module was designed to achieve the twisting actions that would help winding cable into the Figure " ∞ " shape. It was driven by one step motor that has a lead screw which could drive a roller in the vertical direction to create the twist motion. MUNDER Board Microcontroller, L298 motor driver and microstepping stepper motor driver were used to drive the step motors. The paired roller was passive and spring loaded so that the compression force on cable could be adjusted. Test results showed the mechanism worked well and did twist the cable as it required.

A second prototype was designed and fabricated for solving the issues encountered in the tests of the first prototype. It contained two main units: the Cable Manipulation Unit and the Cable Storage Unit. The Cable Manipulation Unit was made by the 3D rapid prototyping machine, and the unit was separated into 12 smaller part and printed in a honeycomb sparse configuration setting to same materials given that the size was relatively large. The Cable Manipulation Unit was constructed mostly using machined aluminum parts and commercially off the shelf components. Three DC servo motors with 512 counts/s optical encoders were readily available from AOSL lab and

were used in the prototype to save cost. Three motors were used in the CRM, ASM, and CTM, and they were all feedback controlled. Mbed microcontroller and Pololu high power motor drivers were used to drive the DC motors. PID parameters were manually tuned and all motors worked well with no observed issues. Motor #1 was speed controlled and other two motors were position controlled following the position of Motor #1.

Dry tests with or without cable were carried out to test the motors and constructed mechanisms. Dry tests with no load (no cable was present) showed all three motors functioned well and observations found no problems. Two speeds were tested for Motor #1 with other two motors positions synchronized: 600 RPM and 2000 RPM. Dry tests running with cable were only carried out with Motor #1 tuned at 200 RPM, which reels the cable at a linear speed of 79.9 inch/min. With the main goal of proving the concept, high speed tests with cable were not completed due to existing issues that would prevent cable from properly wound into the CSU. Two main tests were run with the difference in distance between CSU and CMU (7.5 and 8.5 inches). The results showed that the later test exhibited a higher success rate because of less occurrence of cable jams. Cable Twist Mechanism did not work because both reeling and twisting the cable would make the friction rollers lose grip to the cable. The test results also suggested that better cable deflector should be designed to reduce or eliminate the cable jams. Cable was more likely to get jammed as the ASM was close to both ends of the CSU.

Future work should be focused on the following areas: 1. Design a better Cable Storage Unit. The cable storage unit should have a moving base where the end of the cable would be connected to maintain a constant distance so that the cable can have consistent stiffness at same positions each loop is wound. Passive cable retainers can also be added to the unit to keep cable from bouncing back out of the unit during the

winding process. Investigation into proper sizing of the slot is also beneficial to the success rate of cable winding.

2. Another major area of work can be looking into how twist action can be achieved by the friction rollers of the CRM. Varying the angle of the axes of two friction rollers may induce a twisting torque for the cable. More research can be done to find out proper parameters and experiments can be performed to prove the concept. Moreover, cable slippage detection can also be added to the CRM since the cable reeling action and arm sliding mechanism would immediately be out of sync as soon as any slippage occurs along the cable. This can help keep two motions in synchronization.

Bibliography

- [1] P. Williams, “Towing and Winch Control Strategy for Underwater Vehicles in Sheared Currents,” *International Journal of Offshore and Polar Engineering*, Vol. 16, No. 3, pp. 218–227, September 2006.
- [2] Moog, *Proven Slip Rings*. Retrieved from <http://www.moog.com/products/slip-rings/>
- [3] M. Staff, “Slip Rings.” *McGraw-hill encyclopedia of science & Technology*, McGraw-Hill, pp. 562–563, 2007.
- [4] Willard F. Mason, “Slip rings,” *AccessScience*, McGraw-Hill Education, 2012. Retrieved from <http://www.accessscience.com>
- [5] Michael Markey, “Single Drum Winch Design,” *Handbook of Oceanographic Winch, Wire and Cable Technology*, s.n., Chapter 10, pp. 10–7, 2001.
- [6] Forum Energy Technologies, *Tether Management Systems*. Retrieved from http://www.f-e-t.com/our_products_technologies/subsea-solutions/tether-management-systems-tms/
- [7] M.R. Mitchell, J.G. Dessureault, “A Constant Tension Winch: Design and Test of A Simple Passive System,” *Ocean Engineering*, Pergamon Press Ltd., Vol. 19, No. 5, pp. 489–496, 1992.

- [8] Michael Markey, "Single Drum Winch Design," *Handbook of Oceanographic Winch, Wire and Cable Technology*, s.n., Chapter 10, pp. 10–16, 2001.
- [9] S. Huang, "Dynamic Analysis of Three-Dimensional Marine Cables," *Ocean Engineering*, Elsevier, Vol. 21, No. 6, pp. 587–605, 1994.
- [10] J.W. Kamman, R.L. Huston, "Modeling of Variable Length Towed and Tethered Cable Systems," *Journal of Guidance, Control, and Dynamics*, Springer, Vol 22, No 4, pp 602–608. 1999.
- [11] B. Buckham, M. Nahon, M. Seto, X. Zhao, C. Lambert, "Dynamics and control of a towed underwater vehicle system, part I: model development," *Ocean Engineering*, Elsevier, Vol. 30, No. 4, pp. 453–470, March 2003.
- [12] J. Wu, and A.T. Chwang. "A hydrodynamic model of a two-part underwater towed system," *Ocean Engineering*, Elsevier, Vol. 27, No. 5, pp. 455–472, 2000.
- [13] T.N. Delmer, T.C. Stephens J.M. Coe, "Numerical Simulation of Towed Cables," *Ocean Engineering*, Elsevier, Vol. 10, No. 2, pp. 119–132, 1983.
- [14] P. A. Palo, D. J. Meggitt, W. J. Nordell, "Dynamic Cable Analysis Models," *Offshore Technology Conference*, 1983.
- [15] J.V. Sanders, "A three-dimensional dynamic analysis of a towed system," *Ocean Engineering*, Elsevier, Vol. 9, No. 5, pp. 483–499, 1982.
- [16] C.M. Ablow, S. Schechter, "Numerical simulation of undersea cable dynamics," *Ocean Engineering*, Elsevier, Vol. 10, No. 6, pp. 443–457, 1983.
- [17] R. Driscoll, M. Nahon "Mathematical Modeling and Simulation of a Moored Buoy System," *Oceans '96 MTS, IEEE*, Vol. 1, pp. 517–523, 1996.

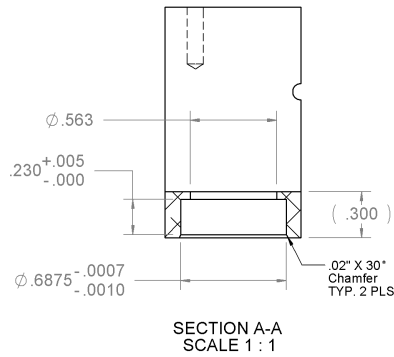
- [18] R. Folb, J.J. Nelligan “Hydrodynamic Loading on Armored Towcables,” *David W. Taylor Navel Ship Research and Development Center, DTNSRDC-82/116*, 1983.
- [19] J. M. Winget, R.L. Huston, “Cable dynamics—a finite segment approach,” *Computers and Structures*, Vol. 6, No. 6 pp. 475–480, 1976.
- [20] M.J. Casarella, “Survey of Investigations on the Configuration and Motion of Cable Systems Under Hydrodynamic Loading,” *Marine Technology Society Journal*, Vol. 4, No. 4, pp. 27–44, 1970.
- [21] Y. Choo, “Hydrodynamic Resistance of Towed Cables,” *Journal of Hydronautics*, Vol. 5, No. 4, pp. 126–131, 1971.
- [22] K. Thrimurthulu, P. M. Pandey, N. V. Reddy, “Optimum Part Deposition Orientation in Fused Deposition Modeling,” *International Journal of Machine Tools and Manufacture, Elsevier*, Vol. 44, No. num, pp. 585–594, 2004.
- [23] STMicroelectronics, “L298 Dual Full Bridge Driver,” *STMicroelectronics*, 2000.
- [24] ARM limited, *mbed LPC1768*. Retrieved from <https://developer.mbed.org/platforms/mbed-LPC1768/>
- [25] Pololu Corporation, *Pololu High-Power Motor Driver 36v9*. Retrieved from <https://www.pololu.com/product/760>
- [26] Wikipedia, *PID Controller*. Retrieved from https://en.wikipedia.org/wiki/PID_controller
- [27] Katsuhiko Ogata, “PID Control and Indtroduction to Robust Control, ” *Modern Control Engineering, s.n.*, Chapter 10, pp. 669–682, 1997.

Appendix

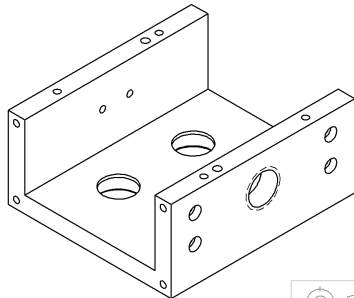
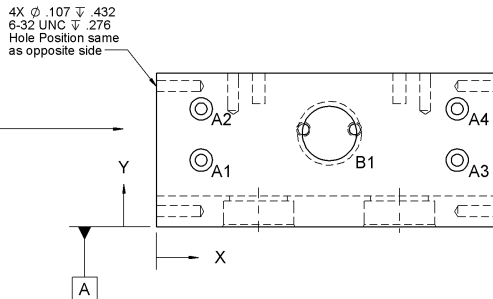
A.1 Prototype Design Drawings

The fabrication drawings of all the parts of the prototypes are included in this appendix. Some parts are made by the Technical Services at MUN, some parts are fabricated in the Student Machine Shop, and some parts are 3D printed at the Rapid Prototyping Center.

TAG	X LOC	Y LOC	SIZE
1	.7500	.1500	$\phi .107 \nabla .370$ 6-32 UNC $\nabla .276$
2	.7500	2.8500	
3	2.6250	.1500	
4	2.6250	2.8500	
5	1.0000	.1500	$\phi .125 \nabla .300$
6	2.3750	2.8500	



TAG	X LOC	Y LOC	SIZE
A1	.4375	.6500	$\phi .116$ THRU $\phi .219 \nabla .112$
A2	.4375	1.1500	
A3	2.9375	.6500	
A4	2.9375	1.1500	
B1	1.6900	.9100	$\phi .531$ THRU 5/8-11 UNC THRU

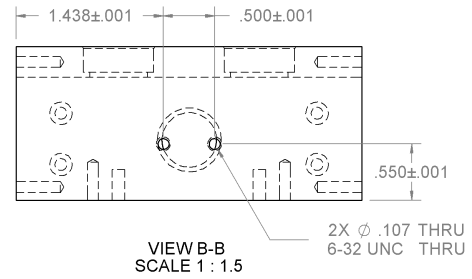
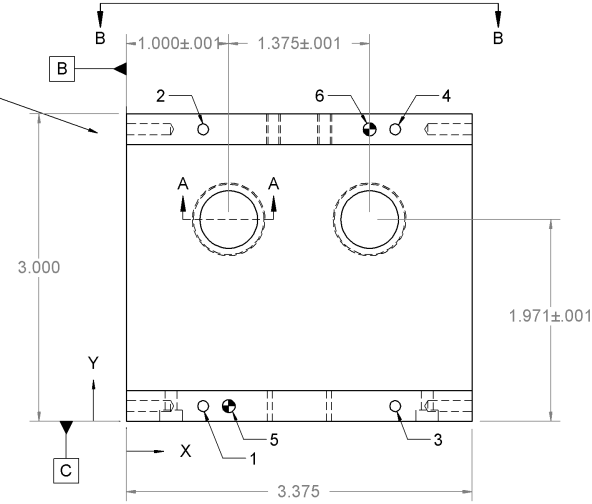


PROPRIETARY AND CONFIDENTIAL
THE INFORMATION CONTAINED IN THIS
DRAWING IS THE SOLE PROPERTY OF
AOSL OF MEMORIAL UNIVERSITY. ANY
REPRODUCTION IN PART OR AS A
WHOLE WITHOUT THE WRITTEN
PERMISSION OF AOSL IS PROHIBITED.

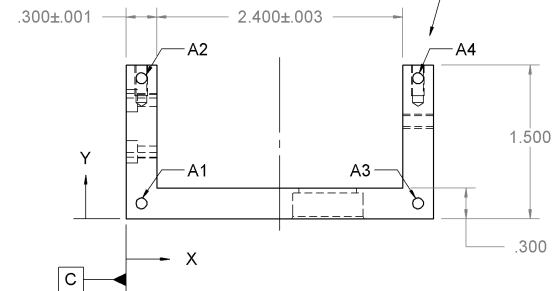
UNLESS OTHERWISE SPECIFIED:
DIMENSIONS ARE IN INCHES
TOLERANCES:
FRACTIONAL $\pm 1/16$
ANGULAR: $\pm 1^\circ$
MACH: BEND ± 0.01
TWO PLACE DECIMAL ± 0.01
THREE PLACE DECIMAL ± 0.005
INTERPRET GEOMETRIC
TOLERANCING PER:
MATERIAL
ALUM 6061 T6
FINISH
DO NOT SCALE DRAWING

NAME	DATE
H. WANG	2012-04-16
DRAWN	
CHECKED	
ENG APPR.	
MFG APPR.	
Q.A.	
COMMENTS:	
QTY.: 1	

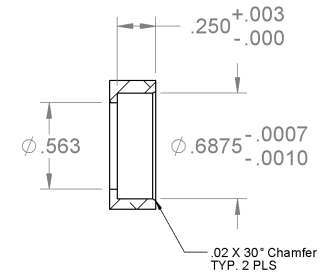
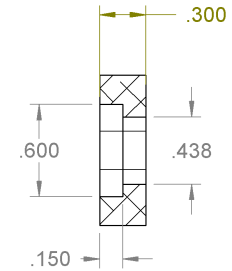
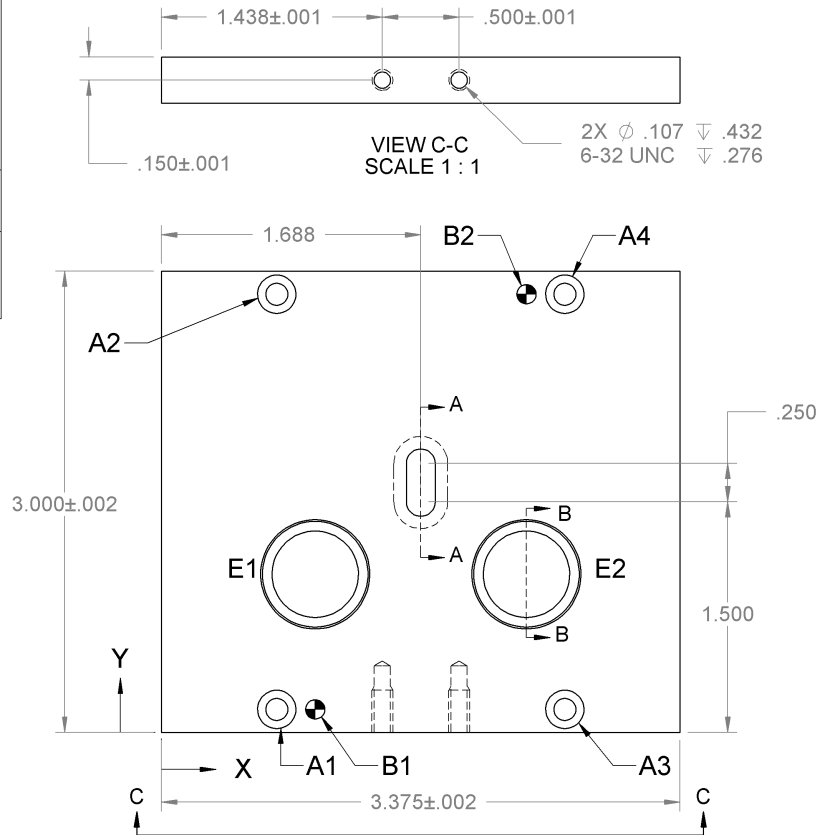
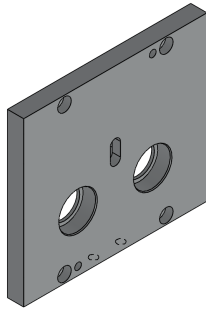
AOSL - Memorial University
TITLE:
Bearing Box
SIZE DWG. NO. REV
A D001
SCALE: 1:2 WEIGHT: SHEET 1 OF 1



TAG	X LOC	Y LOC	SIZE
A1	.1500	.1500	$\phi .107 \nabla .432$ 6-32 UNC $\nabla .276$
A2	.1500	1.3700	
A3	2.8500	.1500	
A4	2.8500	1.3700	



TAG	X LOC	Y LOC	SIZE
A1	.7500	.1500	ϕ .144 THRU ALL ϕ .250 ∇ .138
A2	.7500	2.8500	
A3	2.6250	.1500	
A4	2.6250	2.8500	
B1	1.0000	.1500	ϕ .125 THRU ALL DOWEL
B2	2.3750	2.8500	
E1	1.0000	1.0291	Bearing Housing
E2	2.3750	1.0291	



NOTE:
1. All edges and corners should be free of burs.

UNLESS OTHERWISE SPECIFIED:
DIMENSIONS ARE IN INCHES

TOLERANCES:
FRACTIONAL \pm 1/16
ANGULAR: \pm 1°
MACH: \pm BEND \pm 0.01
TWO PLACE DECIMAL \pm 0.01
THREE PLACE DECIMAL \pm 0.005

INTERPRET GEOMETRIC
TOLERANCING PER:

MATERIAL
ALUM 6061 T6

FINISH

DO NOT SCALE DRAWING

NAME DATE
H. WANG 2012-04-17

DRAWN
CHECKED
ENG APPR.
MFG APPR.

Q.A.
COMMENTS:
QTY.: 1

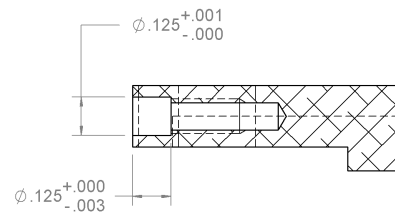
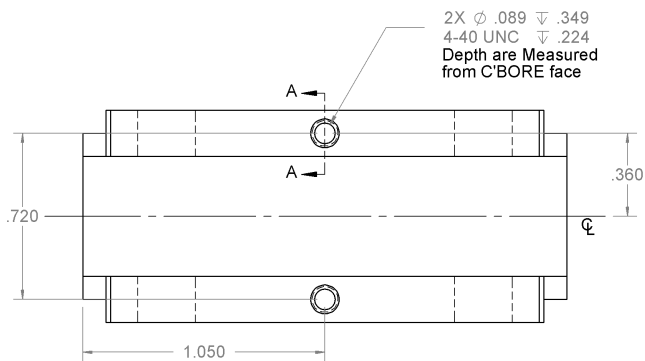
AOSL - Memorial University

TITLE:

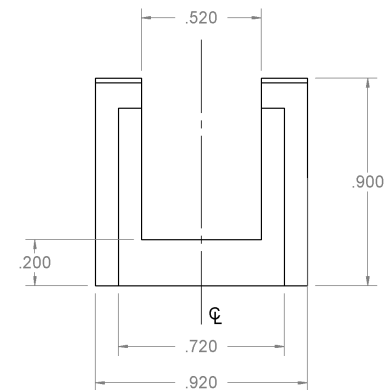
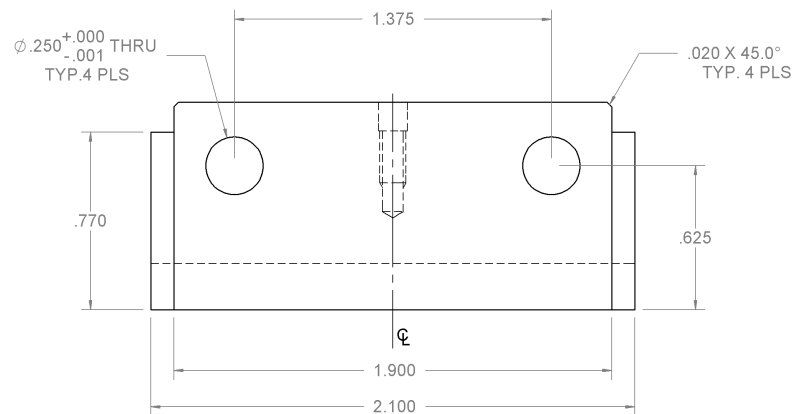
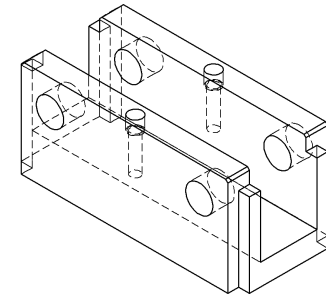
Bearing Box Cover

SIZE DWG. NO. REV
A D002

SCALE: 1:2 WEIGHT: SHEET 1 OF 1



SECTION A-A
SCALE 2 : 1



UNLESS OTHERWISE SPECIFIED:
DIMENSIONS ARE IN INCHES

TOLERANCES:
FRACTIONAL ± 1/16
ANGULAR: ± 1°
MACH: ± BEND ± 0.01
TWO PLACE DECIMAL ± 0.01
THREE PLACE DECIMAL ± 0.005

INTERPRET GEOMETRIC
TOLERANCING PER:

MATERIAL
ALUM 6061 T6

FINISH

DO NOT SCALE DRAWING

PROPRIETARY AND CONFIDENTIAL
THE INFORMATION CONTAINED IN THIS
DRAWING IS THE SOLE PROPERTY OF
AOSL OF MEMORIAL UNIVERSITY. ANY
REPRODUCTION IN PART OR AS A
WHOLE WITHOUT THE WRITTEN
PERMISSION OF AOSL IS PROHIBITED.

NAME DATE

H. WANG 2012-04-17

DRAWN

CHECKED

ENG APPR.

MFG APPR.

Q.A.

COMMENTS:

QTY.: 1



AOSL - Memorial University

TITLE:

Idler Roller Holder

SIZE DWG. NO.

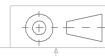
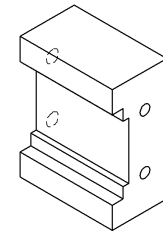
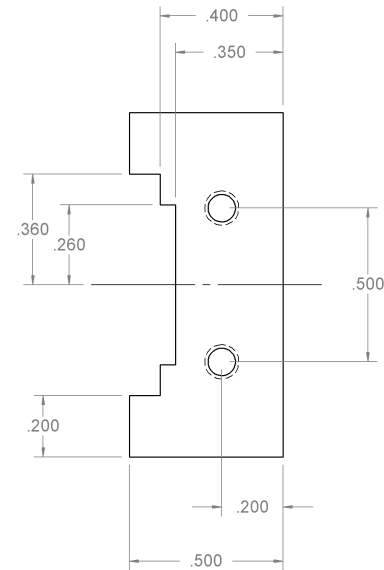
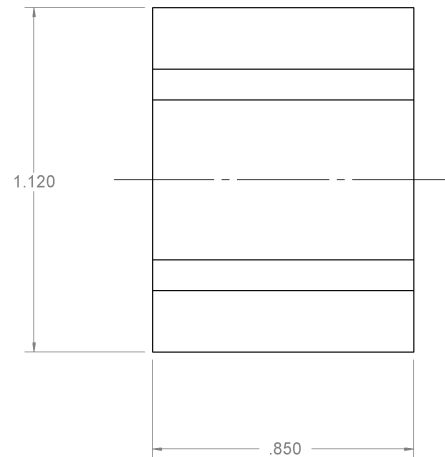
A

D003

REV

SCALE: 1:1 WEIGHT:

SHEET 1 OF 1

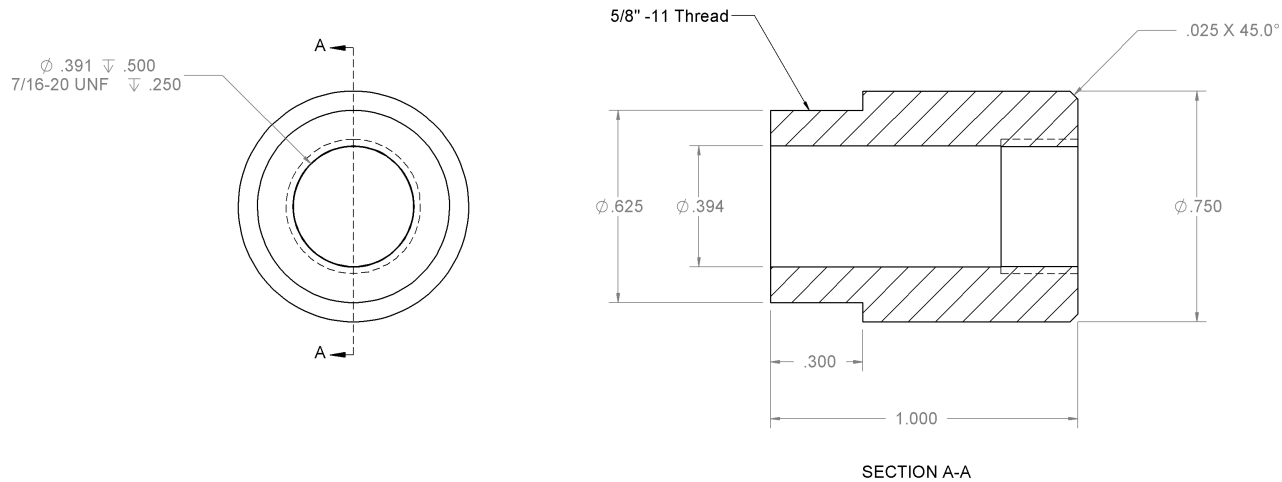


PROPRIETARY AND CONFIDENTIAL
THE INFORMATION CONTAINED IN THIS
DRAWING IS THE SOLE PROPERTY OF
AOSL OF MEMORIAL UNIVERSITY. ANY
REPRODUCTION IN PART OR AS A
WHOLE WITHOUT THE WRITTEN
PERMISSION OF AOSL IS PROHIBITED.

UNLESS OTHERWISE SPECIFIED:
DIMENSIONS ARE IN INCHES
TOLERANCES:
FRACTIONAL $\pm 1/16$
ANGULAR: $\pm 1^\circ$
MACH: BEND ± 0.01
TWO PLACE DECIMAL ± 0.01
THREE PLACE DECIMAL ± 0.005
INTERPRET GEOMETRIC
TOLERANCING PER:
MATERIAL
Delrin
FINISH
DO NOT SCALE DRAWING

	NAME	DATE
DRAWN	H. WANG	2012-04-17
CHECKED		
ENG APPR.		
MFG APPR.		
Q.A.		
COMMENTS:	QTY.: 2	

AOSL - Memorial University		
TITLE: Slider Block		
SIZE A	DWG. NO. D004	REV
SCALE: 2:1	WEIGHT:	SHEET 1 OF 1



UNLESS OTHERWISE SPECIFIED:
DIMENSIONS ARE IN INCHES
TOLERANCES:
FRACTIONAL $\pm 1/16$
ANGULAR: $\pm 1^\circ$
MACH: BEND ± 0.01
TWO PLACE DECIMAL ± 0.01
THREE PLACE DECIMAL ± 0.005

INTERPRET GEOMETRIC
TOLERANCING PER:

MATERIAL
ALUM 6061
FINISH

DO NOT SCALE DRAWING

PROPRIETARY AND CONFIDENTIAL
THE INFORMATION CONTAINED IN THIS
DRAWING IS THE SOLE PROPERTY OF
AOSL OF MEMORIAL UNIVERSITY. ANY
REPRODUCTION IN PART OR AS A
WHOLE WITHOUT THE WRITTEN
PERMISSION OF AOSL IS PROHIBITED.

NAME DATE

H. WANG 2012-04-18

DRAWN

CHECKED

ENG APPR.

MFG APPR.

Q.A.

COMMENTS:

QTY.: 1



AOSL - Memorial University

TITLE:

SIZE DWG. NO.

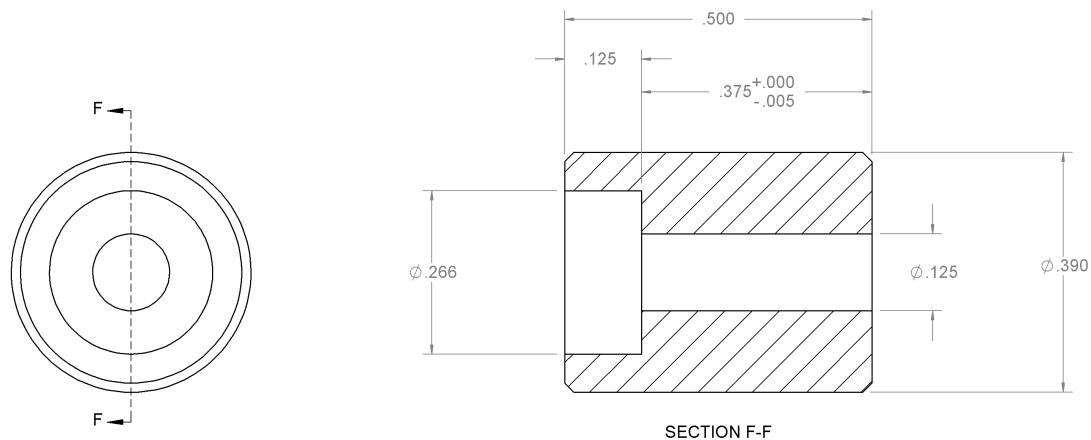
A

D005

REV

SCALE: 2:1 WEIGHT:

SHEET 1 OF 1



UNLESS OTHERWISE SPECIFIED:
DIMENSIONS ARE IN INCHES

TOLERANCES:
FRACTIONAL $\pm 1/16$
ANGULAR: $\pm 1^\circ$
MACH: BEND ± 0.01
TWO PLACE DECIMAL ± 0.01
THREE PLACE DECIMAL ± 0.005

INTERPRET GEOMETRIC
TOLERANCING PER:

MATERIAL

FINISH

DO NOT SCALE DRAWING

PROPRIETARY AND CONFIDENTIAL
THE INFORMATION CONTAINED IN THIS
DRAWING IS THE SOLE PROPERTY OF
AOSL OF MEMORIAL UNIVERSITY. ANY
REPRODUCTION IN PART OR AS A
WHOLE WITHOUT THE WRITTEN
PERMISSION OF AOSL IS PROHIBITED.

NAME DATE

H. WANG 2012-04-24

DRAWN

CHECKED

ENG APPR.

MFG APPR.

Q.A.

COMMENTS:

QTY.: 2



AOSL - Memorial University

TITLE:

SIZE DWG. NO.

A

D006

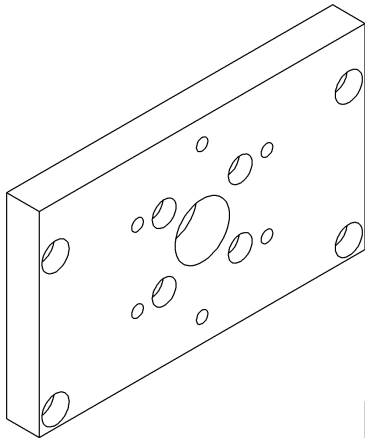
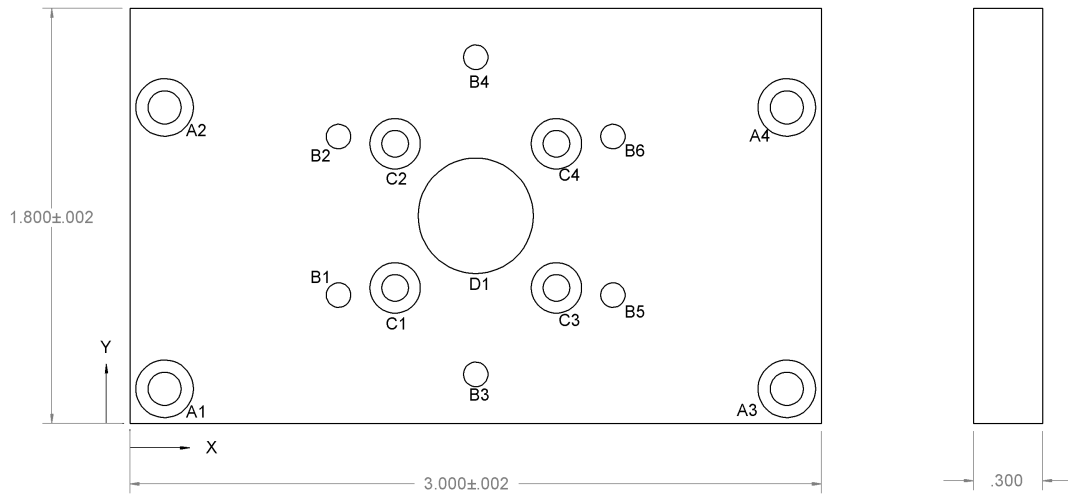
REV

SCALE: 4:1

WEIGHT:

SHEET 1 OF 1

TAG	X LOC	Y LOC	SIZE
A1	.1500	.1500	ϕ .144 THRU ALL └┐ ϕ .250 ∇ .140
A2	.1500	1.3700	
A3	2.8500	.1500	
A4	2.8500	1.3700	
B1	.9046	.5563	ϕ .107 THRU ALL 6-32 UNC THRU ALL
B2	.9046	1.2438	
B3	1.5000	.2125	
B4	1.5000	1.5875	
B5	2.0954	.5563	
B6	2.0954	1.2438	
C1	1.1500	.5875	ϕ .116 THRU ALL └┐ ϕ .219 ∇ .120
C2	1.1500	1.2125	
C3	1.8500	.5875	
C4	1.8500	1.2125	
D1	1.5000	.9000	ϕ .500 THRU

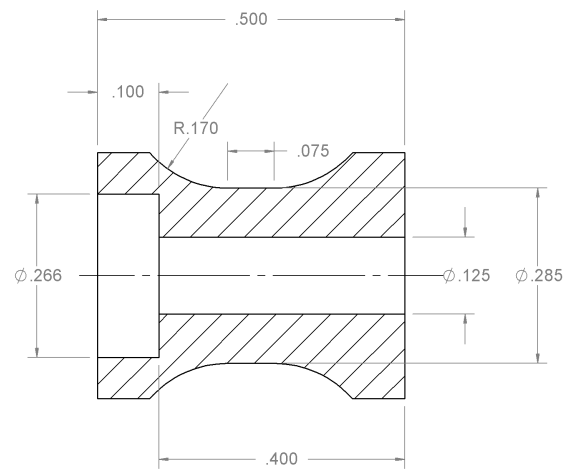
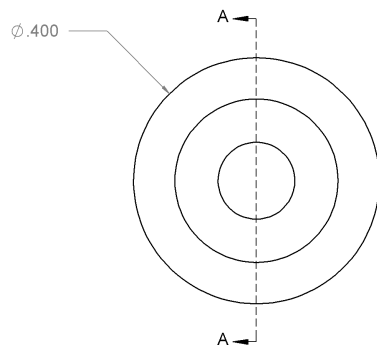


PROPRIETARY AND CONFIDENTIAL
THE INFORMATION CONTAINED IN THIS
DRAWING IS THE SOLE PROPERTY OF
AOSL OF MEMORIAL UNIVERSITY. ANY
REPRODUCTION IN PART OR AS A
WHOLE WITHOUT THE WRITTEN
PERMISSION OF AOSL IS PROHIBITED.

UNLESS OTHERWISE SPECIFIED:
DIMENSIONS ARE IN INCHES
TOLERANCES:
FRACTIONAL \pm 1/16
ANGULAR: \pm 1°
MACH: BEND \pm 0.01
TWO PLACE DECIMAL \pm 0.01
THREE PLACE DECIMAL \pm 0.005
INTERPRET GEOMETRIC
TOLERANCING PER:
MATERIAL
ALUM 6061 T6
FINISH
DO NOT SCALE DRAWING

	NAME	DATE
DRAWN	H. WANG	2012-04-17
CHECKED		
ENG APPR.		
MFG APPR.		
Q.A.		
COMMENTS:		
QTY.: 1		

AOSL - Memorial University		
TITLE:		
End Cover Plate A		
SIZE	DWG. NO.	REV
A	D007	
SCALE: 1:1	WEIGHT:	SHEET 1 OF 1



SECTION A-A

UNLESS OTHERWISE SPECIFIED:
DIMENSIONS ARE IN INCHES

TOLERANCES:
FRACTIONAL $\pm 1/16$
ANGULAR: $\pm 1^\circ$
MACH: BEND ± 0.01
TWO PLACE DECIMAL ± 0.01
THREE PLACE DECIMAL ± 0.005

INTERPRET GEOMETRIC
TOLERANCING PER:

MATERIAL

FINISH

DO NOT SCALE DRAWING

PROPRIETARY AND CONFIDENTIAL
THE INFORMATION CONTAINED IN THIS
DRAWING IS THE SOLE PROPERTY OF
AOSL OF MEMORIAL UNIVERSITY. ANY
REPRODUCTION IN PART OR AS A
WHOLE WITHOUT THE WRITTEN
PERMISSION OF AOSL IS PROHIBITED.

NAME DATE

H. WANG 2012-04-18

DRAWN

CHECKED

ENG APPR.

MFG APPR.

Q.A.

COMMENTS:

QTY.: 2



AOSL - Memorial University

TITLE:

SIZE DWG. NO.

A

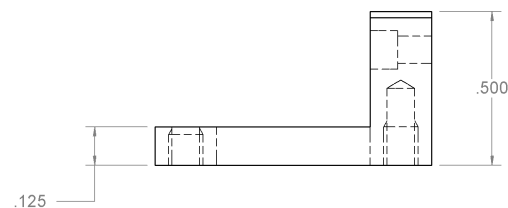
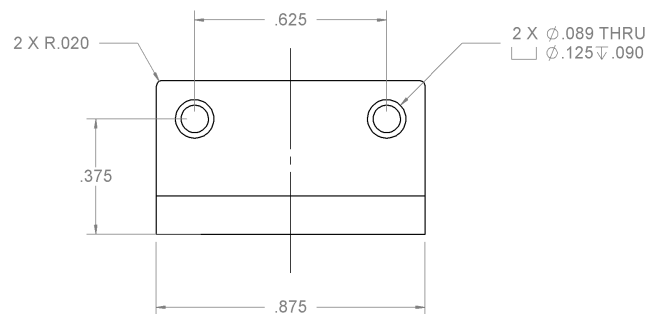
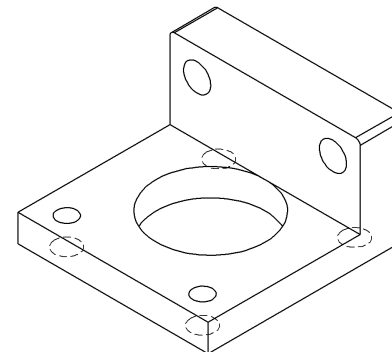
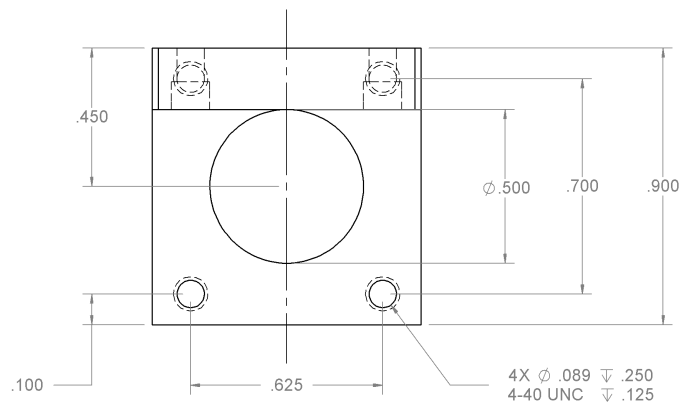
D008

REV

SCALE: 4:1

WEIGHT:

SHEET 1 OF 1



UNLESS OTHERWISE SPECIFIED:
DIMENSIONS ARE IN INCHES

TOLERANCES:
FRACTIONAL $\pm 1/16$
ANGULAR: $\pm 1^\circ$
MACH: ± 0.01
BEND: ± 0.01
TWO PLACE DECIMAL: ± 0.01
THREE PLACE DECIMAL: ± 0.005

INTERPRET GEOMETRIC
TOLERANCING PER:

MATERIAL
ALUM 6061 T6

FINISH

DO NOT SCALE DRAWING

NAME DATE

H. WANG 2012-04-18

DRAWN

CHECKED

ENG APPR.

MFG APPR.

Q.A.

COMMENTS:

QTY.: 2



AOSL - Memorial University

TITLE:

Cable Guide Bracket

SIZE DWG. NO.

A

D009

REV

SCALE: 2:1

WEIGHT:

SHEET 1 OF 1

PROPRIETARY AND CONFIDENTIAL
THE INFORMATION CONTAINED IN THIS
DRAWING IS THE SOLE PROPERTY OF
AOSL OF MEMORIAL UNIVERSITY. ANY
REPRODUCTION IN PART OR AS A
WHOLE WITHOUT THE WRITTEN
PERMISSION OF AOSL IS PROHIBITED.



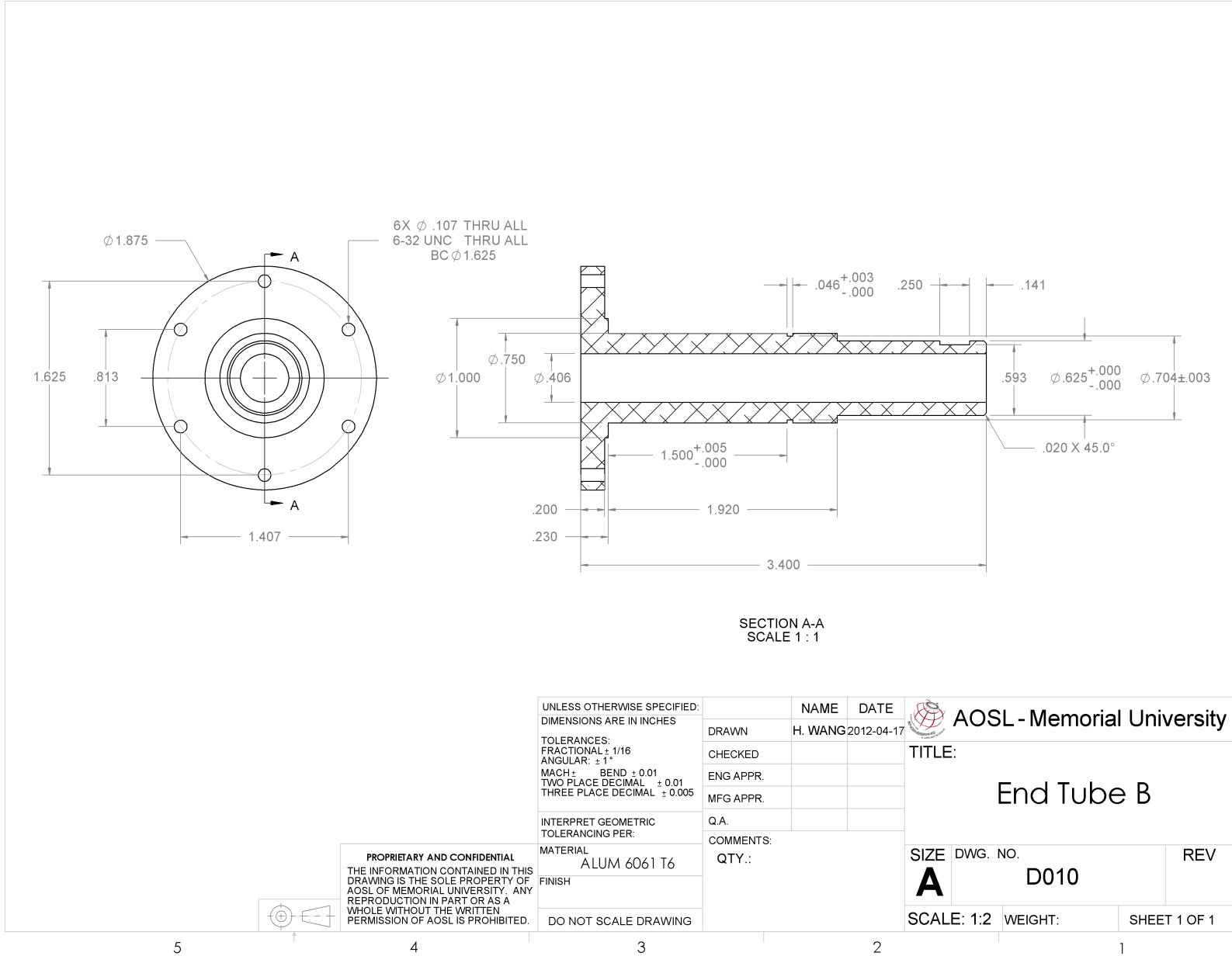
5

4

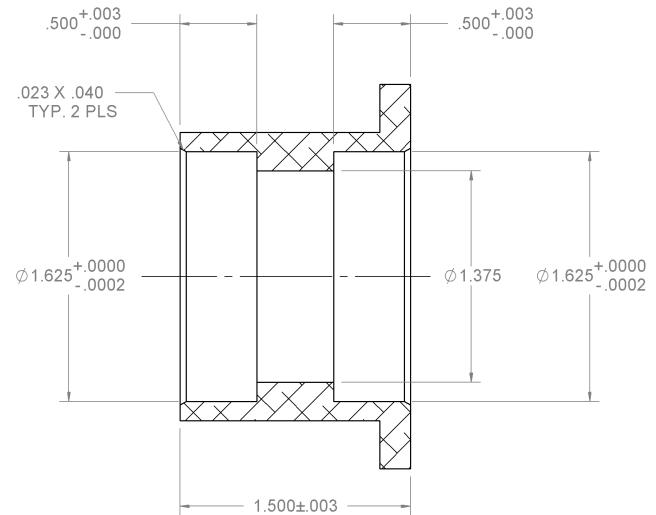
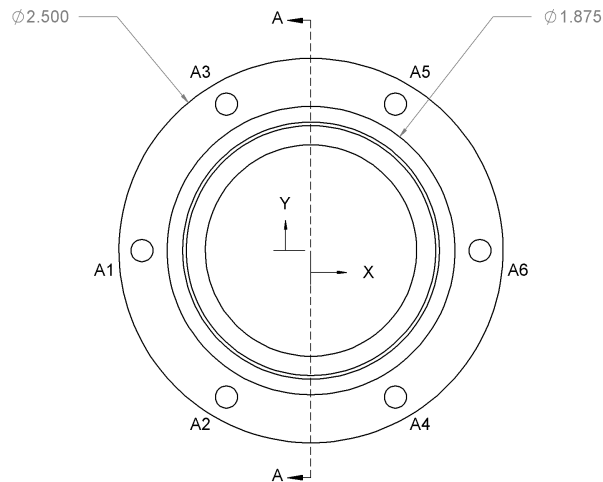
3

2

1



TAG	X LOC	Y LOC	SIZE
A1	-1.1000	.0000	$\phi .144 \nabla .213$
A2	-.5500	-.9526	
A3	-.5500	.9526	
A4	.5500	-.9526	
A5	.5500	.9526	
A6	1.1000	.0000	



SECTION A-A

UNLESS OTHERWISE SPECIFIED:
DIMENSIONS ARE IN INCHES

TOLERANCES:
FRACTIONAL $\pm 1/16$
ANGULAR: $\pm 1^\circ$
MACH: ± 0.01
BEND: ± 0.01
TWO PLACE DECIMAL: ± 0.01
THREE PLACE DECIMAL: ± 0.005

INTERPRET GEOMETRIC
TOLERANCING PER:

MATERIAL
ALUM 6061 T6

FINISH

DO NOT SCALE DRAWING

PROPRIETARY AND CONFIDENTIAL
THE INFORMATION CONTAINED IN THIS
DRAWING IS THE SOLE PROPERTY OF
AOSL OF MEMORIAL UNIVERSITY. ANY
REPRODUCTION IN PART OR AS A
WHOLE WITHOUT THE WRITTEN
PERMISSION OF AOSL IS PROHIBITED.

NAME DATE

H. WANG 2012-04-18

DRAWN

CHECKED

ENG APPR.

MFG APPR.

Q.A.

COMMENTS:

QTY.: 1



AOSL - Memorial University

TITLE:

Bearing Housing

SIZE DWG. NO.

A

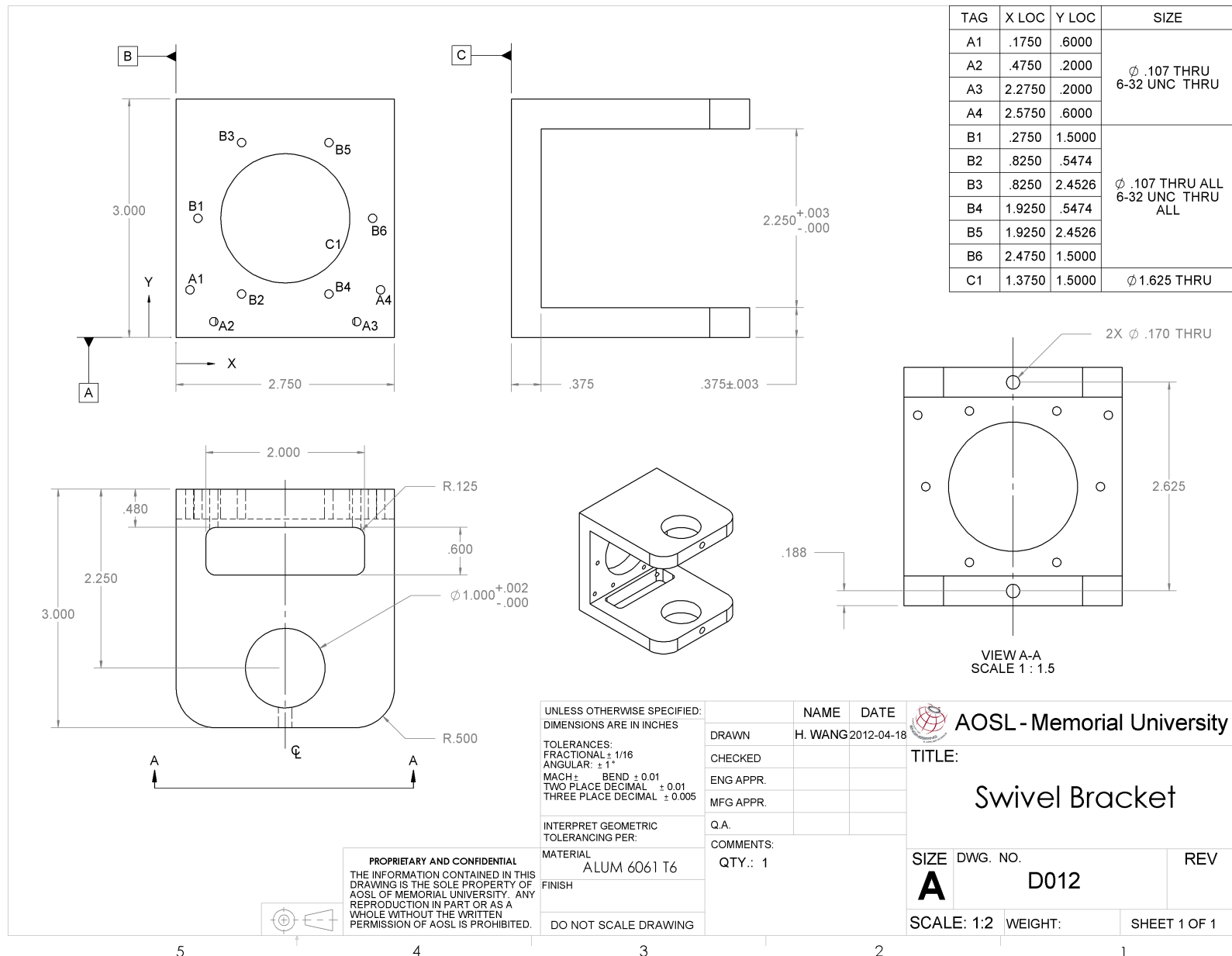
D011

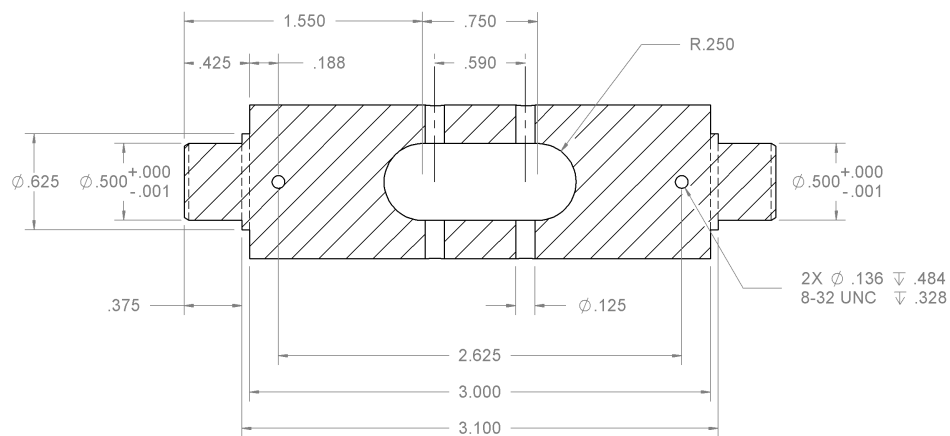
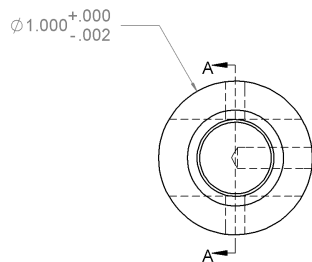
REV

SCALE: 1:1

WEIGHT:

SHEET 1 OF 1





SECTION A-A
SCALE 1 : 1

UNLESS OTHERWISE SPECIFIED:
DIMENSIONS ARE IN INCHES

TOLERANCES:
FRACTIONAL $\pm 1/16$
ANGULAR: $\pm 1^\circ$
MACH: BEND ± 0.01
TWO PLACE DECIMAL ± 0.01
THREE PLACE DECIMAL ± 0.005

INTERPRET GEOMETRIC
TOLERANCING PER:

MATERIAL
ALUM 6061
FINISH

DO NOT SCALE DRAWING

PROPRIETARY AND CONFIDENTIAL
THE INFORMATION CONTAINED IN THIS
DRAWING IS THE SOLE PROPERTY OF
AOSL OF MEMORIAL UNIVERSITY. ANY
REPRODUCTION IN PART OR AS A
WHOLE WITHOUT THE WRITTEN
PERMISSION OF AOSL IS PROHIBITED.

NAME DATE
H. WANG 2012-04-18

DRAWN
CHECKED
ENG APPR.
MFG APPR.

Q.A.
COMMENTS:
QTY.: 1



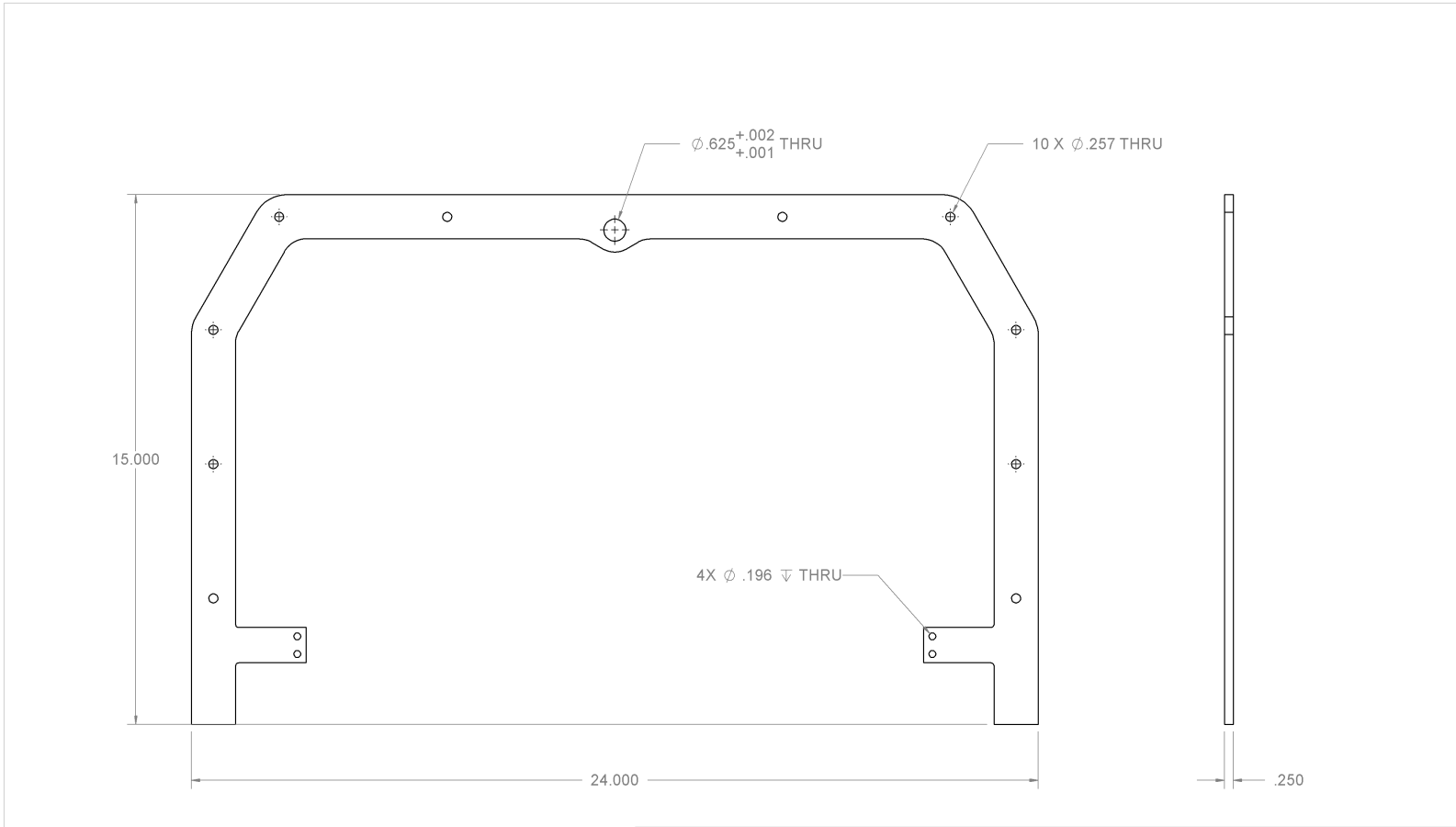
AOSL - Memorial University

TITLE:

Swivel Shaft

SIZE DWG. NO. REV
A **D013**

SCALE: 1:2 WEIGHT: SHEET 1 OF 1

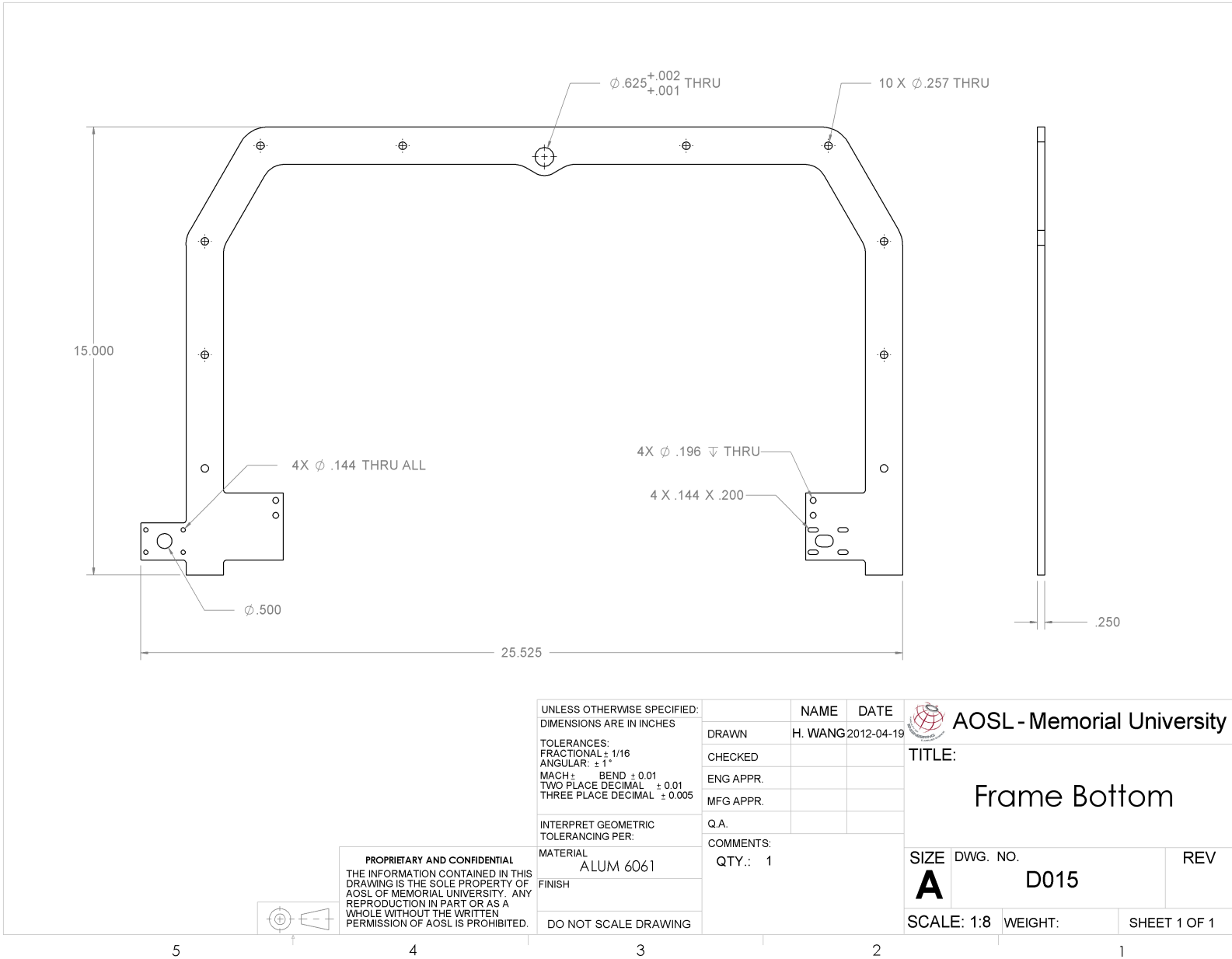


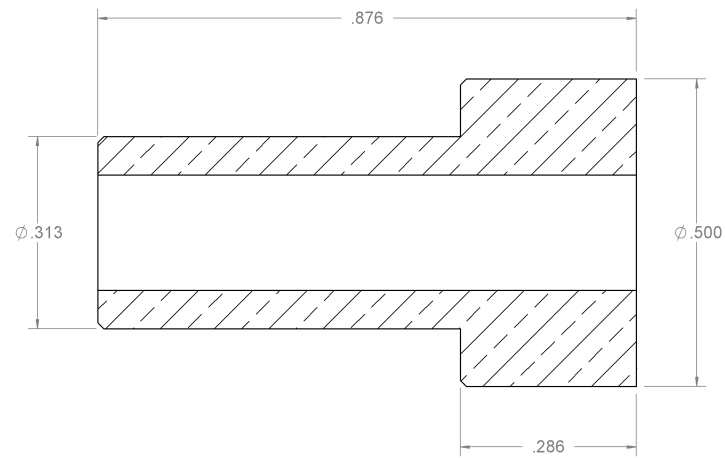
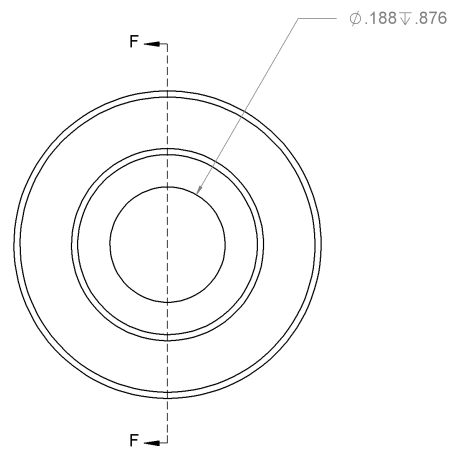
PROPRIETARY AND CONFIDENTIAL
THE INFORMATION CONTAINED IN THIS
DRAWING IS THE SOLE PROPERTY OF
AOSL OF MEMORIAL UNIVERSITY. ANY
REPRODUCTION IN PART OR AS A
WHOLE WITHOUT THE WRITTEN
PERMISSION OF AOSL IS PROHIBITED.

UNLESS OTHERWISE SPECIFIED: DIMENSIONS ARE IN INCHES	
TOLERANCES:	
FRACTIONAL $\pm 1/16$	
ANGULAR: $\pm 1^\circ$	
MACH: BEND ± 0.01	
TWO PLACE DECIMAL ± 0.01	
THREE PLACE DECIMAL ± 0.005	
INTERPRET GEOMETRIC TOLERANCING PER:	
MATERIAL	ALUM 6061
FINISH	
DO NOT SCALE DRAWING	

NAME	DATE
H. WANG	2012-04-19
DRAWN	
CHECKED	
ENG APPR.	
MFG APPR.	
Q.A.	
COMMENTS:	
QTY.: 1	

AOSL - Memorial University	
TITLE:	
Frame Top	
SIZE	DWG. NO.
A	D014
SCALE: 1:8	WEIGHT:
SHEET 1 OF 1	REV





SECTION F-F
SCALE 4 : 1

UNLESS OTHERWISE SPECIFIED:
DIMENSIONS ARE IN INCHES

TOLERANCES:
FRACTIONAL $\pm 1/16$
ANGULAR: $\pm 1^\circ$
MACH: BEND ± 0.01
TWO PLACE DECIMAL ± 0.01
THREE PLACE DECIMAL ± 0.005

INTERPRET GEOMETRIC
TOLERANCING PER:

MATERIAL
Brass

FINISH

DO NOT SCALE DRAWING

NAME DATE

H. WANG 2012-04-24



AOSL - Memorial University

TITLE:

Tensioner Shaft

SIZE DWG. NO.

A

D016

REV

SCALE: 2:1

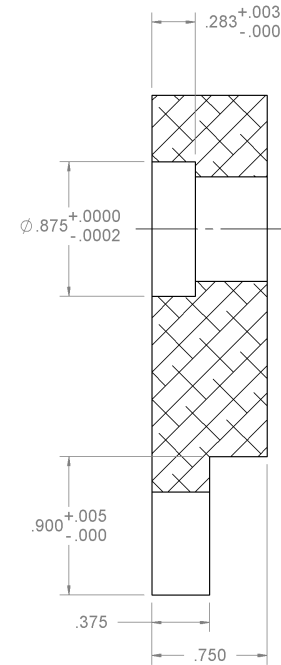
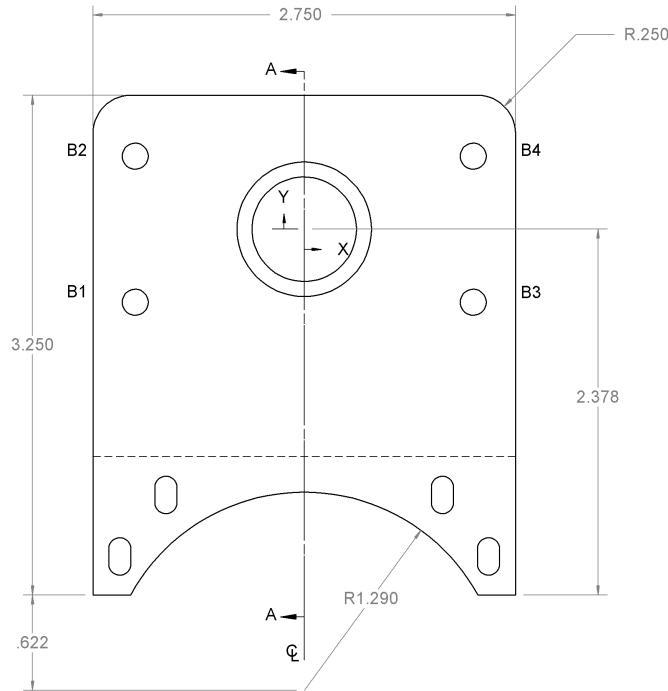
WEIGHT:

SHEET 1 OF 1

PROPRIETARY AND CONFIDENTIAL
THE INFORMATION CONTAINED IN THIS
DRAWING IS THE SOLE PROPERTY OF
AOSL OF MEMORIAL UNIVERSITY. ANY
REPRODUCTION IN PART OR AS A
WHOLE WITHOUT THE WRITTEN
PERMISSION OF AOSL IS PROHIBITED.



TAG	X LOC	Y LOC	SIZE
B1	-1.1000	-.4750	Ø .170 THRU
B2	-1.1000	.4750	
B3	1.1000	-.4750	
B4	1.1000	.4750	



SECTION A-A

UNLESS OTHERWISE SPECIFIED:
DIMENSIONS ARE IN INCHES

TOLERANCES:
FRACTIONAL: $\pm 1/16$
ANGULAR: $\pm 1^\circ$
MACH: $\pm .001$
BEND: ± 0.01
TWO PLACE DECIMAL: ± 0.01
THREE PLACE DECIMAL: ± 0.005

INTERPRET GEOMETRIC
TOLERANCING PER:

MATERIAL
ALUM 6061 T6

FINISH

DO NOT SCALE DRAWING

DRAWN	NAME	DATE
CHECKED	H. WANG	2012-04-18
ENG APPR.		
MFG APPR.		
Q.A.		
COMMENTS:		
QTY.: 1		



AOSL - Memorial University

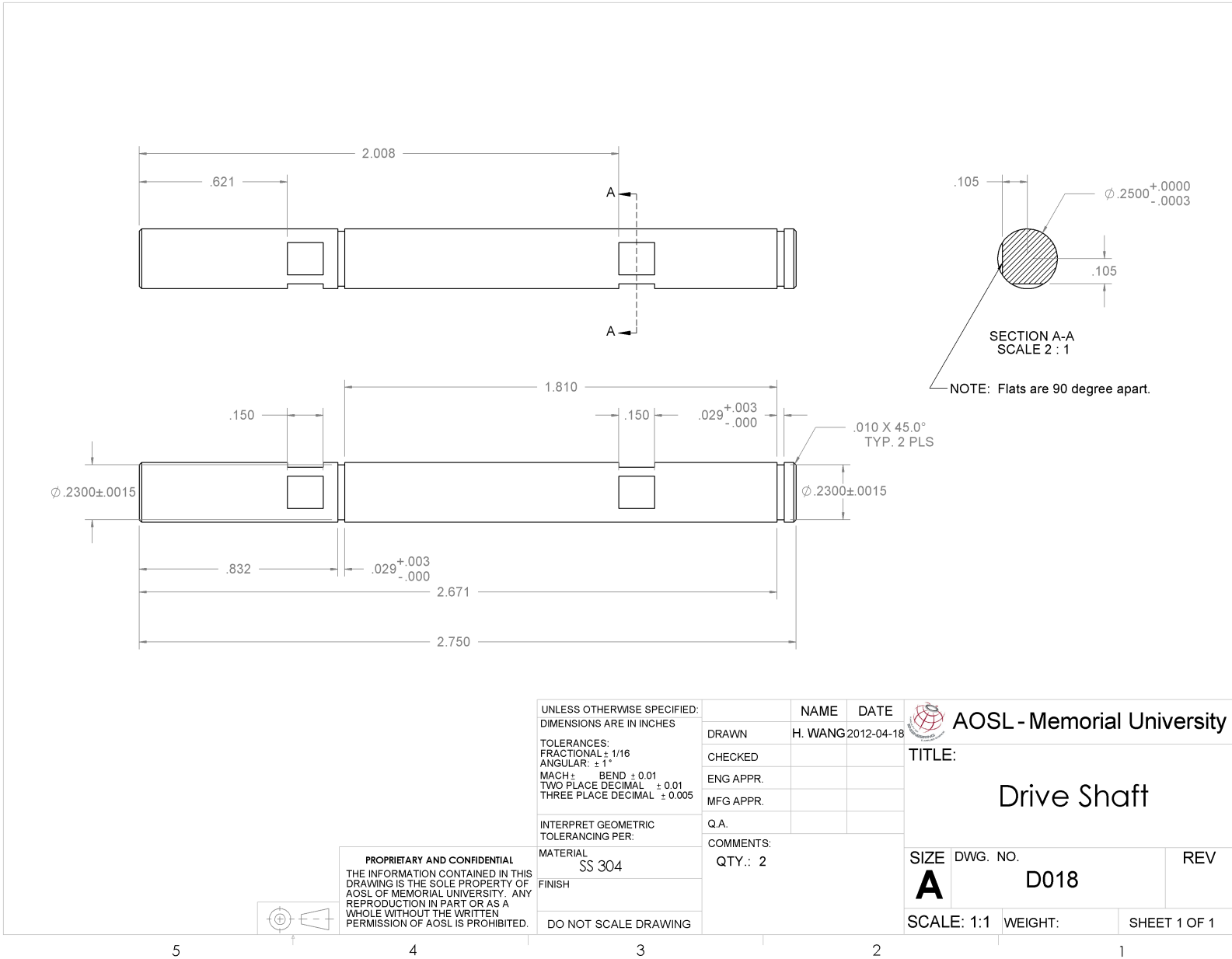
TITLE:

Mounting Bracket

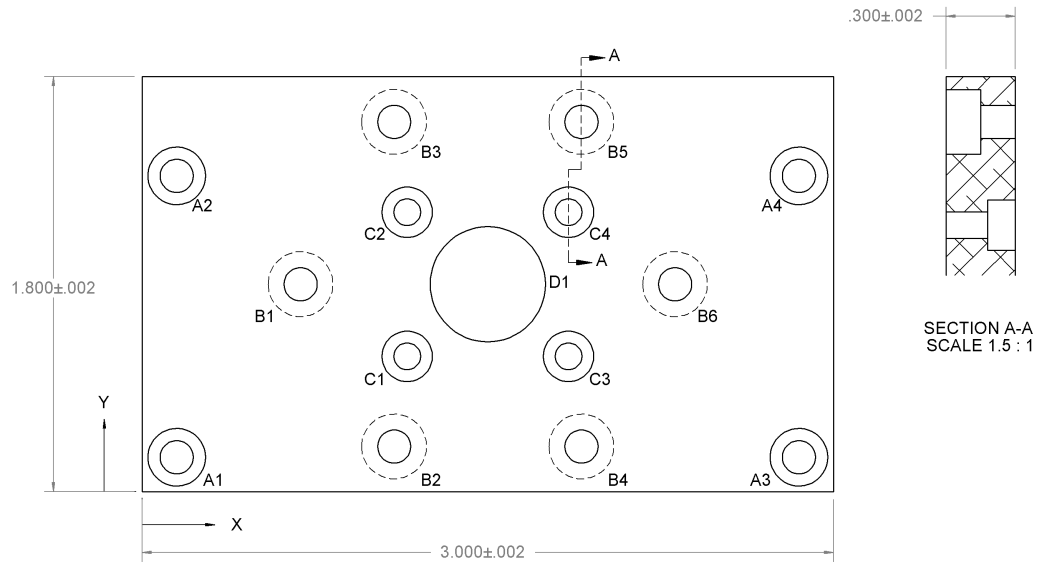
SIZE	DWG. NO.	REV
A	D017	
SCALE: 1:1	WEIGHT:	SHEET 1 OF 1

PROPRIETARY AND CONFIDENTIAL
THE INFORMATION CONTAINED IN THIS
DRAWING IS THE SOLE PROPERTY OF
AOSL OF MEMORIAL UNIVERSITY. ANY
REPRODUCTION IN PART OR AS A
WHOLE WITHOUT THE WRITTEN
PERMISSION OF AOSL IS PROHIBITED.





TAG	X LOC	Y LOC	SIZE
A1	.1500	.1500	$\phi .144$ THRU ALL $\sqcup \phi .250 \nabla .150$
A2	.1500	1.3700	
A3	2.8500	.1500	
A4	2.8500	1.3700	
B1	.6875	.9000	$\phi .144$ THRU ALL $\sqcup \phi .281 \nabla .150$
B2	1.0938	.1964	
B3	1.0938	1.6036	
B4	1.9063	.1964	
B5	1.9063	1.6036	
B6	2.3125	.9000	
C1	1.1500	.5875	$\phi .116$ THRU ALL $\sqcup \phi .219 \nabla .120$
C2	1.1500	1.2125	
C3	1.8500	.5875	
C4	1.8500	1.2125	
D1	1.5000	.9000	$\phi .500$ THRU



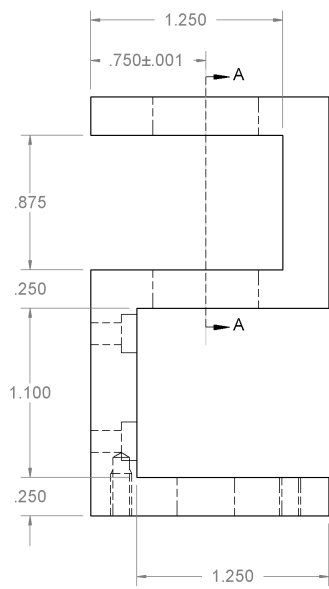
SECTION A-A
SCALE 1.5 : 1

PROPRIETARY AND CONFIDENTIAL
THE INFORMATION CONTAINED IN THIS
DRAWING IS THE SOLE PROPERTY OF
AOSL OF MEMORIAL UNIVERSITY. ANY
REPRODUCTION IN PART OR AS A
WHOLE WITHOUT THE WRITTEN
PERMISSION OF AOSL IS PROHIBITED.

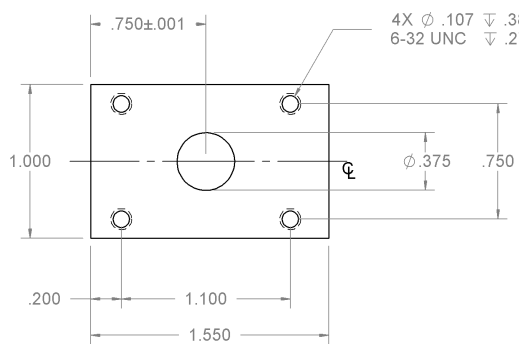
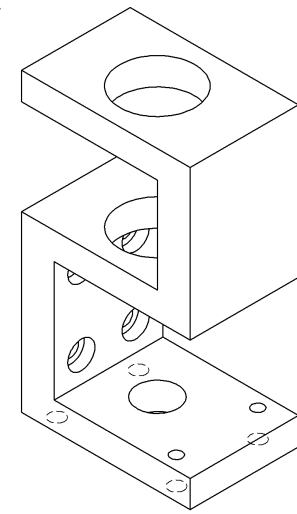
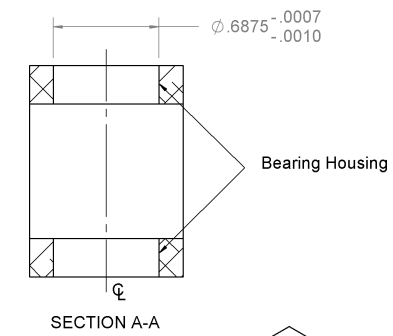
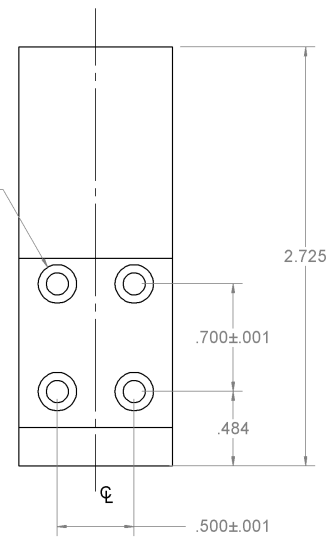
UNLESS OTHERWISE SPECIFIED:
DIMENSIONS ARE IN INCHES
TOLERANCES:
FRACTIONAL $\pm 1/16$
ANGULAR: $\pm 1^\circ$
MACH: $\pm .001$
BEND: ± 0.01
TWO PLACE DECIMAL: ± 0.01
THREE PLACE DECIMAL: ± 0.005
INTERPRET GEOMETRIC
TOLERANCING PER:
MATERIAL
ALUM 6061 T6
FINISH
DO NOT SCALE DRAWING

NAME	H. WANG	DATE	2012-04-17
DRAWN			
CHECKED			
ENG APPR.			
MFG APPR.			
Q.A.			
COMMENTS:	QTY.: 1		

AOSL - Memorial University	
TITLE: End Cover Plate B	
SIZE A	DWG. NO. D019
SCALE: 1:1	WEIGHT:
SHEET 1 OF 1	



4X ϕ .144 THRU ALL
 \perp ϕ .250 ∇ .100



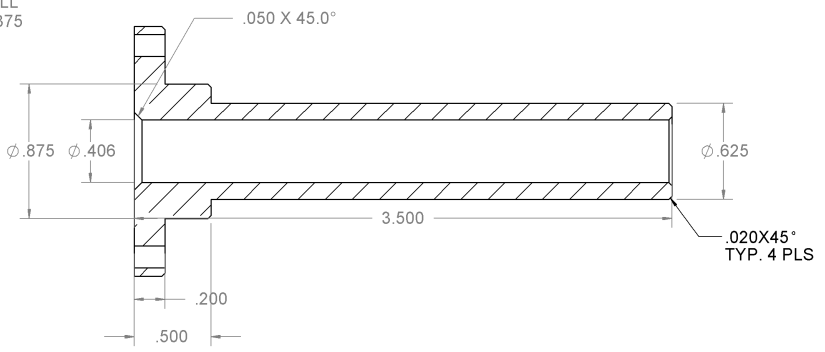
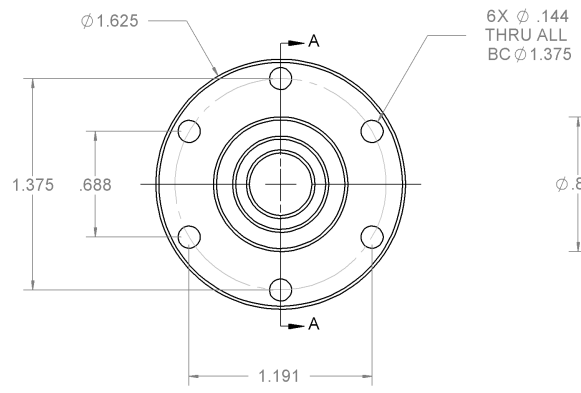
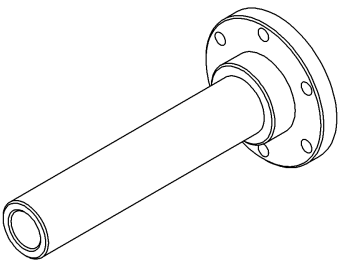
4X ϕ .107 ∇ .380
 6-32 UNC ∇ .276

PROPRIETARY AND CONFIDENTIAL
 THE INFORMATION CONTAINED IN THIS
 DRAWING IS THE SOLE PROPERTY OF
 AOSL OF MEMORIAL UNIVERSITY. ANY
 REPRODUCTION IN PART OR AS A
 WHOLE WITHOUT THE WRITTEN
 PERMISSION OF AOSL IS PROHIBITED.

UNLESS OTHERWISE SPECIFIED: DIMENSIONS ARE IN INCHES	
TOLERANCES:	
FRACTIONAL \pm 1/16	
ANGULAR: \pm 1°	
MACH: BEND \pm 0.01	
TWO PLACE DECIMAL \pm 0.01	
THREE PLACE DECIMAL \pm 0.005	
INTERPRET GEOMETRIC TOLERANCING PER:	
MATERIAL	ALUM 6061 T6
FINISH	
DO NOT SCALE DRAWING	

NAME	DATE
DRAWN H. WANG	2012-04-20
CHECKED	
ENG APPR.	
MFG APPR.	
Q.A.	
COMMENTS:	
QTY.: 1	

AOSL - Memorial University	
TITLE: Main Drive Mounting	
SIZE A	DWG. NO. D020
SCALE: 1:1	WEIGHT:
SHEET 1 OF 1	REV



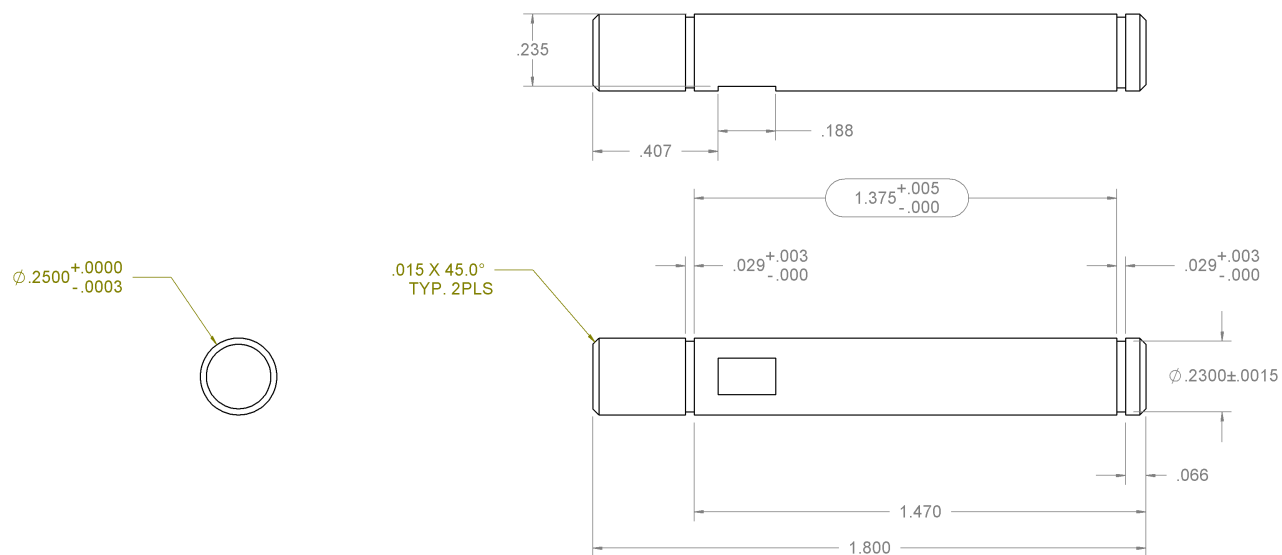
SECTION A-A
SCALE 1 : 1

PROPRIETARY AND CONFIDENTIAL
THE INFORMATION CONTAINED IN THIS
DRAWING IS THE SOLE PROPERTY OF
AOSL OF MEMORIAL UNIVERSITY. ANY
REPRODUCTION IN PART OR AS A
WHOLE WITHOUT THE WRITTEN
PERMISSION OF AOSL IS PROHIBITED.

UNLESS OTHERWISE SPECIFIED:
DIMENSIONS ARE IN INCHES
TOLERANCES:
FRACTIONAL $\pm 1/16$
ANGULAR: $\pm 1^\circ$
MACH: BEND ± 0.01
TWO PLACE DECIMAL ± 0.01
THREE PLACE DECIMAL ± 0.005
INTERPRET GEOMETRIC
TOLERANCING PER:
MATERIAL
ALUM 6061 T6
FINISH
DO NOT SCALE DRAWING

	NAME	DATE
DRAWN	H. WANG	2012-04-17
CHECKED		
ENG APPR.		
MFG APPR.		
Q.A.		
COMMENTS:		
QTY.: 1		

AOSL - Memorial University		
TITLE:		
End Tube A		
SIZE	DWG. NO.	REV
A	D021	
SCALE: 1:2	WEIGHT:	SHEET 1 OF 1



UNLESS OTHERWISE SPECIFIED:
DIMENSIONS ARE IN INCHES

TOLERANCES:
FRACTIONAL $\pm 1/16$
ANGULAR: $\pm 1^\circ$
MACH: BEND ± 0.01
TWO PLACE DECIMAL ± 0.01
THREE PLACE DECIMAL ± 0.005

INTERPRET GEOMETRIC
TOLERANCING PER:

MATERIAL

FINISH

DO NOT SCALE DRAWING

PROPRIETARY AND CONFIDENTIAL
THE INFORMATION CONTAINED IN THIS
DRAWING IS THE SOLE PROPERTY OF
AOSL OF MEMORIAL UNIVERSITY. ANY
REPRODUCTION IN PART OR AS A
WHOLE WITHOUT THE WRITTEN
PERMISSION OF AOSL IS PROHIBITED.

NAME DATE

H. WANG 2012-04-18

DRAWN

CHECKED

ENG APPR.

MFG APPR.

Q.A.

COMMENTS:

QTY.: 1



AOSL - Memorial University

TITLE:

SIZE DWG. NO.

A

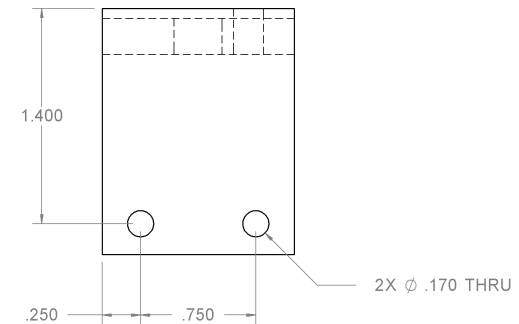
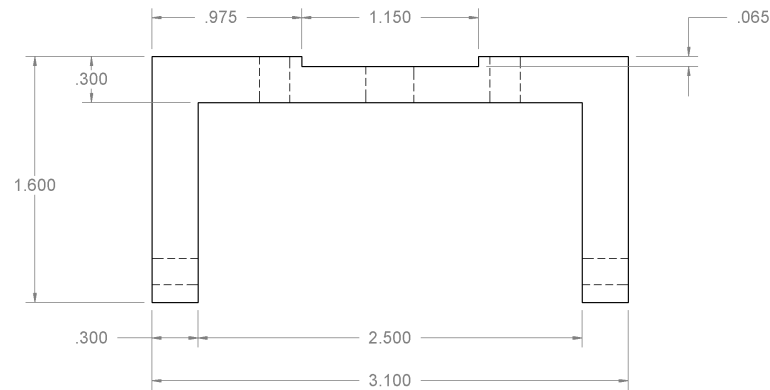
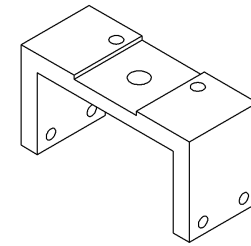
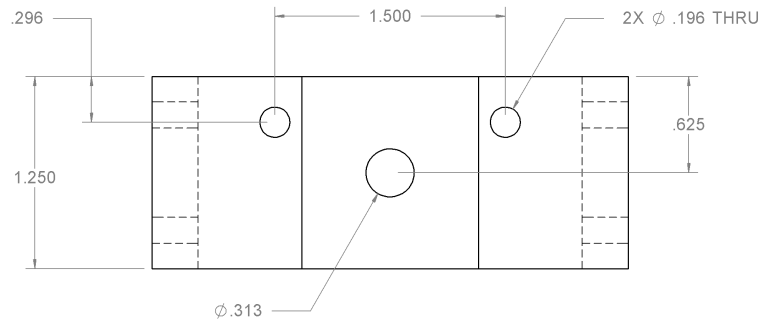
D022

REV

SCALE: 2:1

WEIGHT:

SHEET 1 OF 1



UNLESS OTHERWISE SPECIFIED:
DIMENSIONS ARE IN INCHES

TOLERANCES:
FRACTIONAL $\pm 1/16$
ANGULAR: $\pm 1^\circ$
MACH: ± 0.01
TWO PLACE DECIMAL ± 0.01
THREE PLACE DECIMAL ± 0.005

INTERPRET GEOMETRIC
TOLERANCING PER:

MATERIAL
ALUM 6061

FINISH

DO NOT SCALE DRAWING

PROPRIETARY AND CONFIDENTIAL
THE INFORMATION CONTAINED IN THIS
DRAWING IS THE SOLE PROPERTY OF
AOSL OF MEMORIAL UNIVERSITY. ANY
REPRODUCTION IN PART OR AS A
WHOLE WITHOUT THE WRITTEN
PERMISSION OF AOSL IS PROHIBITED.

NAME DATE

H. WANG 2012-04-18

DRAWN

CHECKED

ENG APPR.

MFG APPR.

Q.A.

COMMENTS:

QTY.: 1



AOSL - Memorial University

TITLE:

Motor Mount T

SIZE DWG. NO.

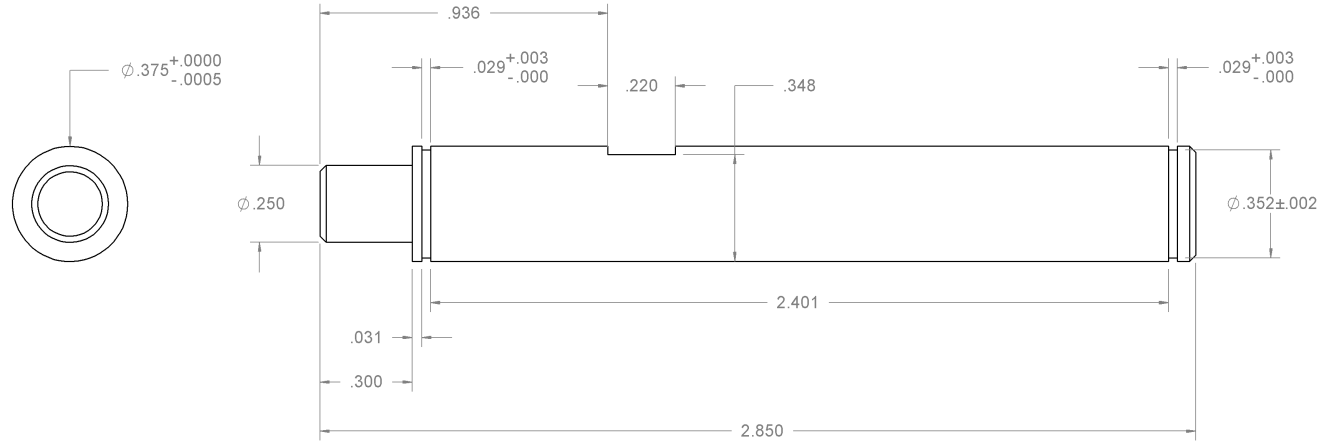
A

D023

REV

SCALE: 1:1 WEIGHT:

SHEET 1 OF 1



UNLESS OTHERWISE SPECIFIED:
DIMENSIONS ARE IN INCHES

TOLERANCES:
FRACTIONAL $\pm 1/16$
ANGULAR: $\pm 1^\circ$
MACH: ± 0.01
BEND: ± 0.01
TWO PLACE DECIMAL: ± 0.005
THREE PLACE DECIMAL: ± 0.005

INTERPRET GEOMETRIC
TOLERANCING PER:

MATERIAL
SS 304

FINISH

DO NOT SCALE DRAWING

NAME DATE

H. WANG 2012-04-18



AOSL - Memorial University

TITLE:

Shaft C

SIZE
A

DWG. NO.
D024

REV

SCALE: 1:1

WEIGHT:

SHEET 1 OF 1

PROPRIETARY AND CONFIDENTIAL
THE INFORMATION CONTAINED IN THIS
DRAWING IS THE SOLE PROPERTY OF
AOSL OF MEMORIAL UNIVERSITY. ANY
REPRODUCTION IN PART OR AS A
WHOLE WITHOUT THE WRITTEN
PERMISSION OF AOSL IS PROHIBITED.



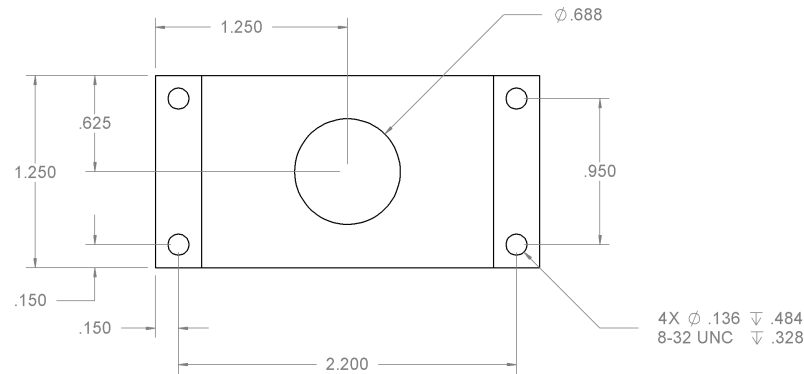
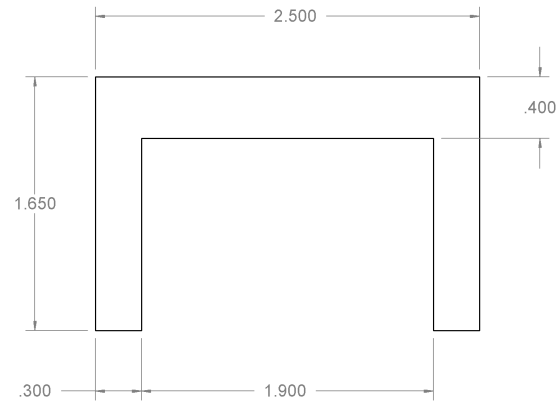
5

4

3

2

1



UNLESS OTHERWISE SPECIFIED:
DIMENSIONS ARE IN INCHES

TOLERANCES:
FRACTIONAL $\pm 1/16$
ANGULAR: $\pm 1^\circ$
MACH: ± 0.01
BEND: ± 0.01
TWO PLACE DECIMAL ± 0.01
THREE PLACE DECIMAL ± 0.005

INTERPRET GEOMETRIC
TOLERANCING PER:

MATERIAL
ALUM 6061

FINISH

DO NOT SCALE DRAWING

NAME DATE

H. WANG 2012-04-18



AOSL - Memorial University

TITLE:

Mounting Bracket C

SIZE DWG. NO.

A

D025

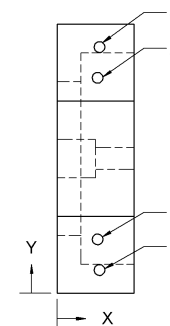
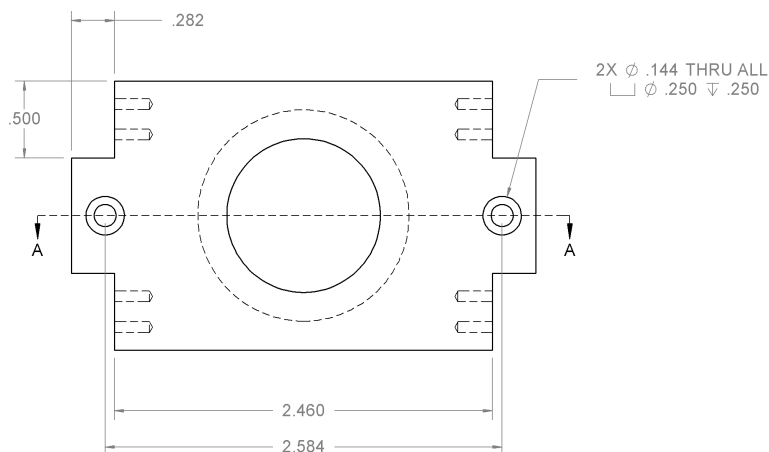
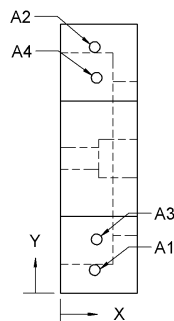
REV

SCALE: 1:1 WEIGHT:

SHEET 1 OF 1

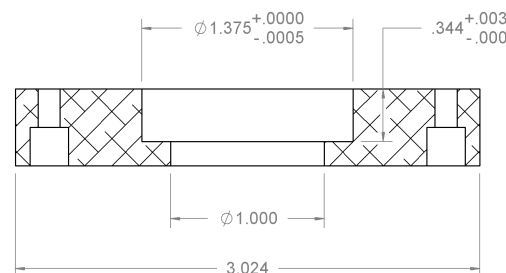
PROPRIETARY AND CONFIDENTIAL
THE INFORMATION CONTAINED IN THIS
DRAWING IS THE SOLE PROPERTY OF
AOSL OF MEMORIAL UNIVERSITY. ANY
REPRODUCTION IN PART OR AS A
WHOLE WITHOUT THE WRITTEN
PERMISSION OF AOSL IS PROHIBITED.





TAG	X LOC	Y LOC	SIZE
A1	.2239	.1500	$\phi .070 \pm .226$ 2-56 UNC $\pm .172$
A2	.2239	1.6000	
A3	.2363	.3496	
A4	.2363	1.4004	

TAG	X LOC	Y LOC	SIZE
1	.2637	.3496	$\phi .070 \pm .226$ 2-56 UNC $\pm .172$
2	.2637	1.4004	
3	.2761	.1500	
4	.2761	1.6000	



SECTION A-A

UNLESS OTHERWISE SPECIFIED:
DIMENSIONS ARE IN INCHES

TOLERANCES:
FRACTIONAL $\pm 1/16$
ANGULAR: $\pm 1^\circ$
MACH: $\pm .001$
BEND ± 0.01
TWO PLACE DECIMAL ± 0.01
THREE PLACE DECIMAL ± 0.005

INTERPRET GEOMETRIC
TOLERANCING PER:

MATERIAL
ALUM 6061 T6

FINISH

DO NOT SCALE DRAWING

NAME DATE

H. WANG 2012-04-18

DRAWN

CHECKED

ENG APPR.

MFG APPR.

Q.A.

COMMENTS:

QTY.: 1



AOSL - Memorial University

TITLE:

End Support

SIZE DWG. NO.

A

D026

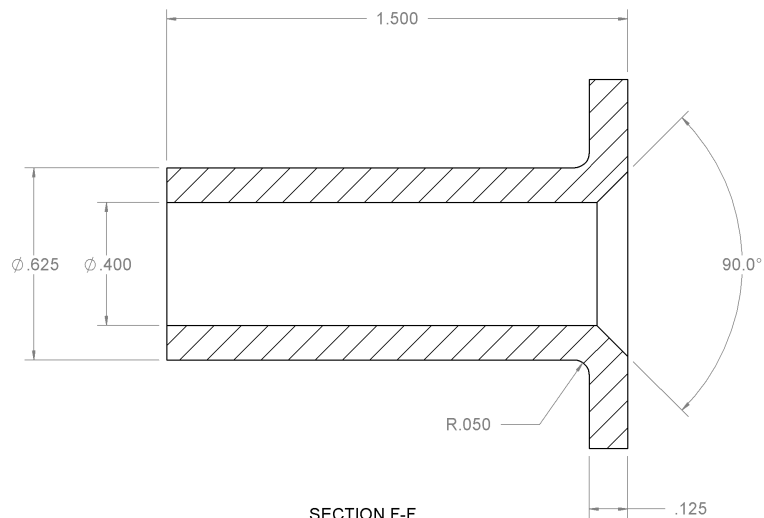
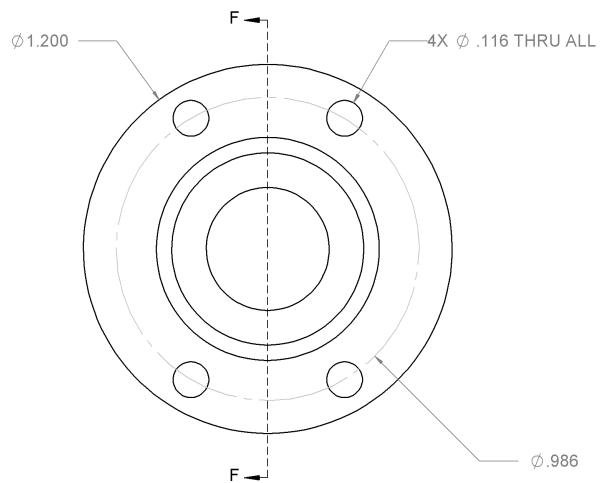
REV

SCALE: 1:1 WEIGHT:

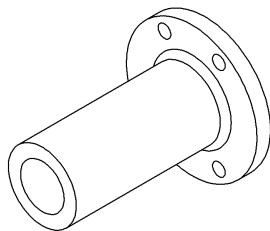
SHEET 1 OF 1

PROPRIETARY AND CONFIDENTIAL
THE INFORMATION CONTAINED IN THIS
DRAWING IS THE SOLE PROPERTY OF
AOSL OF MEMORIAL UNIVERSITY. ANY
REPRODUCTION IN PART OR AS A
WHOLE WITHOUT THE WRITTEN
PERMISSION OF AOSL IS PROHIBITED.





SECTION F-F
SCALE 2 : 1



UNLESS OTHERWISE SPECIFIED:
DIMENSIONS ARE IN INCHES

TOLERANCES:
FRACTIONAL $\pm 1/16$
ANGULAR: $\pm 1^\circ$
MACH: BEND ± 0.01
TWO PLACE DECIMAL ± 0.01
THREE PLACE DECIMAL ± 0.005

INTERPRET GEOMETRIC
TOLERANCING PER:

MATERIAL

FINISH

DO NOT SCALE DRAWING

PROPRIETARY AND CONFIDENTIAL
THE INFORMATION CONTAINED IN THIS
DRAWING IS THE SOLE PROPERTY OF
AOSL OF MEMORIAL UNIVERSITY. ANY
REPRODUCTION IN PART OR AS A
WHOLE WITHOUT THE WRITTEN
PERMISSION OF AOSL IS PROHIBITED.

NAME DATE

H. WANG 2012-04-20

DRAWN

CHECKED

ENG APPR.

MFG APPR.

Q.A.

COMMENTS:

QTY.:



AOSL - Memorial University

TITLE:

SIZE DWG. NO.

A

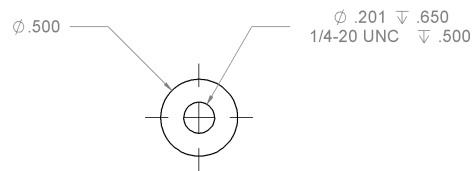
D027

REV

SCALE: 1:1

WEIGHT:


SHEET 1 OF 1

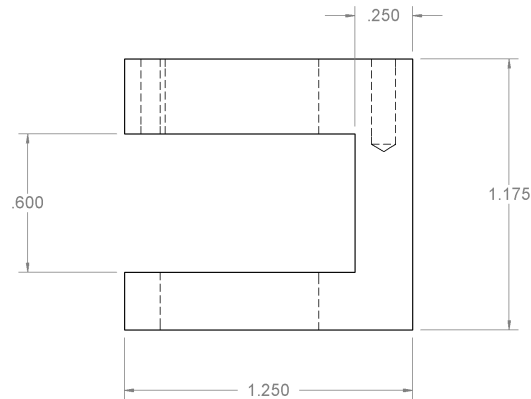
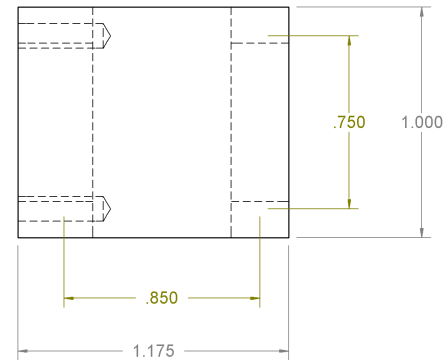
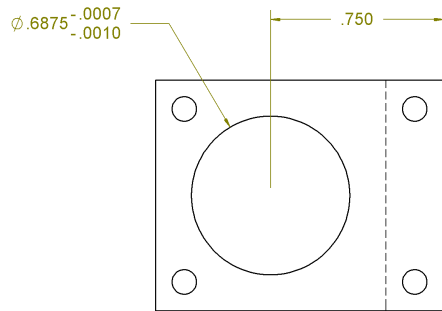


PROPRIETARY AND CONFIDENTIAL
 THE INFORMATION CONTAINED IN THIS
 DRAWING IS THE SOLE PROPERTY OF
 AOSL OF MEMORIAL UNIVERSITY. ANY
 REPRODUCTION IN PART OR AS A
 WHOLE WITHOUT THE WRITTEN
 PERMISSION OF AOSL IS PROHIBITED.

UNLESS OTHERWISE SPECIFIED:
 DIMENSIONS ARE IN INCHES
 TOLERANCES:
 FRACTIONAL $\pm 1/16$
 ANGULAR: $\pm 1^\circ$
 MACH: BEND ± 0.01
 TWO PLACE DECIMAL ± 0.01
 THREE PLACE DECIMAL ± 0.005
 INTERPRET GEOMETRIC
 TOLERANCING PER:
 MATERIAL
 FINISH
 DO NOT SCALE DRAWING

	NAME	DATE
DRAWN	H. WANG	2012-04-26
CHECKED		
ENG APPR.		
MFG APPR.		
Q.A.		
COMMENTS:		
QTY.:		

 AOSL - Memorial University		
TITLE:		
SIZE	DWG. NO.	REV
A	D029	
SCALE: 1:1	WEIGHT:	SHEET 1 OF 1



UNLESS OTHERWISE SPECIFIED:
DIMENSIONS ARE IN INCHES

TOLERANCES:
FRACTIONAL: $\pm 1/16$
ANGULAR: $\pm 1^\circ$
MACH: BEND ± 0.01
TWO PLACE DECIMAL: ± 0.01
THREE PLACE DECIMAL: ± 0.005

INTERPRET GEOMETRIC
TOLERANCING PER:

MATERIAL
ALUM 6061
FINISH

DO NOT SCALE DRAWING

NAME DATE

H. WANG 2012-04-19



AOSL - Memorial University

TITLE:

Wheel Holder

SIZE DWG. NO.

A

D030

REV

SCALE: 2:1

WEIGHT:

SHEET 1 OF 1

PROPRIETARY AND CONFIDENTIAL
THE INFORMATION CONTAINED IN THIS
DRAWING IS THE SOLE PROPERTY OF
AOSL OF MEMORIAL UNIVERSITY. ANY
REPRODUCTION IN PART OR AS A
WHOLE WITHOUT THE WRITTEN
PERMISSION OF AOSL IS PROHIBITED.



5

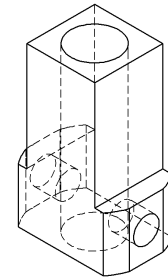
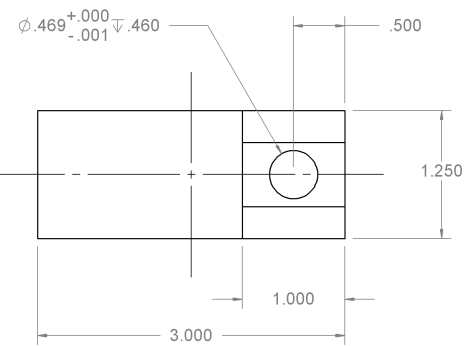
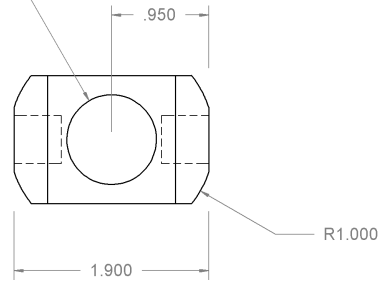
4

3

2

1

$\phi .875^{+.003}_{-.000}$ THRU



UNLESS OTHERWISE SPECIFIED:
DIMENSIONS ARE IN INCHES

TOLERANCES:
FRACTIONAL $\pm 1/16$
ANGULAR: $\pm 1^\circ$
MACH: BEND ± 0.01
TWO PLACE DECIMAL ± 0.01
THREE PLACE DECIMAL ± 0.005

INTERPRET GEOMETRIC
TOLERANCING PER:

MATERIAL
ALUM 6061
FINISH

DO NOT SCALE DRAWING

PROPRIETARY AND CONFIDENTIAL
THE INFORMATION CONTAINED IN THIS
DRAWING IS THE SOLE PROPERTY OF
AOSL OF MEMORIAL UNIVERSITY. ANY
REPRODUCTION IN PART OR AS A
WHOLE WITHOUT THE WRITTEN
PERMISSION OF AOSL IS PROHIBITED.

NAME DATE

H. WANG 2012-04-19

DRAWN
CHECKED
ENG APPR.
MFG APPR.

Q.A.
COMMENTS:
QTY.: 1



AOSL - Memorial University

TITLE:

End Support Bar

SIZE DWG. NO.

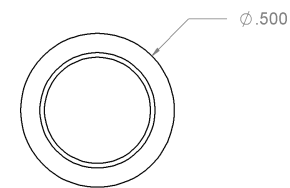
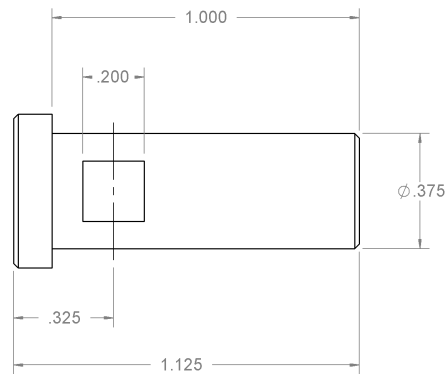
A

D032

REV

SCALE: 1:1 WEIGHT:

SHEET 1 OF 1



UNLESS OTHERWISE SPECIFIED:
DIMENSIONS ARE IN INCHES

TOLERANCES:
FRACTIONAL $\pm 1/16$
ANGULAR: $\pm 1^\circ$
MACH: BEND ± 0.01
TWO PLACE DECIMAL ± 0.01
THREE PLACE DECIMAL ± 0.005

INTERPRET GEOMETRIC
TOLERANCING PER:

MATERIAL
SS 304

FINISH

DO NOT SCALE DRAWING

NAME DATE

H. WANG 2012-04-19

DRAWN

CHECKED

ENG APPR.

MFG APPR.

Q.A.

COMMENTS:

QTY.: 2



AOSL - Memorial University

TITLE:

Shaft Pin Short

SIZE DWG. NO.

A

D033

REV

SCALE: 4:1

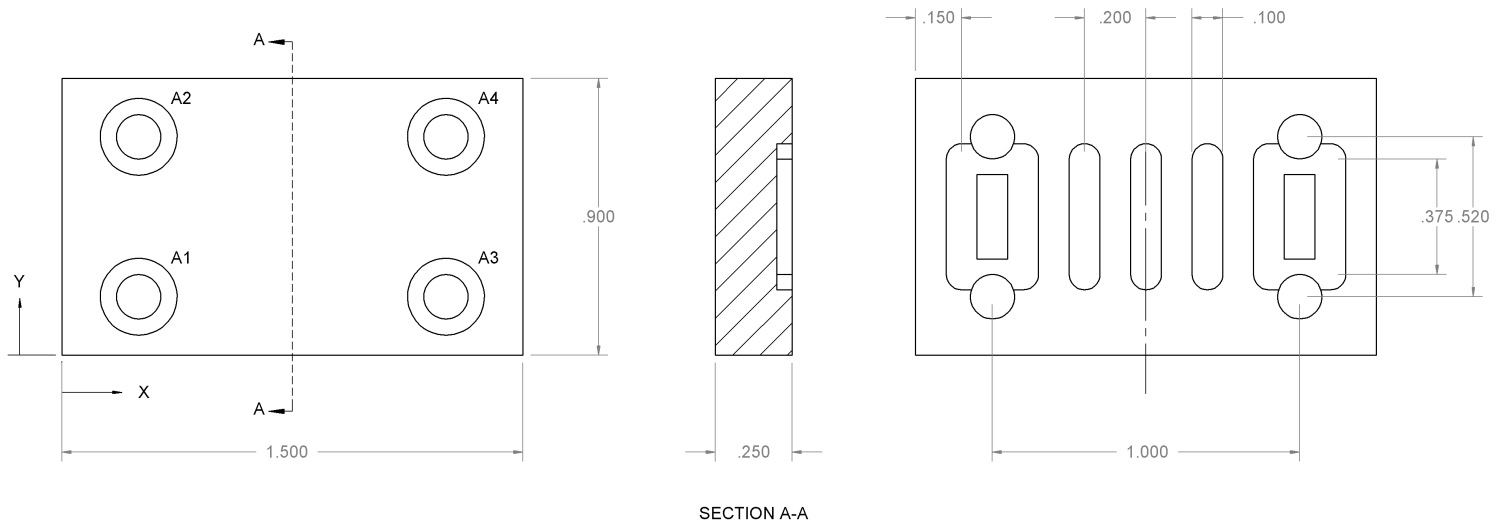
WEIGHT:

SHEET 1 OF 1

PROPRIETARY AND CONFIDENTIAL
THE INFORMATION CONTAINED IN THIS
DRAWING IS THE SOLE PROPERTY OF
AOSL OF MEMORIAL UNIVERSITY. ANY
REPRODUCTION IN PART OR AS A
WHOLE WITHOUT THE WRITTEN
PERMISSION OF AOSL IS PROHIBITED.



TAG	X LOC	Y LOC	SIZE
A1	.2500	.1900	$\phi .144$ THRU ALL $\square \phi .250 \nabla .138$
A2	.2500	.7100	
A3	1.2500	.1900	
A4	1.2500	.7100	



SECTION A-A

UNLESS OTHERWISE SPECIFIED:
DIMENSIONS ARE IN INCHES

TOLERANCES:
FRACTIONAL $\pm 1/16$
ANGULAR: $\pm 1^\circ$
MACH: $\pm .001$
BEND: ± 0.01
TWO PLACE DECIMAL: ± 0.01
THREE PLACE DECIMAL: ± 0.005

INTERPRET GEOMETRIC
TOLERANCING PER:

MATERIAL
ALUM 6061

FINISH

DO NOT SCALE DRAWING

PROPRIETARY AND CONFIDENTIAL
THE INFORMATION CONTAINED IN THIS
DRAWING IS THE SOLE PROPERTY OF
AOSL OF MEMORIAL UNIVERSITY. ANY
REPRODUCTION IN PART OR AS A
WHOLE WITHOUT THE WRITTEN
PERMISSION OF AOSL IS PROHIBITED.

NAME DATE

H. WANG 2012-04-18

DRAWN

CHECKED

ENG APPR.

MFG APPR.

Q.A.

COMMENTS:

QTY.: 1



AOSL - Memorial University

TITLE:

Belt Clamp Top

SIZE DWG. NO.

A

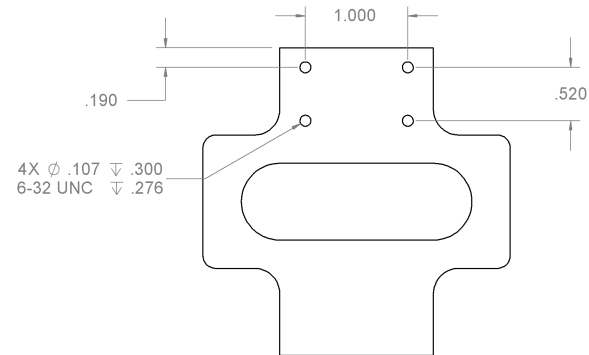
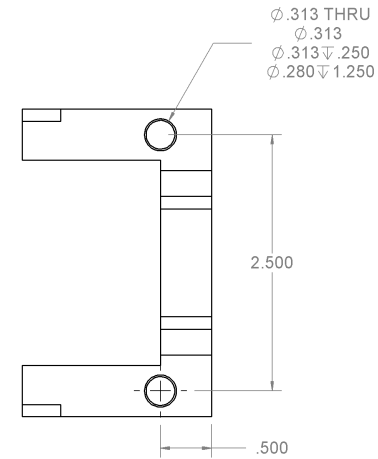
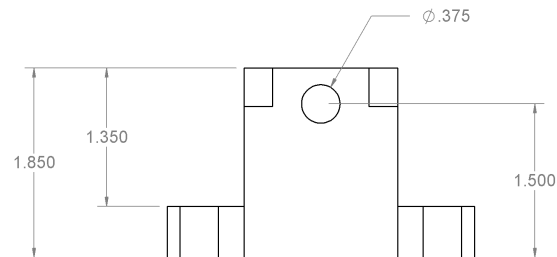
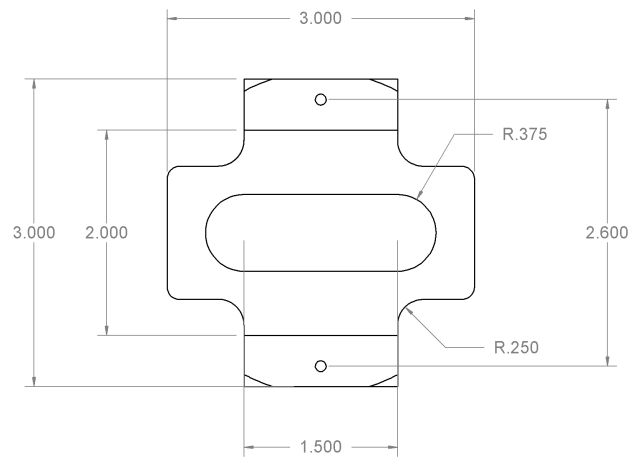
D034

REV

SCALE: 2:1

WEIGHT:

SHEET 1 OF 1



UNLESS OTHERWISE SPECIFIED:
DIMENSIONS ARE IN INCHES

TOLERANCES:
FRACTIONAL $\pm 1/16$
ANGULAR: $\pm 1^\circ$
MACH: BEND ± 0.01
TWO PLACE DECIMAL ± 0.01
THREE PLACE DECIMAL ± 0.005

INTERPRET GEOMETRIC
TOLERANCING PER:

MATERIAL
ALUM 6061

FINISH

DO NOT SCALE DRAWING

PROPRIETARY AND CONFIDENTIAL
THE INFORMATION CONTAINED IN THIS
DRAWING IS THE SOLE PROPERTY OF
AOSL OF MEMORIAL UNIVERSITY. ANY
REPRODUCTION IN PART OR AS A
WHOLE WITHOUT THE WRITTEN
PERMISSION OF AOSL IS PROHIBITED.

NAME DATE

H. WANG 2012-04-18

DRAWN

CHECKED

ENG APPR.

MFG APPR.

Q.A.

COMMENTS:

QTY.: 1



AOSL - Memorial University

TITLE:

Belt Clamp Bottom

SIZE DWG. NO.

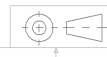
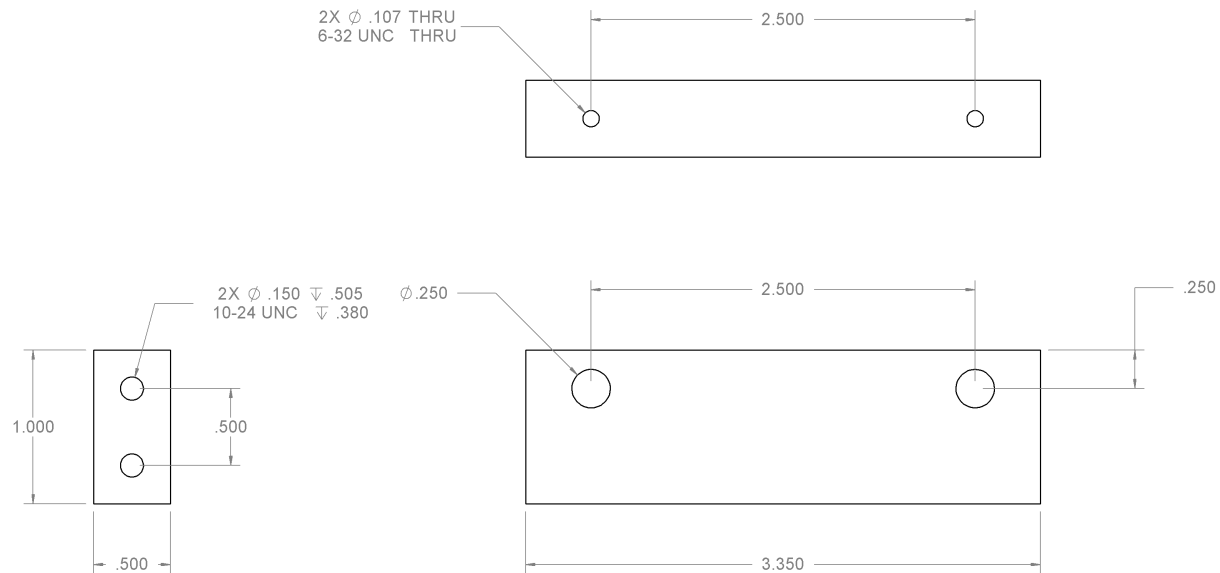
A

D035

REV

SCALE: 2:1 WEIGHT:

SHEET 1 OF 1



PROPRIETARY AND CONFIDENTIAL
THE INFORMATION CONTAINED IN THIS
DRAWING IS THE SOLE PROPERTY OF
AOSL OF MEMORIAL UNIVERSITY. ANY
REPRODUCTION IN PART OR AS A
WHOLE WITHOUT THE WRITTEN
PERMISSION OF AOSL IS PROHIBITED.

UNLESS OTHERWISE SPECIFIED:
DIMENSIONS ARE IN INCHES
TOLERANCES:
FRACTIONAL \pm 1/16
ANGULAR: \pm 1°
MACH: BEND \pm 0.01
TWO PLACE DECIMAL \pm 0.01
THREE PLACE DECIMAL \pm 0.005
INTERPRET GEOMETRIC
TOLERANCING PER:
MATERIAL
ALUM 6061
FINISH
DO NOT SCALE DRAWING

	NAME	DATE
DRAWN	H. WANG	2012-04-19
CHECKED		
ENG APPR.		
MFG APPR.		
Q.A.		
COMMENTS:		
QTY.: 2		

AOSL - Memorial University		
TITLE: Belt Rod Hanger		
SIZE A	DWG. NO. D037	REV
SCALE: 2:1	WEIGHT:	SHEET 1 OF 1

Ø .250^{+.0000}
 ^{-.0003}



.188

.125

17.875

.125

.020 X 45.0°
TYP. 2 PLS

18.500

UNLESS OTHERWISE SPECIFIED:
DIMENSIONS ARE IN INCHES

TOLERANCES:
FRACTIONAL ± 1/16
ANGULAR: ± 1°
MACH: BEND ± 0.01
TWO PLACE DECIMAL ± 0.01
THREE PLACE DECIMAL ± 0.005

INTERPRET GEOMETRIC
TOLERANCING PER:

MATERIAL
SS 304
FINISH

DO NOT SCALE DRAWING

NAME DATE

H. WANG 2012-04-19

DRAWN

CHECKED

ENG APPR.

MFG APPR.

Q.A.

COMMENTS:

QTY.: 2



AOSSL - Memorial University

TITLE:

Timing Shaft Long

SIZE DWG. NO.

A

D038

REV

SCALE: 1:8 WEIGHT:

SHEET 1 OF 1

PROPRIETARY AND CONFIDENTIAL
THE INFORMATION CONTAINED IN THIS
DRAWING IS THE SOLE PROPERTY OF
AOSSL OF MEMORIAL UNIVERSITY. ANY
REPRODUCTION IN PART OR AS A
WHOLE WITHOUT THE WRITTEN
PERMISSION OF AOSSL IS PROHIBITED.



5

4

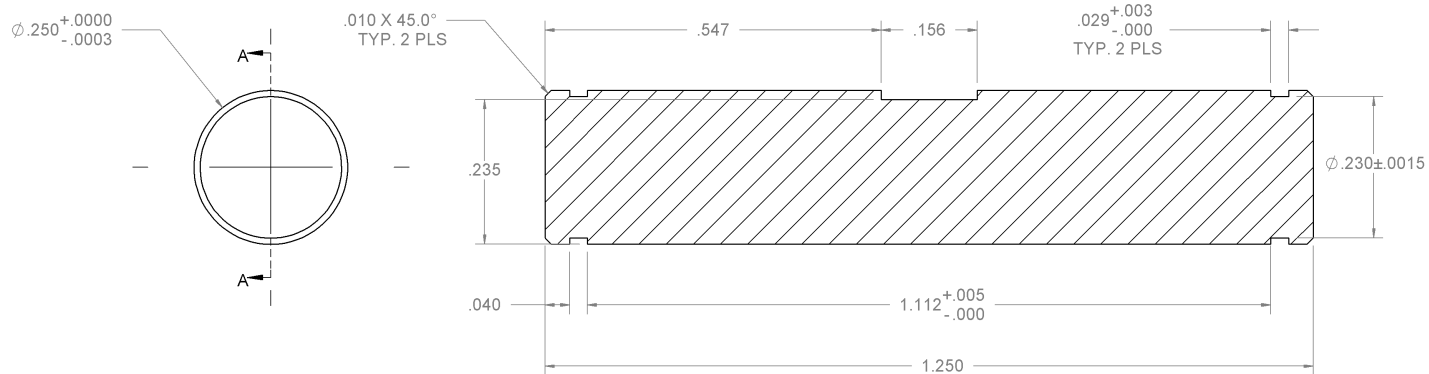
3

2

1



PROPRIETARY AND CONFIDENTIAL
THE INFORMATION CONTAINED IN THIS
DRAWING IS THE SOLE PROPERTY OF
AOSL OF MEMORIAL UNIVERSITY. ANY
REPRODUCTION IN PART OR AS A
WHOLE WITHOUT THE WRITTEN
PERMISSION OF AOSL IS PROHIBITED.



SECTION A-A
SCALE 4 : 1

UNLESS OTHERWISE SPECIFIED:
DIMENSIONS ARE IN INCHES

TOLERANCES:
FRACTIONAL $\pm 1/16$
ANGULAR: $\pm 1^\circ$
MACH: BEND ± 0.01
TWO PLACE DECIMAL ± 0.01
THREE PLACE DECIMAL ± 0.005

INTERPRET GEOMETRIC
TOLERANCING PER:

MATERIAL
SS 304

FINISH

DO NOT SCALE DRAWING

NAME DATE

H. WANG 2012-04-19

DRAWN

CHECKED

ENG APPR.

MFG APPR.

Q.A.

COMMENTS:

QTY.: 1



AOSL - Memorial University

TITLE:

Timing Wheel Shaft

SIZE DWG. NO.

A

D041

REV

SCALE: 2:1

WEIGHT:

SHEET 1 OF 1

PROPRIETARY AND CONFIDENTIAL
THE INFORMATION CONTAINED IN THIS
DRAWING IS THE SOLE PROPERTY OF
AOSL OF MEMORIAL UNIVERSITY. ANY
REPRODUCTION IN PART OR AS A
WHOLE WITHOUT THE WRITTEN
PERMISSION OF AOSL IS PROHIBITED.



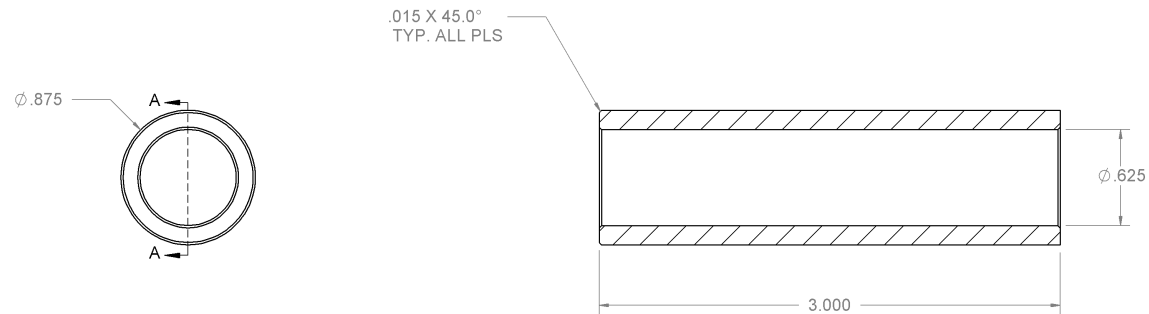
5

4

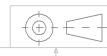
3

2

1



SECTION A-A
SCALE 1 : 1



PROPRIETARY AND CONFIDENTIAL
THE INFORMATION CONTAINED IN THIS
DRAWING IS THE SOLE PROPERTY OF
AOSL OF MEMORIAL UNIVERSITY. ANY
REPRODUCTION IN PART OR AS A
WHOLE WITHOUT THE WRITTEN
PERMISSION OF AOSL IS PROHIBITED.

UNLESS OTHERWISE SPECIFIED:
DIMENSIONS ARE IN INCHES


TOLERANCES:
FRACTIONAL $\pm 1/16$
ANGULAR: $\pm 1^\circ$
MACH: BEND ± 0.01
TWO PLACE DECIMAL ± 0.01
THREE PLACE DECIMAL ± 0.005

INTERPRET GEOMETRIC
TOLERANCING PER:

MATERIAL
Delrin AF
FINISH

DO NOT SCALE DRAWING

	NAME	DATE
DRAWN	H. WANG	2012-04-19
CHECKED		
ENG APPR.		
MFG APPR.		
Q.A.		
COMMENTS:		
QTY.: 1		

 AOSL - Memorial University		
TITLE:		
End Support Bushing		
SIZE	DWG. NO.	REV
A	D043	
SCALE: 4:1	WEIGHT:	SHEET 1 OF 1

A.2 Matlab and Mbed Source Codes

PID Controller Simulation Parameters

```
% Motor parameters are obtained from the motor manufacturer's spec sheet
% Assumptions are made on system inertia (gears, rollers etc.)
```

```
P = 1;
```

```
I = 0;
```

```
D = 0;
```

```
Ra = 3.91;                %% Motor resistance (ohms)
```

```
L = 4.24E-3;             %% Motor inductance (H)
```

```
KT = 5.8E-2;             %% Motor torque constant (N-m/A)
```

```
Jm = 7.06E-6;           %% Motor rotor inertia (kg-m^2)
```

```
fm = 1.8E-6;             %% Motor viscous damping coefficient (N-m-s)
```

```
FL = 5.4E-6;
```

```
KE = 5.83E-2;           %% Motor back-EMF constant (V/r/s)
```

```
Ft = fm + FL/5.9;
```

```
FT = 3.0E-4;            %% Friction Torque (N-m)
```

```
JL = 2.0E-5;
```

```
Jt = Jm + JL/5.9^2 ;    %% Total mass moment of inertia (kg-m^2)
```

```
KENC = 512/(2*pi);      %% Encoder gain (pulses/rad)
```

```
Ktach = 2/(1000*2*pi/60);    %% Tachometer gain (V/r/s)
```

Motor 2 pulses recording for ASM swing measurement

```
//This program records # of pulses as ASM swings back and forth
```

```
#include "QEI.h"
```

```
#include "Motor.h"
```

```
#include "mbed.h"
```

```
#include "PinDetect.h"
```

```
/*Communication*/
```

```
Serial pc(USBTX, USBRX);
```

```
/*Analog speed ajustment*/
```

```
AnalogIn input(p15);
```

```
/*Encoder Setup*/
```

```
/*Use X4 encoding*/
```

```
QEI encoderA(p29, p30, NC, 512, QEI::X4_ENCODING);
```

```
QEI encoderB(p27, p28, NC, 512, QEI::X4_ENCODING);
```

```
/*Motors Setup*/
```

```
Motor mA(p21, p22); // pwm forward, pwm backward
```

```
Motor mB(p23, p24); // pwm forward, pwm backward
```



```

/*Timers*/
Ticker timerA, timerB, dswitch;

/*Interpurts*/
//limitswitch setup
PinDetect switchLeft(p5);
PinDetect switchRight(p6);

/*Working Variable*/
volatile float controloutputA = 0.0;
volatile float controloutputB = 0.0;

//Set point setup
volatile float speedmA = 0.0, setspeedmA = 0.0;
volatile float setPositionB = 0.0;

float errorA = 0.0, errorAprev = 0.0, accuErrorA = 0.0;
float errorB = 0.0, errorBprev = 0.0, accuErrorB = 0.0;

```

```

float proportionalA = 0.0, derivativeA = 0.0;
float proportionalB = 0.0, derivativeB = 0.0;

volatile float cobiasA = 0.0, cobiasB = 0.0;
volatile float maxRPM = 3734.0;

volatile float thetaA = 0, thetaAprev = 0;
volatile float thetaB = 0, thetaBprev = 0;

volatile long encoderApulses = 0;
volatile long encoderBpulses = 0, MBpulses = 0;

volatile int k = 1, i = 0, j = 0, ds = 1;
volatile float speedmARPM = 0.0;

/*Private Prototypes*/
void initialize();
void PIDB();

/* Initialize Function */
void initialize()
{
//    setspeedmA = 200.0; //set point speed range from 0-3734RPM.
//    cobiasA = ;

```

```
}
```

```
void flip () {
```

```
    MBpulses = encoderBpulses;
```

```
    pc.printf("%ld\n", MBpulses);
```

```
    encoderB.reset();
```

```
    encoderBpulses = 0;
```

```
    k = -1*k;
```

```
}
```

```
/*PID loop function for Motor B – Position Control of  
Arm Swing Motion*/
```

```
void PIDB()
```

```
{
```

```
    //assign encoder pulses value to encoderBpulses variable.
```

```
    encoderBpulses = encoderB.getPulses();
```

```
    //Calculate control output.
```

```
    mB.speed(controloutputB*k);
```

```

}

int main() {

    pc.baud(115200);
    pc.printf("Start Recording\n");

    controloutputB = 0.2;

    //Switch operations to change direction of motor
    switchLeft.mode( PullUp );
    switchLeft.attach_asserted( &flip );
    switchLeft.setSampleFrequency(); // Defaults to 20ms.

    switchRight.mode( PullUp );
    switchRight.attach_asserted( &flip );
    switchRight.setSampleFrequency(); // Defaults to 20ms.

    timerB.attach(&PIDB, 0.001); //execute Motor B Position PID
                                loop every milisecond.
}

```

Mbed Source Code for Cable Manipulation Test

```

#include "QEI.h"
#include "Motor.h"
#include "mbed.h"

```

```

#include "PinDetect.h"

/*Defines PID Gain*/
//Motor A
#define KpA 1.2
#define TiA 1.2
#define TdA 0.8
//Motor B
#define KpB 5.0
#define TiB 100
#define TdB 0.0

/*Communication*/
Serial pc(USBTX, USBRX);

/*Analog speed ajustment*/
AnalogIn input(p15);

/*Files*/
//LocalFileSystem local("local");
// Open "out.txt" on the local file system for writing
//FILE *fp = fopen("/local/out.txt", "w");

/*Encoder Setup*/

```

```

/*Use X4 encoding.
QEI wheel(p29, p30, NC, 624, QEI::X4_ENCODING);
Use X2 encoding by default.*/
QEI encoderA(p29, p30, NC, 512, QEI::X2_ENCODING);
QEI encoderB(p27, p28, NC, 512, QEI::X2_ENCODING);


/*Motors Setup*/
Motor mA(p21, p22); // pwm forward, pwm backword
Motor mB(p23, p24); // pwm forward, pwm backword


/*Timers*/
Ticker timerA, timerB, SpeedTimer;


/*Interpurts*/
PinDetect switchLeft(p5);
PinDetect switchRight(p6);


/*Working Variable*/
volatile float controloutputA = 0.0;
volatile float controloutputB = 0.0;


//Set point setup

```

```
volatile float speedmA = 0.0, setspeedmA = 0.0;  
volatile float setPositionB = 0.0;
```

```
float errorA = 0.0, errorAprev = 0.0, accuErrorA = 0.0;  
float errorB = 0.0, errorBprev = 0.0, accuErrorB = 0.0;
```

```
float proportionalA = 0.0, derivativeA = 0.0;  
float proportionalB = 0.0, derivativeB = 0.0;
```

```
volatile float cobiasA = 0.0, cobiasB = 0.0;  
volatile float maxRPM = 3734.0;
```

```
volatile float thetaA = 0, thetaAprev = 0;  
volatile float thetaB = 0, thetaBprev = 0;
```

```
volatile long encoderApulses = 0;  
volatile long encoderBpulses = 0;
```

```
volatile int k = 1, i = 0, j = 0;  
volatile long mlspeed = 0;  
volatile float speedmARPM = 0.0;
```

```
volatile float buffer[100];
```

```

/*Private Prototypes*/
void initialize();
void PIDA();
void PIDB();
//void RPMOUTA();

/* Initialize Function */
void initialize()
{
    setspeedmA = 200.0; //set point speed range from 0–3734RPM.
    setspeedmA = setspeedmA/maxRPM; //scale setspeedmA to 0–100%
    cobiasA = setspeedmA;

}

void flip() {

    encoderA.reset();
    encoderB.reset();

    encoderApulses = 0;
    encoderBpulses = 0;

```



```
thetaA = 0;
```

```
thetaB = 0;
```

```
thetaAprev = 0;
```

```
thetaBprev = 0;
```

```
k = -1*k;
```

```
}
```

```
/*PID loop function for Motor A – Speed Control of  
Cable Rolling Motion*/
```

```
void PIDA()
```

```
{
```

```
//assign encoder pulses value to encoderApulses variable.
```

```
encoderApulses = encoderA.getPulses();
```

```
thetaA = encoderApulses; //read encoder feedback from Motor A.
```

```
//calculate speed of Motor A in counts/ms.
```

```
speedmA = thetaA - thetaAprev;
```

```
speedmARPM = speedmA*29.3;
```

```
/* if(i < 100){
```

```
buffer[i] = speedmARPM;
```

```
i++;
```

```
}*/
```

```

pc.printf("%f\n", speedmARPM);

//scale the actual speed of Motor A to 0–100%.
speedmA = speedmA/637.3;
errorA = setspeedmA - speedmA; //calculate the error speed in %.

//Calculate proportinal term.
proportionalA = errorA;

//Calculate derivative term.
derivativeA = errorA - errorAprev;
errorAprev = errorA;

//Calculate accumulated error.
accuErrorA += errorA;

//Calculate control output.
controloutputA = cobiasA + KpA*(proportionalA +
(1.0/TiA)*accuErrorA + TdA*derivativeA );

//Check if controloutput has saturated.
if (controloutputA > 1.0)
{
controloutputA = 1.0;
}
if (controloutputA < -1.0)

```

```

{
  controloutputA = -1.0;
}

//Write the control output to the motor
mA.speed(controloutputA);

thetaAprev = thetaA; // Update encoder

}

/*PID loop function for Motor B – Position Control of
Arm Swing Motion*/

void PIDB()
{
  //assign encoder pulses value to encoderBpulses variable.
  encoderBpulses = encoderB.getPulses();
  //position of Motor B follows the position of Motor A to a ratio
  setPositionB = k*(float)encoderApulses*33591.0/76958.0;
  thetaB = encoderBpulses; //read encoder feedback from Motor B.
  errorB = setPositionB - (float)thetaB;
  errorB = errorB/1024.0;

  //Calculate proportional term.
  proportionalB = errorB;

```

```

//Calculate derivative term.
derivativeB = errorB - errorBprev;
errorBprev = errorB;

//Calculate accumulated error.
accuErrorB += errorB;

//Calculate control output.
controloutputB = cobiasB + KpB*(proportionalB +
(1.0/TiB)*accuErrorB + TdB*derivativeB);

//Check if controloutput has saturated.
if (controloutputB > 1.0)
{
controloutputB = 1.0;
}
if (controloutputB < -1.0)
{
controloutputB = -1.0;
}
//Write the control output to the motor
mB.speed(controloutputB);

thetaBprev = thetaB; // Update encoder

```

```
}
```

```
int main() {
```

```
    initialize(); //initialize all parameters.
```

```
    pc.baud(115200);
```

```
    //Open results file.
```

```
    //fp = fopen("/local/pidtest.csv", "w");
```

```
    //Switch operations to change direction of motor
```

```
    switchLeft.mode( PullUp );
```

```
    switchLeft.attach_asserted( &flip );
```

```
    switchLeft.setSampleFrequency(); // Defaults to 20ms.
```

```
    switchRight.mode( PullUp );
```

```
    switchRight.attach_asserted( &flip );
```

```
    switchRight.setSampleFrequency(); // Defaults to 20ms.
```

```
    //execute Motor A PID loop every milisecond.
```

```
    timerA.attach(&PIDA, 0.01);
```

```
    //execute Motor B Position PID loop every milisecond.
```

```
    timerB.attach(&PIDB, 0.01);
```

```
}
```

Matlab Code for Dynamics Cable Model Simulation

```

%*****
%Title: cable2dm.m
%Author: Haibing Wang
%
%*****

clear all

clc

options = odeset('RelTol',1e-3,'AbsTol',1e-3);

% Setting up
lu = 0.5; % Element Unit length
ne = 20; % Number of elements
nd = 21; % Number of nodes
n=1;

% Assign initial values
for i = 1:2*nd*2;
    if i == 1
        X0(1) = 1.8;
    elseif i > 2*nd+2 && rem(i,2) == 0

        X0(i) = lu*n;
        n = n+1;
    end
end

```

```

else
X0(i) = 0;
end
end
% X0 = [1.2 0 0 0 0 0 0 0 0 0 0 0.5 0 1 0 1.5];

[t,x] = ode45('funcm',[0 8],X0,options);

%*****
% Calculating Forces at Node 0. *
%*****

nd = 21;

Cd = 1.2; % Drag coefficient
Cv = 0.1; % Damping coefficient
lu = 0.5; % Initial length of cable element
E = 2e9; % Young's Modulus of cable
dc = 0.011; % Diameter of Cable
ds = 0.15; % Diameter of towfish
A = pi*dc^2/4; % Cross sectional area of cable
Vc = A*lu; % Volume of cable element
g = 9.81; % Gravitational acceleration
rho_w = 1030; % Density of seawater
rho_tf = 3000; % Density of towfish
rho_c = 1050; % Density of cable
mc = rho_c*Vc; % Mass of cable element

```

```

ma = rho_w*Vc; % Mass of displaced water by cable element
Af = pi/4*ds^2; % Cross sectional area of towfish
Vtf = pi/6*ds^3; % Volume of towfish
ms = rho_tf*Vtf; % Mass of towfish

xsize = size(x);
step = xsize(1);

theta1 = atan2((x(step,(2*(nd+2))) - x(step,(2*(nd+1)))) ,...
(x(step,(2*(nd+1)+1))-x(step,(2*(nd+1)-1))));

RIB1 = [cos(theta1) sin(theta1);
-sin(theta1) cos(theta1)];

%l1 = sqrt((x(2*(nd+1)+1)-x(2*(nd+1)-1))^2+(x(2*(nd+1+1))...
%      -x(2*(nd+1)))^2);
l1 = sqrt((x(step,45)-x(step,43))^2 + (x(step,46)-x(step,44))^2);
s1 = (l1-lu)/lu;
T1 = E*A*s1;

V1 = RIB1*[x(step,1);x(step,2)]; % Element 1 node 0
% Tangential velocity of node 0 in Element 1 local coord
Vt1 = V1(1);

```



```

V2 = RIB1*[x(step,3);x(step,4)]; % Element 1 node 1
% Tangential velocity of node 1 in Element 1 local coord
Vt2 = V2(1);

P1 = Cv*(Vt2 - Vt1); % Damping force in cable element 1

Fg = mc*g; % Gravity force of element
Fb = rho_w*Vc*g; % Boyancy force

VG1x = (x(step,1)+x(step,3))/2; % Velocity of Element 1(
                                center point) in x and y dir
VG1y = (x(step,2)+x(step,4))/2;

VG1B = RIB1'*[VG1x;VG1y];
VG1t = VG1B(1);
VG1n = VG1B(2);

ft1 = 0.01*(2.008 - 0.3858*theta1 + 1.9159*theta1^2 -
4.16147*theta1^3 + 3.5064*theta1^4 - 1.187299*theta1^5);
fn1 = 0.5-0.1*cos(theta1)+0.1*sin(theta1)-0.4*cos(2*theta1)-
0.011*sin(2*theta1);

FdB1t = -sign(VG1t)*0.5*rho_w*Cd*dc*lu*ft1*(VG1t^2+VG1n^2);
FdB1n = -sign(VG1n)*0.5*rho_w*Cd*dc*lu*fn1*(VG1t^2+VG1n^2);

```

```

FdI1 = RIB1*[FdB1t;FdB1n];
FdI1x = FdI1(1); % Drag forces of element 1 in x-direction
FdI1y = FdI1(2); % Drag forces of element 1 in y-direction

Ftx = T1*cos(theta1) + P1*cos(theta1) + 0.5*FdI1x;
Fty = T1*sin(theta1) + P1*sin(theta1) + 0.5*Fg - 0.5*Fb + 0.5*FdI1y;

%*****

% Plotting

%*****

d = size(t);

ts = 0;
tid = zeros(20,1); % tid gets the time step ID for every
                    nearest 0.2s interval

for jj=1:25

    ts = ts + 0.4;
    for p = 1:d(1)
        if abs(t(p)-ts) - min(abs(t-ts)) < 0.00001
            tid(jj) = p;
        end
    end
end
end

```

```
end
```

```
dd = size(tid);
```

```
%Plotting cable postions every 0.2s
```

```
for k = 1:dd(1)
```

```
for m = 1:ne
```

```
plot([x(tid(k),(2*nd+(2*m-1))),x(tid(k),(2*nd+(2*m+1)))],...
```

```
[x(tid(k),(2*nd+2*m)),x(tid(k),(2*nd+(2*m+2)))], 'b-');
```

```
hold on
```

```
plot([x(tid(k),(2*nd+(2*m-1))),x(tid(k),(2*nd+(2*m+1)))],...
```

```
[x(tid(k),(2*nd+2*m)),x(tid(k),(2*nd+(2*m+2)))], '*');
```

```
end
```

```
xlim([-1 14])
```

```
ylim([0 10.5])
```

```
set(gca, 'YDir', 'rev')
```

```
xlabel('x position in meters')
```

```
ylabel('y position in meters')
```

```
title('Position of Cable in 2D Space')
```

```
hold on
```

```
end
```

```
%
```

```
% subplot(4,2,2)
```

```
% plot(t,x(:,10));
```

```

% xlabel('t')
% ylabel('position in meters')
% title('Y position of point B')
%
% subplot(4,2,3)
% plot(t,x(:,11));
% xlabel('t')
% ylabel('position in meters')
% title('X position of point A')
%
% subplot(4,2,4)
% plot(t,x(:,12));
% xlabel('t')
% ylabel('position in meters')
% title('Y position of point A')
%
% subplot(4,2,5)
% plot(t,x(:,7));
% xlabel('t')
% ylabel('Velocity in m/s')
% title('Velocity in x-direction for point B')
%
% subplot(4,2,6)
% plot(t,x(:,8));
% xlabel('t')
% ylabel('Velocity in m/s')

```

```

% title('Velocity in y-direction for point B')
%
% subplot(4,2,7)
% plot(t,x(:,1));
% xlabel('t')
% ylabel('Velocity in m/s')
% title('Velocity in x-direction for point A')
%
% subplot(4,2,8)
% plot(t,x(:,2));
% xlabel('t')
% ylabel('Velocity in m/s')
% title('Velocity in y-direction for point A')

%%%%%%%%%%%%%%%%%%%%%%%%%%%%%%%%%%%%%%%%%%%%%%%%%%%%%%%%%%%%%%%%%%%%%%%%
% plot([x(m,7),x(m,9)], [x(m,8),x(m,10)], 'r');
% hold on
% plot([x(m,9),x(m,11)], [x(m,10),x(m,12)]);
% xlim([-2.5 1])
% ylim([0 3.5])
% set(gca, 'YDir', 'rev')
% xlabel('x position in meters')
% ylabel('y position in meters')
% title('position of cable')
% hold on

```

```
% subplot(3,1,1)
% plot(t,x(:,16));
% xlabel('t')
% ylabel('position in meters')
% title('Y position of Node 1')
%
% subplot(3,1,2)
% plot(t,x(:,18));
% xlabel('t')
% ylabel('position in meters')
% title('Y position of Node 2')
%
% subplot(3,1,3)
% plot(t,x(:,20));
% xlabel('t')
% ylabel('position in meters')
% title('Y position of Node 3')

% subplot(4,2,4)
% plot(t,x(:,12));
% xlabel('t')
% ylabel('position in meters')
```

```

% title('Y position of point A')
%
% subplot(4,2,5)
% plot(t,x(:,7));
% xlabel('t')
% ylabel('Velocity in m/s')
% title('Velocity in x-direction for point B')
%
% subplot(4,2,6)
% plot(t,x(:,8));
% xlabel('t')
% ylabel('Velocity in m/s')
% title('Velocity in y-direction for point B')
%
% subplot(4,2,7)
% plot(t,x(:,1));
% xlabel('t')
% ylabel('Velocity in m/s')
% title('Velocity in x-direction for point A')
%
% subplot(4,2,8)
% plot(t,x(:,2));
% xlabel('t')
% ylabel('Velocity in m/s')
% title('Velocity in y-direction for point A')

```

```

%*****

%Title: funcm.m

%Author: Haibing Wang

%

%*****


function xdot = funcm(t,x)

% state variable x = [V0x,V0y,V1x,V1y,V2x,V2y,V3x,V3y,
X0,Y0,X1,Y1,X2,Y2,X3,Y3]


% ne = number of elements , nd = # of nodes , nd = ne +1
ne = 20;
nd = 21;
nv = 2*(2*(ne+1));

xdot = zeros(1, nv);


% Constants and parameters.


Cd = 1.2; % Drag coefficient
Cv = 0.1; % Damping coefficient
lu = 0.5; % Initial length of cable element
E = 2e9; % Young's Modulus of cable

```



```

dc = 0.011; % Diameter of Cable
ds = 0.15; % Diameter of towfish
A = pi*dc^2/4; % Cross sectional area of cable
Vc = A*lu; % Volume of cable element
g = 9.81; % Gravitational acceleration
rho_w = 1100; % Density of seawater
rho_tf = 3000; % Density of towfish
rho_c = 1100; % Density of cable
mc = rho_c*Vc; % Mass of cable element
ma = rho_w*Vc; % Mass of displaced water by cable element
Af = pi/4*ds^2; % Cross sectional area of towfish
Vtf = pi/6*ds^3; % Volume of towfish
ms = rho_tf*Vtf; % Mass of towfish

MB = [mc 0;0 mc+ma]; % Cable mass & added mass

% Rotation Matrix
for i = 1:ne

theta(i) = atan2((x(2*(nd+i+1))-x(2*(nd+i))),
(x(2*(nd+i)+1)-x(2*(nd+i)-1)));

% Mass matrices
RIB{i} = [cos(theta(i)) sin(theta(i));
-sin(theta(i)) cos(theta(i))];

```

end

```
MI0 = 0.5*RIB{1}*MB*RIB{1}'; % Node 0 mass: 1/2 of mass
                                from element 1
```

```
for i = 1:ne
```

```
if i < 3
```

$$MI\{i\} = 0.5 * RIB\{i\} * MB * RIB\{i\}' + 0.5 * RIB\{i+1\} * MB * RIB\{i+1\}';$$

else

$$MI\{i\} = 0.5 * RIB\{i\} * MB * RIB\{i\}';$$

end

% Internal Forces

```
l(i) = sqrt((x(2*(nd+i)+1)-x(2*(nd+i)-1))^2+(x(2*(nd+i+1))-...
-x(2*(nd+i)))^2); % Cable length under towing
```

```
s(i) = (l(i)-lu)/lu; % Strain of cable
```

```
T(i) = E*A*s(i); % Tension forces in cable
```

```
V{2*i-1} = RIB{i}*[x(2*i-1);x(2*i)]; % Element 1 node 0
```

$$V_t(2*i-1) = V\{2*i-1\}(1); \text{ \% Tangential velocity of node 0}$$

in Element 1 local coord

```

V{2*i} = RIB{i}*[x(2*i+1);x(2*i+2)]; % Element 1 node 1
Vt(2*i) = V{2*i}(1); % Tangential velocity of node 1
                        in Element 1 local coord

% Damping force in cable element 1
P(i) = Cv*(Vt(2*i) - Vt(2*i-1));

end

% External Forces
Fg = mc*g; % Gravity force of element
Fb = rho_w*Vc*g; % Boyancy force
Fbs = rho_w*Vtf*g;

for i= 1:ne

VGx(i) = (x(2*i-1)+x(2*i+1))/2; % V of Element 1(center point)
                        in x and y dir
VGy(i) = (x(2*i)+x(2*i+2))/2;

VGB{i} = RIB{i}'*[VGx(i);VGy(i)];
VGt(i) = VGB{i}(1);
VGn(i) = VGB{i}(2);

ft(i) = 0.01*(2.008 - 0.3858*theta(i) + 1.9159*(theta(i))^2

```

```

- 4.16147*(theta(i))^3+3.5064*(theta(i))^4
- 1.187299*(theta(i))^5);

```

```

fn(i) = 0.5-0.1*cos(theta(i))+0.1*sin(theta(i))
-0.4*cos(2*theta(i)) - 0.011*sin(2*theta(i));

```

```

FdBt(i) = -sign(VGt(i))*0.5*rho_w*Cd*dc*lu*ft(i)*((VGt(i))^2
+(VGn(i))^2);

```

```

FdBn(i) = -sign(VGn(i))*0.5*rho_w*Cd*dc*lu*fn(i)*((VGt(i))^2
+(VGn(i))^2);

```

```

FdI{i} = RIB{i}*[FdBt(i);FdBn(i)];

```

```

FdIx(i) = FdI{i}(1); % Drag forces of element 1 in x-direction

```

```

FdIy(i) = FdI{i}(2); % Drag forces of element 1 in y-direction

```

```

end

```

```

% Drag force in x-dir

```

```

Dsx = -0.5*Cd*rho_w*x(2*ne+1)*abs(x(2*ne+1))*Af;

```

```

% Drag force in y-dir

```

```

Dsy = -0.5*Cd*rho_w*x(2*ne+2)*abs(x(2*ne+2))*Af;

```

```

% Newton's laws for node 0

```

```

xdot(1) = 0;

```

```

xdot(2*ne+3) = x(1);

```

```

xdot(2) = 0;

```

```

xdot(2*ne+4) = x(2);
% F0x = 0 = -Ftx + T1*cos(theta1) + P1*cos(theta1) + 0.5*FdI1x;
% F0y = 0 = -Fty + T1*sin(theta1) + P1*sin(theta1) + 0.5*Fg
% - 0.5*Fb + 0.5*FdI1y
Ftx = T(1)*cos(theta(1)) + P(1)*cos(theta(1)) + 0.5*FdIx(1);
Fty = T(1)*sin(theta(1)) + P(1)*sin(theta(1)) + 0.5*Fg
      - 0.5*Fb + 0.5*FdIy(1);

for i = 1:ne

% Newton's laws for node 1,2,3
xdot(2*(ne+i)+3) = x(2*i+1);
xdot(2*(ne+i)+4) = x(2*i+2);

if i < ne
Fx(i) = 0.5*(FdIx(i)+FdIx(i+1))+0.5*T(i+1)*cos(theta(i+1))+
0.5*P(i+1)*cos(theta(i+1))-0.5*T(i)*cos(theta(i)) - ...
0.5*P(i)*cos(theta(i));
Fy(i) = 0.5*(FdIy(i)+FdIy(i+1))+Fg-Fb+0.5*T(i+1)*sin(theta(i+1))+
0.5*P(i+1)*sin(theta(i+1))-0.5*T(i)*sin(theta(i)) ...
-0.5*P(i)*sin(theta(i));
else
Fx(i) = 0.5*FdIx(i)-0.5*T(i)*cos(theta(i))-0.5*P(i)*cos(theta(i))
+Dsx;
Fy(i) = 0.5*FdIy(i) + 0.5*Fg-0.5*Fb -0.5*T(i)*sin(theta(i)) -
0.5*P(i)*sin(theta(i)) + ms*g - Fbs + Dsy;

```

```
end  
AA = MI{i}\[Fx(i);Fy(i)];  
xdot(2*i+1) = AA(1);  
xdot(2*i+2) = AA(2);  
  
end  
  
% Integrator wants a column vector  
  
xdot = xdot';
```

A.3 Specification Sheet for COTS Components

Falmat Xtreme Underwater Data Cable



UNDERWATER NETWORK DATA/POWER CABLES

Applications: Homeland Security, Oceanographic, Observation, and other extreme marine environments.

Part Number	Power Comp	Data Comp **	Break Strength	Diameter	Wgt/1000'
FMCAT51205K24	5C- 12AWG	Cat 5e -24awg	2400 lbs	.700"	256 lbs
FMCAT51207K24	7C- 12AWG	Cat 5e -24awg	2400 lbs	.700"	297 lbs
FMCAT51606K24	6C- 16AWG	Cat 5e -24awg	2400 lbs	.564"	157 lbs
FMCAT51610K24	10C-16AWG	Cat 5e -24awg	2400 lbs	.564"	191 lbs
FMCAT51812K12	12C-18AWG	Cat 5e -24awg	1200 lbs	.500"	143 lbs
FMCAT51806K12	6C- 18AWG	Cat 5e -24awg	1200 lbs	.500"	110 lbs
FMCAT52218K12	18C-22AWG	Cat 5e -24awg	1200 lbs	.447"	120 lbs
FMCAT52218	18C-22AWG	Cat 5e -24awg	0	.433"	117 lbs
FMCAT52824K8	24C-28AWG	Cat 5e -24awg	800 lbs	.415"	90 lbs
FMCAT52824	24C-28AWG	Cat 5e -24awg	0	.400"	88 lbs
FMCAT50000 *	N/A	Cat 5e -24awg	0	.325"	47 lbs
FMCAT50000K12 *	N/A	Cat 5e -24awg	1200 lbs	.340"	52 lbs

* Cat 5 cable only, with rugged Xtreme-Green™ Polyurethane, no power conductors, or water-block.

** Stranded conductors for added flexibility.

Data Network/Power Composite Cables featuring:

- Extreme ruggedness, yet flexible water-blocked construction.
- Designed for underwater use with high-speed network data, video, and sensor equipment.
- Cables can be used for bottom-laid, vertical deployment, winch systems, and ROV applications.
- Our Cat 5e 4 pair stranded conductors meets or exceeds TIA 568-B. Suitable for 10Base-T and 100Base-T.
- Custom variations of these listed cables can be supplied with added breaking strength, steel armor package, additional jackets, or neutrally buoyant constructions.

Xtreme-Cat™ Cables are designed to maintain their flexibility in harsh and challenging environments. These cables feature Falmat's specially formulated "Xtreme-grade" polyurethane jacket for easier payout, tighter bends, and better tractor control with extremely low coefficient of friction. The Xtreme-Cat™ Cables with reduced diameter offer even smaller bend radius for tighter bends and compact, portable handling systems.



1873 DIAMOND STREET SAN MARCOS, CA 92078 U.S.A.
TEL: (760) 471-5400 FAX: (760) 471-4970 WEB: WWW.FALMAT.COM

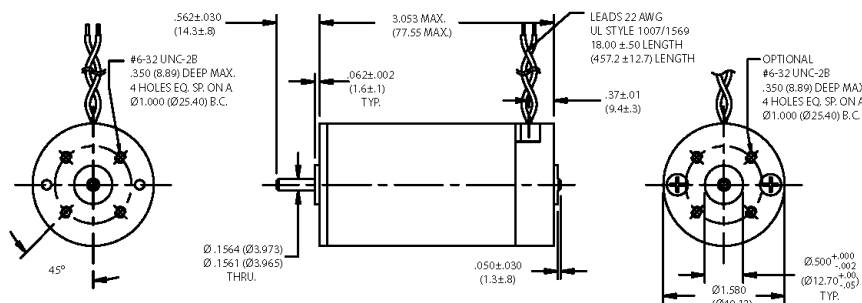
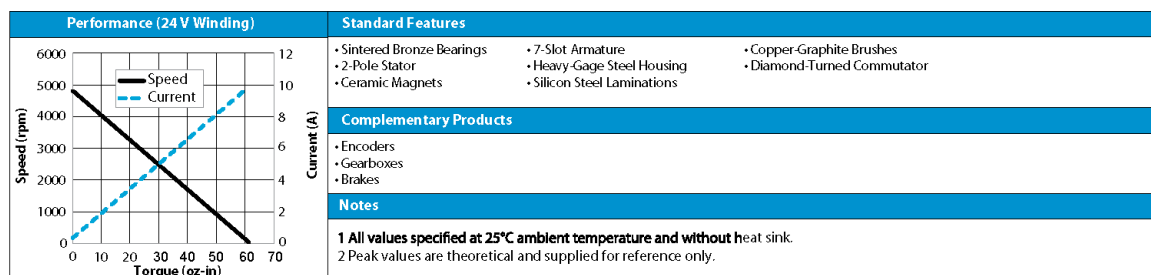
Last Revised 5-26-10

Pittman DC Servo Motor 9236 30.3V

Brush Commutated DC Servo Motors

9236 Series

PITTMAN®

[illegible]

This document is for informational purposes only and should not be considered as a binding description of the products or their performance in all applications. The performance data on this page depicts typical performance under controlled laboratory conditions. Actual performance will vary depending on the operating environment and application. AMETEK reserves the right to revise its products without notification. The above characteristics represent standard products. For products designed to meet specific applications, contact PITTMAN Motor Sales Department.

PITTMAN PRODUCTS
343 Godshall Drive, Harleysville, PA 19438
USA: +1 267 933 2105 - Europe: +33 240928751 - Asia: +86 21 5763 1258
www.pittman-motors.com

G 17

AMETEK®
PRECISION MOTION CONTROL

A.4 Cable Twisting Test

Cable Twist exists in almost every application where cable winding and storing is required such as in the winch systems. As it is unavoidable, understanding the limit becomes important and necessary. Different cables exhibit very different cable properties such as tension and torsional stiffness. Identifying the cable parameters becomes a little more complicated because the non-homogeneous nature of em cables, which always consist of a few different materials. A typical marine cable has at least the following components: copper conductors, conductor shield, insulation, reinforcement/armour layer, outer jacket.

In this thesis, finding the relationship between the twisting angle and torque involved is required. Thus, a simple cable twist test was performed to study the torsional behaviour of the selected the marine cable FALMAT underwater network data cable FMXCAT50000K12 (see in Appendix A3), which was capable of 1200 lbs of towing capacity. A 2 foot long piece of cable was cut and mounted on the test device as shown in Figure 5.1, one end of the cable was clamped so that the cable was fixed on all degrees of freedom, the other end of the cable was clamped on a pulley wheel that can rotate around its center axis. The pulley wheel has a groove in where it wound a string which hung the weights. The pulley wheel friction drove a small wheel that was mounted on a incremental encoder for obtaining the rotational position information. The encoder used in this test setup was A Model 755A from The Encoder Product Company, and it has 1000 counts per revolution. The Encoder was connected to the digital input of the MUnDer board, and the twisted cable angle was displayed on the screen through Tera Terminal, an open source emulator.

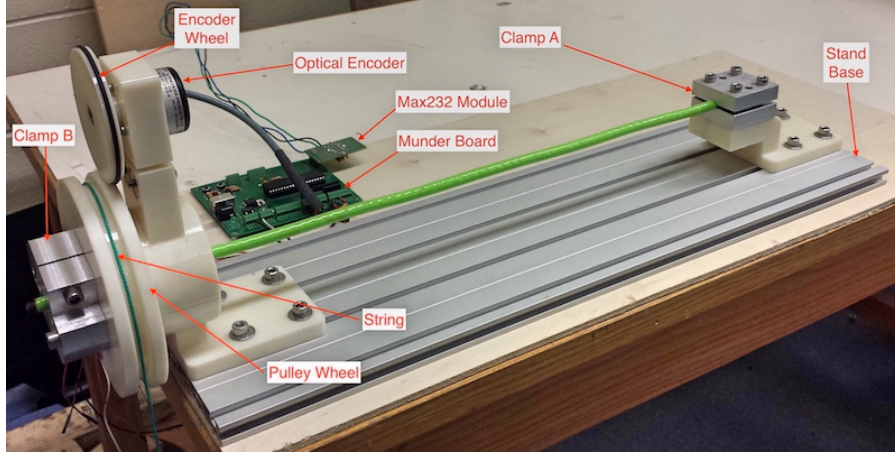


Figure 5.1: Marine Cable Twist Test Setup

The twisted angle of the cable can be calculated as follows:

$$\Theta_{twist} = P_{en} \cdot \frac{360.0}{1000.0} \cdot \frac{D_{en}}{D_{pu}} \quad (5.1)$$

In the above equation,

Θ_{twist} - Twisted Cable Angle

P_{en} - Encoder pulses for cable test

D_{en} - Diameter of cable test setup encoder wheel is 3.092 inches

D_{pu} - Diameter of cable test setup pulley wheel is 5.075 inches

The available resolution of the torsional cable movement is 0.0219° , which is sufficient for this cable test. The cable was twisted in both the clockwise direction and counterclockwise directions, This was to investigate the consistency of the cable twist in both directions.

Cable Twist Angle VS. Applied Torque Test			
Cable Length(mm)			
Clockwise			
Weight (g)	Torque (N-cm)	Pulses	Angle (deg)
10	0.59	8	1.688
57	3.36	149	31.441
104	6.12	350	73.856
151	8.89	525	110.784
198	11.65	669	141.171
245	14.42	811	171.135
292	17.19	898	189.494
339	19.95	988	208.485
386	22.72	1072	226.211
433	25.49	1148	242.248
480	28.25	1223	258.75
527	31.02	1286	271.369
574	33.79	1362	287.406
621	36.55	1436	303.21
668	39.32	1468	309.774
715	42.08	1530	322.857
Counter Clockwise			
10	0.59	5	1.55
57	3.36	121	25.533
104	6.12	322	67.947
151	8.89	434	91.581
198	11.65	582	122.812
245	14.42	770	162.483
292	17.19	845	178.31
339	19.95	933	196.879
386	22.72	1005	212.73
433	25.49	1065	224.734
480	28.25	1115	235.285
527	31.02	1182	249.212
574	33.79	1228	259.13
621	36.55	1287	270.158
668	39.32	1338	282.342
715	42.08	1401	295.636

Figure 5.2: Marine Cable Twist Test Data

In Figure 5.2, the first column is the incremental weights that was hung on the string, which is converted to the form of torque load based on the pulley wheel diameter. The last column is the twisted angle values. The data is used to plot the cable twist angle Vs. Applied Torque chart in Figure 5.3. As seen in the chart, there is only a small deviation between the clockwise and counterclockwise rotation tests. The deviation tends to get a little larger at higher torque loading. The plotted chart exhibits only a slight nonlinearity.

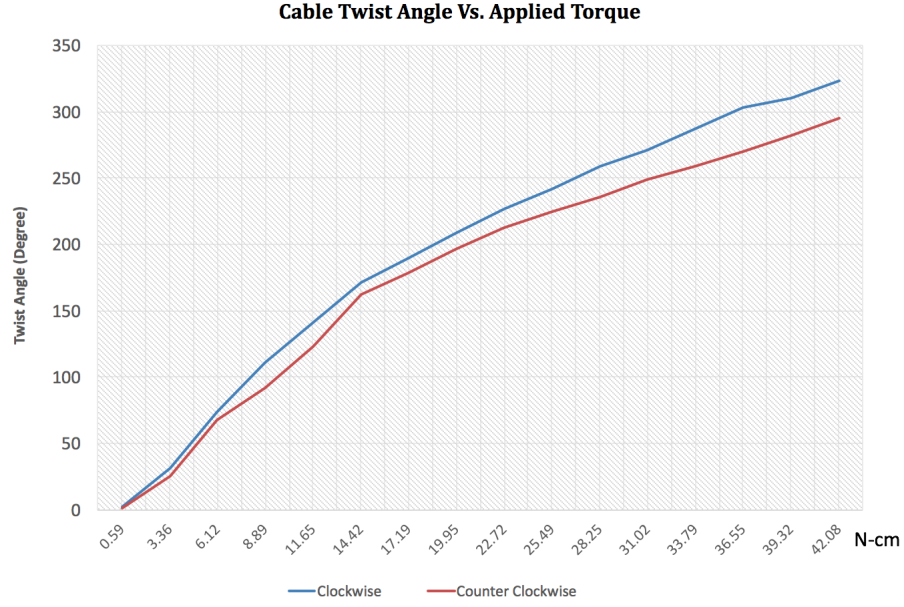


Figure 5.3: Marine Cable Twist Test chart

By using the Excel 2nd order polynomial curve fitting, equations for clockwise and counterclockwise can easily be obtained as follows,

Clockwise:

$$y = -1.0457 \cdot x^2 + 38.473 \cdot x - 32.384 \quad (5.2)$$

The coefficient of correlation is $R^2 = 0.99674$

Counterclockwise:

$$y = -1.0531 \cdot x^2 + 36.853 \cdot x - 35.012 \quad (5.3)$$

The coefficient of correlation is $R^2 = 0.99483$

By applying these equations, the torque required to twist the cable to a certain angle can be predicted accurately.